Dissolved Ammonia and Ammonia Gas Sorption Behavior in Porous Coordination Polymers (PCPs)

January 2019

JIANG YONG

Dissolved Ammonia and Ammonia Gas Sorption Behavior in Porous Coordination Polymers (PCPs)

A Dissertation Submitted to
the Graduate School of Life Environmental Sciences,
the University of Tsukuba
in Partial Fulfillment of the Requirements
for the Degree of Doctor of Philosophy in Environmental Studies
(Doctoral Program in Sustainable Environmental Studies)

JIANG YONG

Abstract

Ammonia including NH_4^+ in water bodies and gaseous NH_3 has been caused serious pollution problems, such as water eutrophication, soil acidification and $PM_{2.5}$, which have potential risk to human health. Up to now, many methods have been developed to remove NH_4^+ from aqueous solutions, such as breakpoint chlorination, air stripping, membrane technology, ozonation, adsorption, ion exchange etc. In the case of gaseous NH_3 treatment, the main methods including catalytic oxidation, biological filtration, liquid absorption and solid adsorption have been developed. Owing to the adsorption has the advantages of low operation cost and easy control, adsorption technology was chosen in this study.

Prussian blue (PB) and its analogues have been received considerable attention for their great NH_4^+/gas sorption because they have a simple cubic and nano-scale crystal structure with linear bridging of the octahedral metal ions by cyanide anions. More importantly, the target adsorbent for wastewater treatment and gas sorption, respectively, can be prepared by crystal engineering, metal substitution, and control of its vacancy density. For the NH_4^+ removal from wastewater or digestion liquids, adsorbents with high-selectivity are essential as there are many coexisting cations in the aqueous solution. In particular, for digestion liquids, a large capacity is also necessary because its NH_4^+ concentration is pretty high. For the gaseous NH_3 sorption from atmosphere, PB and its analogues have been demonstrated their highest sorption capacity among porous and open framework materials at room temperature. However, little information is available on the NH_3 sorption performance of PB analogues under high working temperature condition.

This study aimed to develop a new adsorbent with larger sorption capacity and high selectivity for NH_4^+ in aqueous solutions, and to study the sorption performances of NH_3 sorbent at high working temperature, regarding sufficient capacity, stability during cycle use and less volume change during the sorption-desorption process.

Firstly, the removal of NH_4^+ from NH_4Cl aqueous solutions and salty water were studied. For NH_4^+ sorption, a new PB analogue, namely sodium cobalt (II) hexacyanoferrate (II) (NaCoHCF), $Na_yCo(II)\ [Fe^{2+}(CN)_6]_x\ zH_2O$ with high capacity and selectivity was prepared. The adsorption performance was investigated by varying the mixing ratio (R_{mix}) of $[Fe(CN)_6]^{4-}$ to

Co^{2+} during synthesis. The NH_3 capacity was found to be proportional to R_{mix}, indicating that the NH_4^+ capacity can be increased by increasing the Na^+ ion content in NaCoHCF. Furthermore, R_{mix}=1.00 with homogeneous nanoparticles was prepared by flow synthesis using a micromixer. Even in a salty solution prepared by using NaCl at a Na^+ ion concentration of 9,350 mg/L, the maximum adsorption capacity (q_{max}, 4.28 mol/kg) was maintained. Using Markham–Benton analysis, the selectivity factor defined by the ratio of equilibrium constants for NH_4^+ to that for Na^+ was calculated to be α=96.2. The high selectivity of NaCoHCF results in good NH_4^+ adsorption performance, even from artificial seawater. In comparison with other adsorbents under the same condition and even in the NH_4Cl solution, NaCoHCF showed the highest capacity. Also, the co-existing Na^+ in aqueous solution has no interference with the adsorption of NH_4^+ by NaCoHCF, whereas the other adsorbents exhibited very low NH_4^+ adsorption from the salty solution.

Secondly, gaseous NH_3 sorption/capture under a wide range of temperature was studied using cobalt hexacyanocobaltate (CoHCCo). The comprehensive sorption performances were studied when operation temperature varied from 20 to 250 °C. The results show that it is possible to develop adsorbents which can be applied in the temperature swing adsorption (TSA). The largest NH_3 sorption capacity of CoHCCo were 25.2, 18.6, 8.6, and 2.1 mmol/g at 20, 100, 150, and 250 °C, respectively. Also, the stable structure was maintained during the sorption-desorption cycles by injecting 8 vol% NH_3 gas mixed with room air.

Thirdly, to compare with the CoHCCo, another new adsorbent called zinc hexacynanocobaltate (ZnHCCo) was developed. The isotherm test shows ZnHCCo has unique properties, i.e. it not only has similar the same sorption capacity with CoHCCo but also adsorbed NH_3 can be desorbed by pressure swing adsorption (PSA) process at moderate high working temperature (100 °C). At last, the effect of air containing moderate humidity (RH: 76%) on the NH_3 sorption performance of ZnHCCo and CoHCCo was discussed.

Results from this study indicate the adsorbents for NH_4^+ and gaseous NH_3 treatment and recovery were succeeded prepared. They would be useful in the field of wastewater or digestion liquids treatment system containing high NH_4^+/NH_3 concentration, as its largest sorption capacity, good selectivity and recyclability.

Keywords: Prussian blue analogue; ammonium; gaseous ammonia; sorption; energy

Contents

List of tables

List of figures

Chapter 1 Introduction

1.1 Environmental issues caused by NH_4^+/ NH_3

The total concentration of ionized ammonia (NH_4^+) and un-ionized ammonia (NH_3) in water is defined as the total ammonia nitrogen (NH_3-N) [1]. The NH_4^+ can be transformed to the form of NO_3^-, and if the concentration of NO_3-N≥10 mg⁄L, people who drink that water would be ill or die [2]. Moreover, excess ammonia in aquatic systems can cause eutrophication, harmful algal blooms, anoxic in estuaries, rivers, and even in coastal oceans. Consequently, the biodiversity, biology, fisheries, and overall ecosystem health are adversely affected by this N nutrient imbalance [3–5]. NH_3-N is present in two forms in water bodies, ammonium (NH_4^+) or ammonia (NH_3), according to the following chemical reaction.

$$NH_3 + H_3O+ \leftrightarrow NH_4^+ + H_2O \quad (1\text{-}1)$$

$$NH_4^+ + OH^- \leftrightarrow NH_3 + H_2O \quad (1\text{-}2)$$

Except the problems caused by NH_3-N wastewater, another problem is caused by NH_3 gas which is always be discharged into air directly and accompanied with bad odors, and it is hazardous to public health. As we know [6], (i) agriculture is mainly responsible for ammonia emissions, greater than 90% coming from manure and inorganic fertilizers, (ii) ammonia is able to react in the air with SO_2 and NO_x, thereby forming ammonium sulphate ($(NH_4)_2SO_4$) and ammonium nitrate (NH_4NO_3)), which eventually leads to create $PM_{2.5}$ that is harmful to human health, (iii) the ammonia deposition contributes to water eutrophication and soil acidification. Hence, reduction of ammonia emission is also important in our lives. On the other hand, up to now, the problem that hydrogen provides extremely low quantities of energy per unit of volume as compared to the conventional fuels used in transportation vehicles. Moreover, the development of the hydrogen distribution infrastructure includes complicated safety issues, such as hydrogen is volatile, and has wide flammability limits, presents high explosion danger, and its flame is invisible. Hence, the potential of ammonia gas can be used as fuels and hydrogen alternative energy, which has received much attention in recent years [7–9]. The main features of several fuels are shown in Table 1-1 [8], indicating NH_3 has a narrow flammability range, and therefore it is generally considered non-

Table 1-1 Some features of ammonia as compared to other conventional fuels [8].

Property	Gasoline	Diesel	Natural gas	H_2	NH_3
Flammability limit, volumes % in air	1.4-7.6	0.6-5.5	5-15	4-75	16-25
Auto-ignition temperature, ℃	300	230	450	571	651
Peak flame temperature, ℃	1977	2053	1884	2000	1850

flammable and no explosion danger if being properly transported. In addition, NH_3 can be thermally cracked into hydrogen and nitrogen using low energy, i.e., ~12% from the higher heating vale (HHV) [10] to produce H_2 for fuel-cells, furthermore it is fully recyclable because it can be made from nitrogen and water, the substances available everywhere in the environment. Another important point is it does not generate CO_2 and can easily be stored and transported as a liquid (around 8 atm at room temperature) [11].

According to the above, there are two major problems or environmental issues concerning NH_4^+/NH_3, one is NH_4^+-N in aqueous solution, NH_4^+-N should be removed properly from wastewater before entering into aquatic systems; another is gaseous NH_3, which should be adsorbed or captured because NH_3 has bad odor and it also contributes to the water eutrophication. The whole concept is shown in Fig. 1-1. The current techniques for the ammonium ions removal from wastewater are shown in Fig. 1-2 [12], among them, ion exchange method was selected in this study as it has the advantages of easily controllable and high removal efficiency. The sorbents belonging to nanomaterial were chosen because it has the benefits of a large specific surface area. and high surface reactivity. On the other hand, the main techniques for gaseous NH_3 sorption/capture are shown in Fig. 1-3. Among them, the method of solid adsorption was selected in this study as it has the advantages of simplicity, economy in configuration and operation. The adsorbent of Prussian blue analogue was chosen because one of PB analogue has been demonstrated its highest sorption capacity for NH_3 among the recyclable porous adsorbents up to now at room temperature (RT).

1.2 Methods for NH_4^+ and gaseous NH_3 removal

1.2.1 NH_4^+-N removal

The most widely used methods for ammonia removal from wastewaters are chemical precipitation, adsorption, ion exchange, and biological nitrification/denitrification [13]. Among these removal technologies, ion exchange as a kind of sorption method [14], has effective performances under varying water chemistry and can be employed in centralized or decentralized systems, which is also flexible regarding the operation mode, reactor configurations, and sequence in a treatment train. Therefore, its advantages provide opportunities for safe, effective, and affordable water treatment [15].

(1) Biological processes

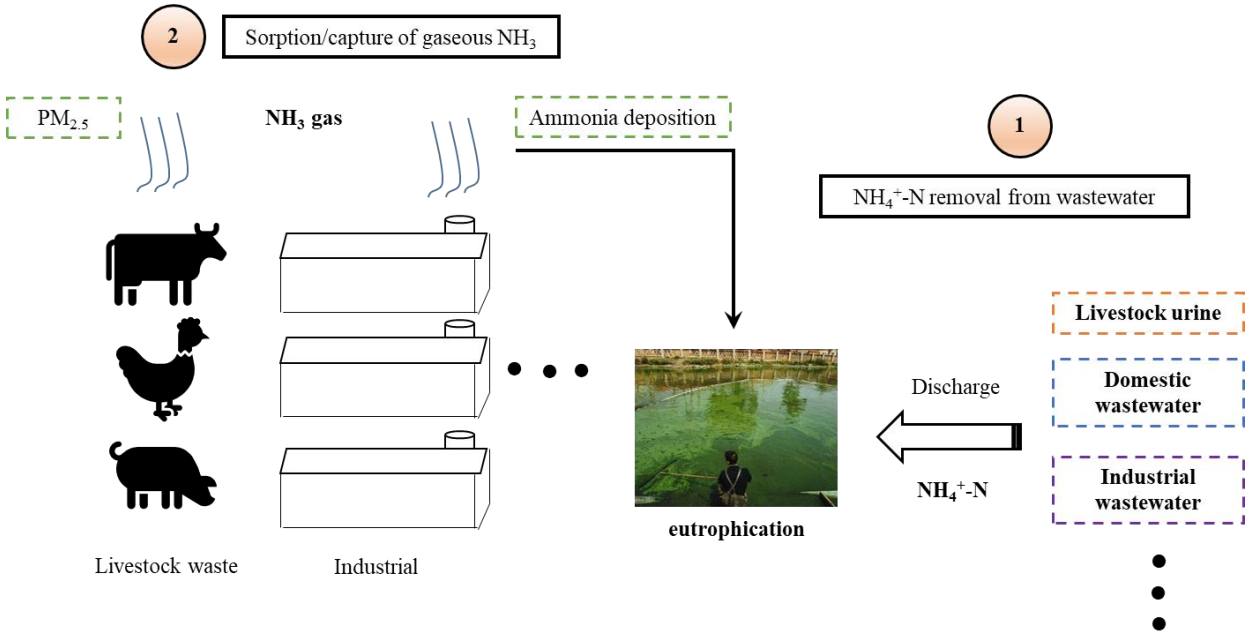

Fig. 1-1 The whole concept for NH_3 gas and dissolved NH_3 (NH_4^+-N) removal.

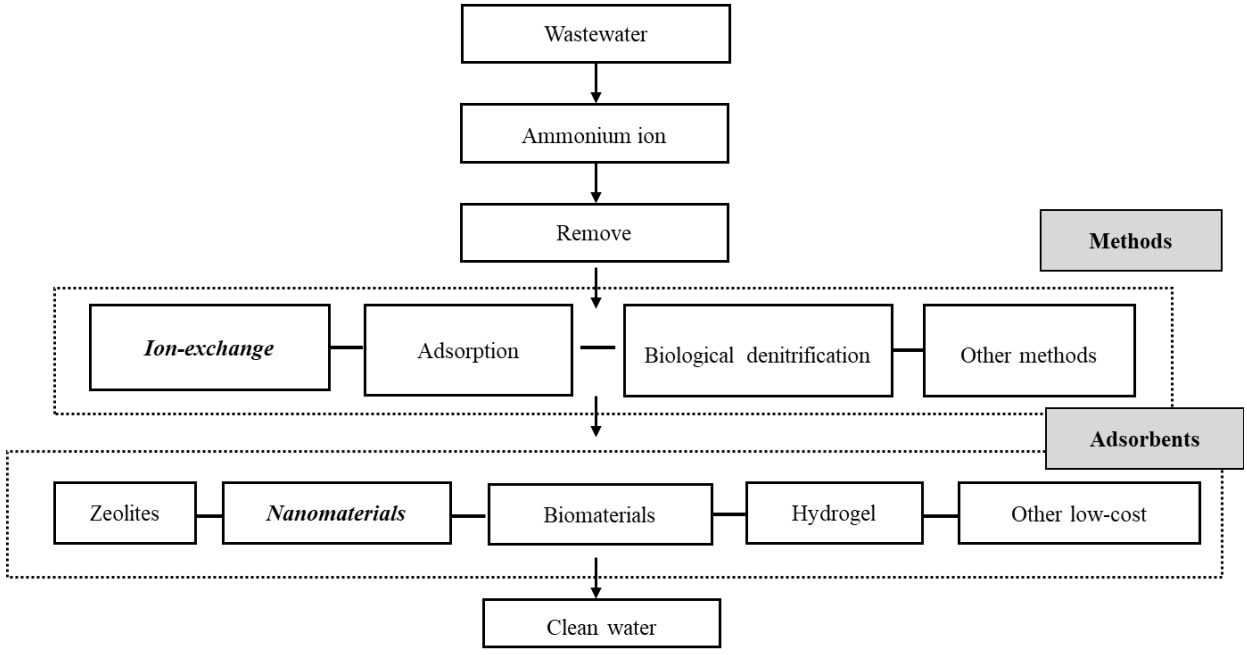

Fig. 1-2 Options for ammonium ions removal from wastewater [12].

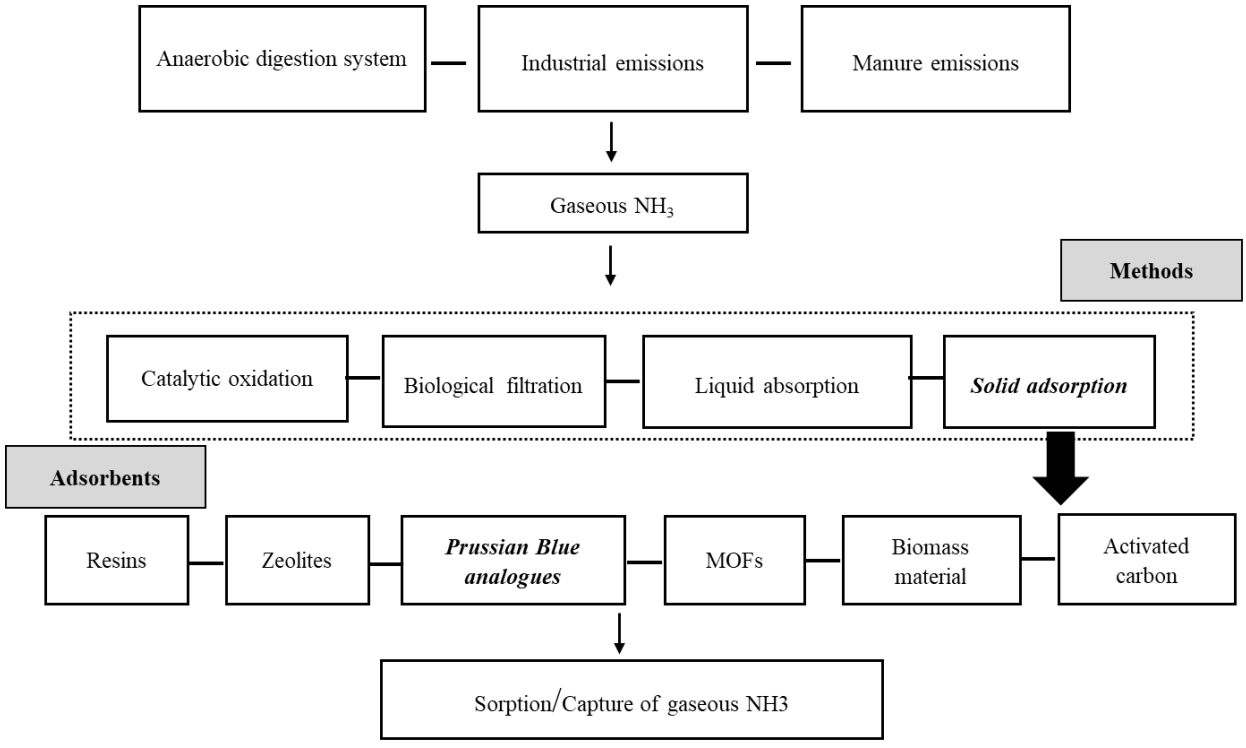

Fig. 1-3 Options for gaseous NH_3 sorption from ambient atmosphere.

Biological processes are widely applied to the treatment of both municipal and industrial wastewaters [16]. The major biological processes used for wastewater treatment can be separated into five major groups: aerobic process, anoxic process, anaerobic process, combined aerobic-anoxic-anaerobic processes, and pond processes. The principal application of the processes are as below: 1) the removal of the carbonaceous organic matter in wastewater; 2) nitrification; 3) denitrification; 4) phosphorus removal; and 5) waste stabilization [17].

Recently, anammox system has been found to be feasible and extremely suitable for treatment of highly concentrated ammonia-containing industrial effluents. However, the main drawbacks for anammox bacteria are their isolation in pure form and slow growth rate [18]. Hence, to make the costs of wastewater treatment systems to be competitive, a novel microbial processes like a combination of anammox and partial nitrification process in one reactor namely CANON process (Complete Autotrophic Nitrogen removal Over Nitrite) was developed [19].

However, some factors can affect the biological NH_4^+-N removal efficiency to a great extent.

The first factor is salinity. Partial nitrification/anammox process can be successfully applied for various wastewaters like livestock wastewater, landfill leachate, industrial wastewater etc. However, these wastewaters as contain high salt concentration which was considered as an inhibition factor for the biological nitrogen removal process [20]. Mosquera-Corral et al. [21] claimed that salt concentration over 100 mM would inhibit ammonia oxidation in a SHARON bioreactor treating fish water effluents. However, recently, marine anammox bacteria has been enriched in continuous culture system for more than one year, which demonstrated the anammox bacteria can inherently prefer high salt concentration and live in high salt habitats and would be available for industrial purposes [22, 23].

The second one is temperature. Cannavo et al. [24] indicated that at temperatures below 24 ℃, nitrification stopped and methanol loading rate was decreased progressively when treating sanitary landfill leachate containing an ammonia concentration of over 2200 mg N/L. Furthermore, the system suffered major nitrification and denitrification inhibition at 100 ℃.

Dosta et al. [25] evaluated the effects of moderately low temperatures on the stability of anammox process, and found the system was successfully operated at temperature 18 ℃. However, when the temperature decreased to 15 ℃, nitrite accumulation was observed and the system lost its stability.

The third factor is pH. As we know, without pH control or buffers nitrification rates would drop off very quickly due to the production of HNO_2, and HNO_3. The pH range preferred by heterotrophic denitrifiers is between 5.95 and 7.9 [26], although the optimal pH level in an anoxic/oxic membrane bioreactor with over 99.9% of nitrate removal and without accumulation of nitrite is 7.5-8.5 [27]. The pH values beyond this range may hinder the denitrification process, but in general, the optimal pH is site-specific due to some effects of acclimation and adaptation to the microbial ecosystem.

(2) Adsorption

Adsorption is now recognized as an effective and economical method for ammonium ions removal [28, 29]. There are two types of adsorption, physisorption and chemisorption. Some adsorbents such as biochar, activated carbon (AC), zeolite with and without modification have been trialed for removing ammonium via the water treatment process [30–35].

As the adsorption efficiency depends on the type of adsorbents, different kinds of low-cost adsorbents have been developed and tested to remove ammonium ions. There are kinds of literature reported on the adsorption of ammonium ion by these low-cost adsorbents, e.g. polyvinyl alcohol (PVA) hydrogel [36], aerobic granular sludge, activated sludge and anammox granules [37, 38], powders of leaves, stems or barks of some plants [39], municipal sludge [40]. Furthermore, adsorbents should have good selectivity, as if resources are different, the wastewater would contain a variety of co-existing ions, resulting in the high requirement for selectivity. That is to say, if adsorbents do not have high selectivity, the sorption capacity in real practice would always decrease. Hence, the selectivity of adsorbents for the target treatment substances is extremely important.

Also, since adsorption sometimes is reversible, adsorbents can be regenerated by a suitable desorption process [41], which makes the adsorption cost-effective in the applications.

Two main sorption isotherm models, Langmuir and Freundlich model are commonly applied. The Langmuir model assumes that adsorption takes place at specific homogeneous sites within the adsorbent and has been successfully applied in many adsorption processes of monolayer adsorption. The following assumptions are considered for Langmuir model [42]:

1) The surface containing the adsorbing sites is a perfectly flat plane with no corrugations (assume the surface is homogeneous).

2) The adsorbing gas become an immobile state.

3) All sites are equivalent.

4) Each site can hold at most one molecule of A (mono-layer coverage only).

5) There are no interactions between adsorbate molecules on adjacent sites.

In contrast, the Freundlich isotherm is the most important multisite adsorption isotherm for rough surfaces [43].

(3) Ion exchange

Along with absorption and adsorption, ion exchange is regarded as a form of sorption [14]. An ion-exchanger in aqueous solution consists of anions, cations and water, where either the cations or the anions are chemically bound to an insoluble matrix. The chemically bound ions are referred as the fixed ions, and the ions of opposite charge are referred to as the counter-ions [44].

Ion exchange is used in water treatment to remove the unwanted soluble ionized substances from water [45]. Exchange sorbents are usually ion exchange resins, zeolites, clay or soil humus, including either cation exchangers that exchange positively charged ions or anion exchangers that exchange negatively charged ions.

The ion exchange process can be illustrated by considering an anion exchange material, in which the counter-ion is E^-. The exchanger can, therefore, be represented as M^+E^-, where M^+ denotes the insoluble matrix material containing the fixed (positive) ion. When a solution containing a different anion, A^-, is brought into contact with the ion-exchanger, an equilibrium is established between the two mobile ions E^- and A^- as follows [44]:

$$M^+E^- + A^-_{aq} \leftrightarrow M^+A^- + E^-_{aq} \quad (1\text{-}3)$$

Ion exchanges can be unselective or have binding preferences for certain ions or classes of ions, depending on their chemical structure. It can be dependent on the size of the ions, their charge, or their structure. Typical examples of ions that can bind to ion exchangers are as follows [46]:

1) H^+ (proton) and OH^- (hydroxide).

2) Singly charged monatomic ions like Na^+, K^+, and Cl^-.

3) Doubly charged monatomic ions like Ca^{2+} and Mg^{2+}.

4) Polyatomic inorganic ions like SO_4^{2-} and PO_4^{3-}.

5) Organic bases, usually molecules containing the amine functional group $-NR_2H^+$.

6) Organic acids, often molecules containing $-COO^-$ (carboxylic acid) functional groups.

7) Biomolecules that can be ionized: amino acids, peptides, proteins, etc.

Ion exchange has been widely applied for the removal of ammonium ions from wastewater. However, regeneration of ion exchange resins by chemical reagents when they are exhausted, always cause seriously secondary pollution [12]. Therefore, if the ion exchange system is not designed and managed properly, ion exchange can provide significant disadvantages for small potable water systems.

The Langmuir and Freundlich isotherms can also be used to model ion exchange [47].

1.2.2 Methods for gaseous ammonia sorption/capture

In the case of gaseous NH_3 sorption/capture, kinds of removal methods, such as catalytic oxidation, biological filter, liquid absorption, and solid adsorption were compared, the results of advantages and disadvantages are shown in Table 1-2 [48–58].

Ammonia gas separation is conventionally accomplished by cryogenic distillation. However, the method is economical only on a very large scale, since both the investment and operating costs are high [58]. On small and medium scales, ammonia can be separated by absorption, which is a process containing transfer of one or more species from the gas phase to a liquid solvent. However, this technique has some drawbacks, such as difficult operability, high investment costs, and the loss of absorbing solutions due to degradation [59].

Among these methods, ammonia gas separation by adsorption and its recovery for reuse is considered as a heat exchange fluid in adsorption heat pumps, fuels and H_2 alternative energy [9, 60, 61, 62].

1.3 Adsorbents used for NH_4^+-N and gaseous NH_3 removal

As a sorbent, whether it is adsorbing wastewater or gases, firstly, it must have high selectivity, as co-existing ions in water bodies may decrease the sorption capacity of specific adsorbate. Moreover, the same requirement in the case of adsorption and storage of specific gas, as the gas stream generated from industries, is always mixed with kinds of gases. For instance, the flue gas is composed of high concentrations of N_2 (>70%), H_2S, SO_2, and low concentration of CO_2 (<15%) [63, 64], and natural gas contains high concentrations of methane (>80%), and other trace gases [65]. Secondly, the sorption capacity of the sorbents should be considered. Thirdly, the regenerability, in particular, is an important property for industrial applications, since some gases

Table 1-2 Comparison among various removal methods for gaseous NH_3 in ambient atmosphere.

Methods	Advantages	Disadvantages	Ref.
Catalytic oxidation	Higher thermal stable, high conversion efficiency.	High operating temperature (i.e. 800–900 ℃).	[48,49]
Biological filter	The best cost-effective control technology for simultaneous ammonia and odor reduction from composting process.	The reductive nature of biogas constitutes unfortunately reduces the applicability of biological treatment in ammonia removal from the biogas.	[51–53]
Liquid absorption	Recover water-dissolvable ammonia from air stream containing up to a few per cent of gas phase ammonia.	Uneconomical for the ammonia recovery; the operation and maintenance costs are relatively high.	[54–56]
Solid adsorption	Simplicity and economy in configuration and operation.	Sorption capacity is limited at higher working temperature; structures become unstable after sorption.	[50,57,58]

are adsorbed very strongly on the sorbents, leading to difficulties in resource recovery and less or one-time use of sorbent, thus high cost for operation.

1.3.1 Sorption materials for NH_4^+-N containing wastewater

Zeolites are the most widely used sorbents in the field of wastewater treatment and commercial water purification, in which there are mainly two types, natural zeolite and modified zeolite, including natural zeolite [32], Zeolite 13X [66], zeolite clinoptilolite [67], sodium hydroxide modified zeolite [68] and NaCl-modified zeolites [69] and so on. Because microporous aluminosilicate minerals which could be used as ion exchanger [70] are contained, and due to the porosity and their high cationic exchange property, zeolite can be employed to free ammonia and ammonium capture/removal.

Other sorbents, mainly consisting of organic sorbents, industrial byproducts, agricultural wastes and synthetic materials, such as activated carbon [71], fly ash [72], chitosan beads [73], clay minerals [74], oxide nanoparticles [75], were reported to have interesting performances. Among these sorbents, nanoparticles, in recent years, have also aroused many concerns, such as nano zero-valent iron, due to its small particle size (the average diameter of iron nanoparticles was in the range of 50–100 nm), large specific surface area, and high surface reactivity [76]. Bimetallic nanoparticles [77], the one named Fe/Cu particles which can enhance the rate of ammonium and ammonia reduction in aqueous solution, have better properties of air stability and an optimum reduction rate at nearly neutral pH.

1.3.2 Sorption materials for gaseous NH_3 treatment

Different solid media like potting soil, peat, zeolite and activated carbon [78, 79] have the potential ability to adsorb exhaust gases, ammonia, which is evolving during composting of tobacco and grape waste. Besides, zeolite, alumina, silica gel, and activated carbon can be used as a sorbent to separate ammonia from the gas streams in the ammonia manufacturing process [59, 80 , 81].

Also, in the last decade, much attention has been paid to the applications of metal-organic frameworks (MOFs), functional materials and catalytic activities [82, 83] in the fields of separation [84], storage [85], and removal/capture of a certain gas [86–88]. Because of their unique chemical

and physical properties including higher chemical versatility, ultrahigh porosity, large surface area, and tunable structure than other porous materials, such as zeolites and activated carbons [89, 90], which make MOFs can be rationally designed to adsorb ammonia and amines selectively. Indeed, several research groups have recently reported MOFs for ammonia capture [91–94] and sensor [95] applications. However, in general, MOFs are less stable than inorganic porous materials at high working temperature or after NH_3 sorption. Even several porous coordination polymers (PCPs) showing sufficient thermal stability (>500 ℃) [96], however, the stability has been reported independently, such as MOF-177 [97], with Zn_4O clusters and MOF-5 [98], and HKUST-1 [99], consisting of Cu_2-paddlewheel building units, have been reported to be unstable against ammonia [100, 101]. More recently, the instability of other Zn_4O-based PCPs against ammonia has also been documented [102]. To the best of our knowledge, there have been only a few examples stating that the framework structure of the MOF is maintained after the adsorption of ammonia at ambient temperature [93, 94, 103–106]. Many MOFs were also unstable against ammonia at room temperature (RT) or higher temperatures between 200 and 300 ℃, although several MOFs were stable up to 350 ℃ under an ammonia atmosphere at ambient pressure [105], the sorption capacity was not shown.

1.4 Prussian blue families for NH_4^+-N/gaseous NH_3 adsorption

Prussian Blue Analogues (PBAs), also known as PCPs, the applications for NH_4^+-N/gaseous NH_3 adsorption have been widely studied. Recently, one kind of PBAs called metal hexacyanoferrate (MHCF), such as copper hexacyanoferrate (CuHCF) [107], has applied on recovering dissolved ammonia in pure water and co-existing Na^+ added NaCl in solution, respectively, showed fast adsorption kinetics and the least impact of coexisting sodium ion, hold an impressive ammonium adsorption capacity of 1.94 mol/kg in pure water solution. The sorption mechanism of the CuHCF is ion exchange, as NH_4^+ was adsorbed by exchanging with the K^+ ions [107]. Therefore, to enhance the adsorption capacity, $[Fe(CN)_6]$ vacancies should be eliminated, as the number of alkali A^+ ions increasing with the number of vacancies decreasing which decided by charge balance. Another reason is the vacancy site does not play a role in NH_4^+ adsorption. The crystal structure of MHCF with less and high vacancy concentration is shown in Fig. 1-4. The purple spheres represent the alkali A^+ and A^+can exchange with the NH_4^+ in aqueous solution.

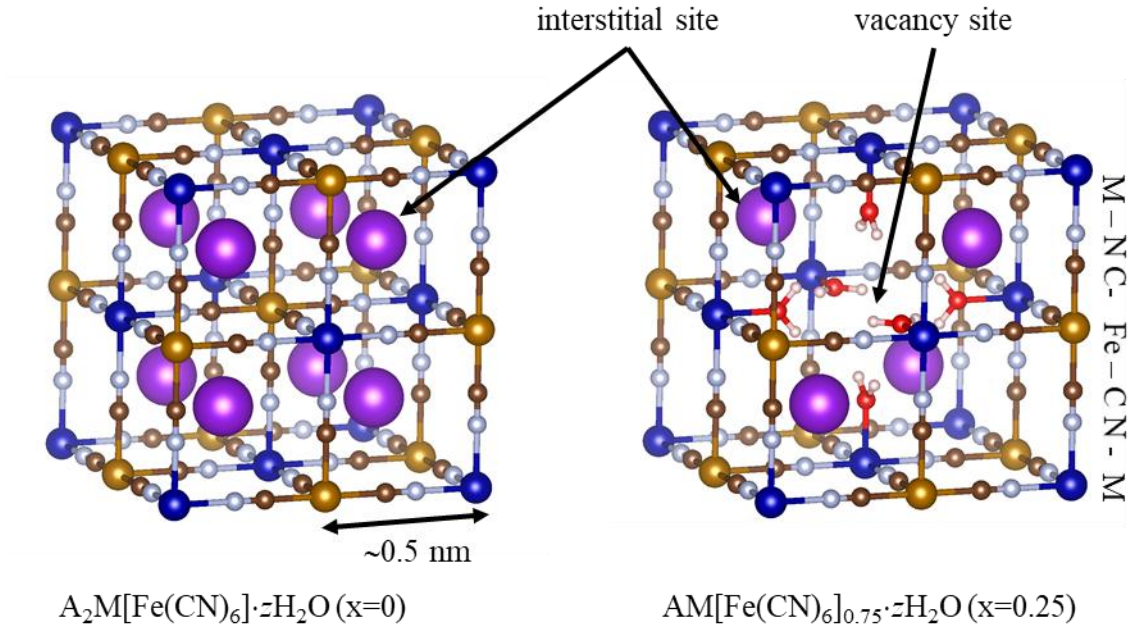

Fig. 1-4 The crystal structure of metal hexacyanoferrate (MHCF, $A_yM[Fe(CN)_6]_{1-x}\ zH_2O$) with different vacancy concentrations, *x*. Purple spheres represent A^+ cations, the ion exchange species in NH_4^+ adsorption.

Also, utilizing PBAs as an adsorbent for ammonia sorption/detection at the conditions with low and high concentrations has also aroused much attention [108, 109]. PB, CuHCF, and cobalt hexacyanocobaltate (CoHCCo) in the anhydrous form [110] have been employed on the gaseous ammonia sorption, shows 12.5, 20.2, 21.9 mmol/g of sorption capacity at RT, 0.1 MPa, especially to the sorption capacity of CuHCF and CoHCCo, showing the highest value among the recyclable porous adsorbents up to now. However, the chemical state of the adsorbed gaseous NH_3 depends on the presence of the water in the atmosphere, i.e. NH_3, which was stored as in the dehydrated case, tended to be converted into NH_4^+ in the hydrated case. Hence, developing PBAs for adsorbing stable NH_3 form by optimizing the chemical composition is necessary. Furthermore, the strategy for the developing gaseous adsorbents of PBAs was different with those PBAs employed in wastewater treatment. In the case of gaseous sorption/capture, the $[M'(CN)_6]$ vacancies play an important role in sorption performance, i.e. moderate vacancies can raise the sorption capacity. The crystal structure of Prussian blue (PB) employed in the gaseous NH_3 sorption is shown in Fig. 1-5.

1.5 Objectives of this research

To effectively remove dissolved ammonia in wastewater at RT, and sorption/capture gaseous ammonia in a wide temperature range, three sorbents, i.e. three PBAs were developed and prepared. The adsorption and desorption behaviors of these three sorbents were studied, and possible mechanisms were also discussed. The specific objectives are listed as follows:

(1) According to the requirements for adsorbents applied in wastewater, develop a new adsorbent with larger sorption capacity and high selectivity for the target adsorbate.

(2) Based on the sorbent of CoHCCo that we have developed, which showed the largest sorption capacity in ammonia gas sorption at RT compared with other traditional sorbents at the same conditions. Further study the sorption performances of CoHCCo applied in the fields of ammonia gas sorption/recovery containing humid atmosphere at high working temperature processes.

(3) Developing another metal hexacyanocobaltate with lower cost than CoHCCo, make the sorption capacity is similar with that of CoHCCo, other differences in sorption properties between the new one and CoHCCo are also expected, such as more stable NH_3 form would be kept even in the humid atmosphere.

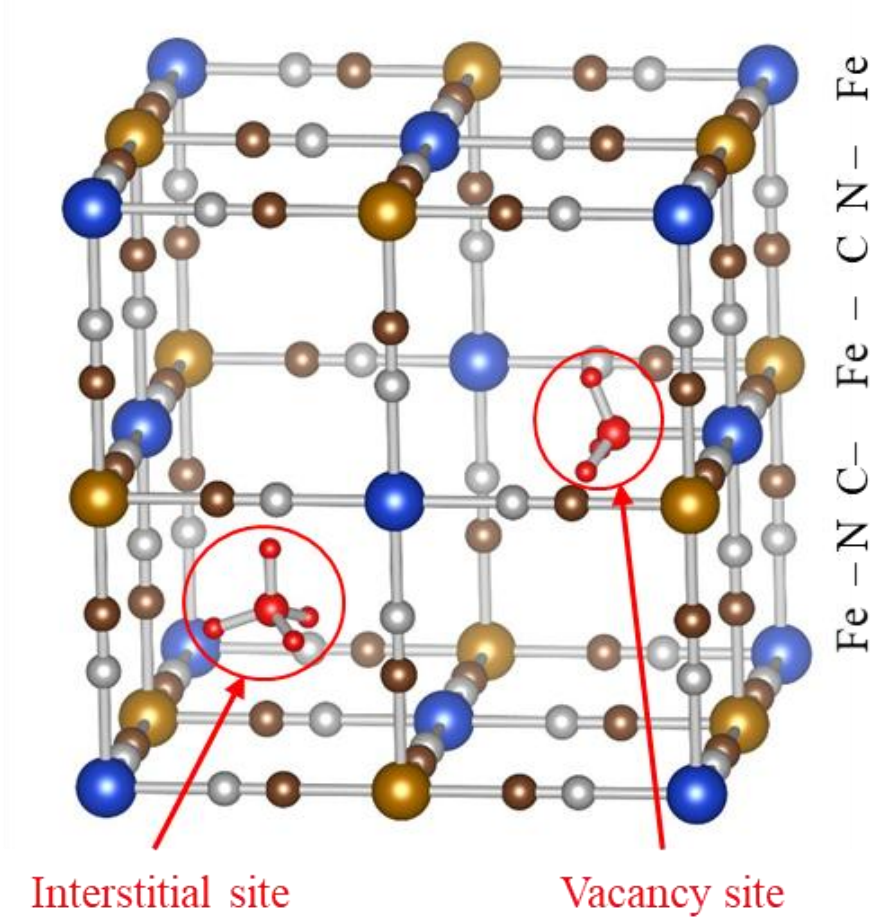

Fig. 1-5 The crystal structure of PB [110].

1.6 Originality and structure of the dissertation

A new sorbent with high sorption capacity (q_{max}, 4.28 mol/kg) and selectivity (α=96.2) for NH_4^+-N removal from aqueous solution, called sodium cobalt hexacyanoferrate (NaCoHCF) was prepared, and its potential for recycling use was also demonstrated. In the case of sorption/capture of gaseous NH_3, to my best knowledge, the CoHCCo was employed on the NH_3 sorption and desorption process under heating conditions up to 260 ℃ for the first time. Besides, to compare with CoHCCo, another new NH_3 sorbent named zinc hexacynanocobaltate (ZnHCCo) was developed. The stability during cycle use, sorption capacity, regenerability, and durability to a humid atmosphere were studied at moderate working temperature.

Based on those above, the study was divided into three parts, and the structure of the dissertation is shown in Fig. 1-6**.**

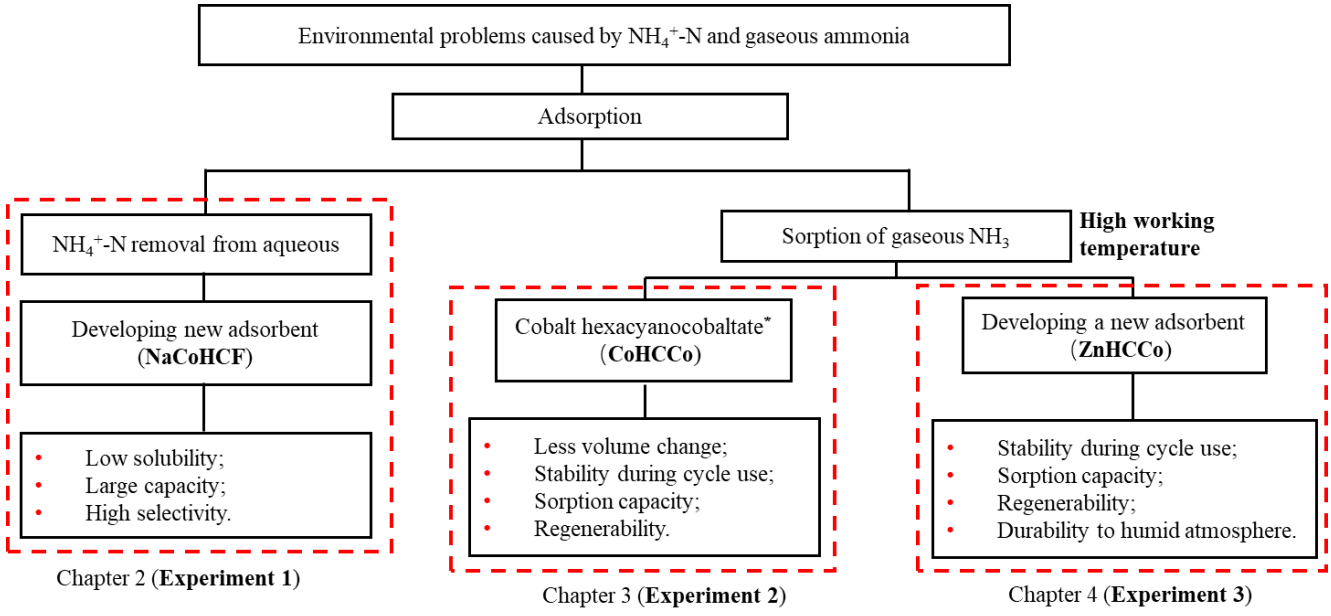

Note: "*****" indicates sorbent was developed previously, and was studied at RT.

Fig. 1-6 Structure of the dissertation

Chapter 2 Ammonium removal from water using sodium cobalt hexacyanoferrates with high capacity and selectivity

2.1 Introduction

Ammonium, NH_4^+, is a widely synthesized chemical, most of which is used as a fertilizer. This distributing ammonium is oxidized to nitrite, NO_2^-, and then further converted to nitrate, NO_3^-, in rivers, lakes, and oceans through nitrification processes. When humans and animals drink water containing ammonia ($NO_3^- \geqslant 45$ mg/L or NO_3-N $\geqslant 10$ mg/L) [2], they can become ill or even die. In aquatic systems, especially those near densely populated settlements or large-scale livestock facilities, the high concentrations of ammonia in water cause concern. Excess ammonia in aquatic systems can cause eutrophication, harmful algal blooms, and anoxic conditions in estuaries, rivers, and even the coastal environment. Consequently, biodiversity, fisheries, and overall ecosystem health are adversely affected by this N nutrient imbalance [4, 5, 111].

Various nations have set standards for ammonia in effluent or environmental water. For example, the U.S. Environmental Protection Agency (EPA) lowered the limit in 2013 for aquatic life in ambient water bodies to 17 and 1.9 mg/L total ammonia nitrogen one-hour and 30-day averages, respectively [112]. China and India have also established standards for effluents of 15–50 and 50 mg/L ammonium nitrogen [113, 114]. Reducing the ammonium concentration is also important for bio-gasification technology with anaerobic digestion because the digestion is inhibited by high concentrations of ammonium. Depending on the conditions, 1500–5000 mg/L of total ammonium nitrogen can cause the slow down or failure of digestion [115, 116]. For the removal of NH_4^+ from wastewater or digestion liquids, methods for the selective removal of NH_4^+ are necessary because various ions coexist in these solutions.

For the uptake of NH_4^+, removal with an adsorbent is an easily controllable and highly efficient method. Strong acid cation (SAC) exchange resins, analogues of Amberlite IR-120 (Alfa Aesar, UK), show the highest adsorption capacity, reaching 5.34 mol kg^{-1} for an aqueous solution without coexisting cations and using glass-packed bed columns [117]. Nevertheless, SAC resins have low selectivity to NH_4^+ when other competing ions are present. He et al. studied alkaline-activated and lanthanum-impregnated zeolites [33] and found a maximum adsorption capacity, q_{max}, of 1.54 mol kg^{-1} in a pure water solution. However, the removal efficiency, P_R, decreased from 90%

to 36% in the presence of Na^+. Soetardji et al. reported that sodium-hydroxide-modified zeolite mordenite has q_{max} = 3.0 mol kg^{-1} in aqueous solution and that P_R decreased from 81% to 66.9% when competing with other ions [68]. Guaya et al. studied a hydrated aluminum-oxide-modified zeolite [118], which showed q_{max} = 2.14 mol kg^{-1} in aqueous solution and P_R = 12% with coexisting Na^+ ions.

In an earlier study, potassium copper hexacyanoferrate, KCuHCF, has a high ammonium adsorption capacity of 1.94 mol kg^{-1} was found, as well as high selectivity for dissolved ammonia [107]. The KCuHCF, one metal hexacyanoferrate (MHCF), is a Prussian blue analogue. MHCFs have the chemical composition of $A_yM[Fe(CN)_6]_{1-x}$ zH_2O, where A and M, respectively, denote alkali and transition metals, and x indicates the concentration of $[Fe(CN)_6]$ vacancies. With respect to MHCFs, many researchers have studied their use in catalysis [119–121], electrodes in secondary batteries [122–125], electrochromism [126–130], sensors [29],[132] gas storage [110, 133, 134], photomagnets [135–137], and adsorbents for radioactive Cs^+ ions [138–142]. The ionic radii of hydrated Cs and NH_4 are similar (3.29 and 3.31 Å, respectively). Therefore, assuming a size-based adsorption model, MHCFs could also have substantial adsorption capability for NH_4^+ [143].

Based on these considerations, in this paper, another MHCF, sodium cobalt hexacyanoferrate (NaCoHCF) was investigated, to enhance the adsorption capacity. The most important difference between KCuHCF and NaCoHCF is the difference between Cu and Co (see Fig. 2-1). In the case of KCuHCF, KCuHCF with fewer $[Fe(CN)_6]^{4-}$ vacancies causes material instability in the aqueous solution [144]. However, with substitution with Co, the introduction of a small number of $[Fe(CN)_6]^{4-}$ vacancies becomes possible. Additionally, the affinity of MHCF for the mono-cation is known to depend on the hydrated radius, implying that utilization of Na^+ instead of K^+ can increase the NH_4^+ adsorption performance.

There are two parts in this study. The first is a composition-dependent study. Five kinds of NaCoHCF-nanoparticles (NaCoHCF-NPs) $Na_yCo[Fe(CN)_6]_x$ zH_2O, were synthesized by changing the molar concentration ratio of the reagent solution (R_{mix}) using a batch method. The second part is a detailed study of R_{mix} = 1.00. Quantitative analysis into the adsorption capacity and selectivity was conducted. The changes to the crystal structure are also discussed. By comparison with earlier studies, our NaCoHCF exhibits a very high capacity was found when using the batch-adsorption method. Particularly for NH_4^+ adsorption from saline solutions, the benefits of NaCoHCF are enhanced by its high selectivity. Finally, we demonstrate its potential for recyclability.

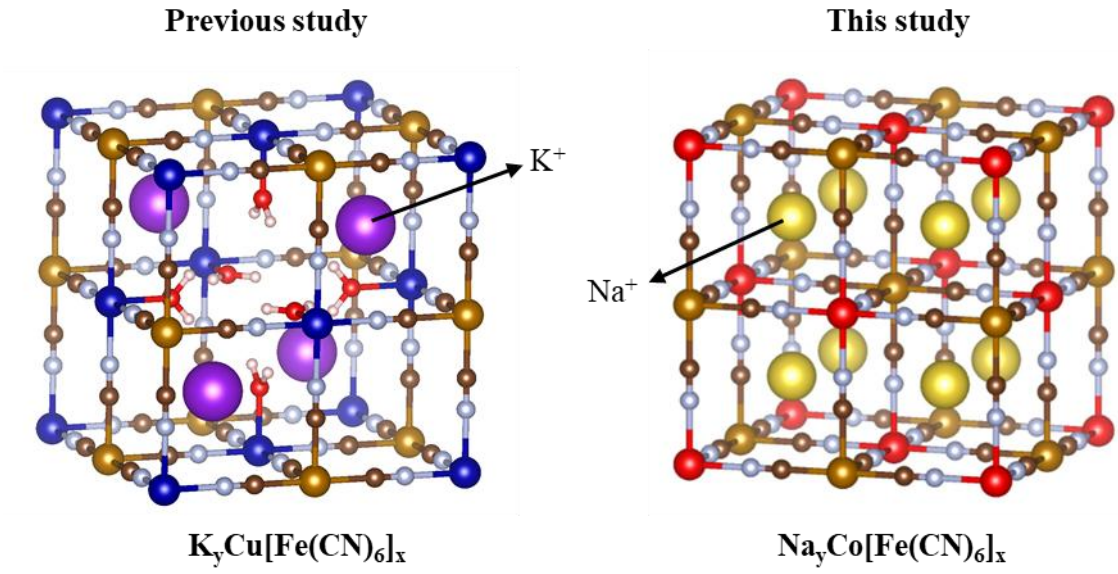

Fig. 2-1 The crystal structure of metal hexacyanoferrate (MHCF, $A_yM[Fe(CN)_6]_x$) with different vacancy concentrations, *x*. Purple and yellow spheres represent A^+ cations, the ion exchange species in NH_4^+ adsorption.

2.2 Experimental section

2.2.1 Synthesis of NaCoHCF-NPs

First, NaCoHCF-NPs with compositions of $Na_{4x-2}Co[Fe(CN)_6]_x$ (water omitted) were prepared according to the following chemical reaction.

$$Co(NO_3)_2 + xNa_4[Fe(CN)_6] \rightarrow Na_{4x-2}Co[Fe(CN)_6]_x + 2NaNO_3 \qquad (2\text{-}1)$$

To study the composition dependence, the NaCoHCF-NPs were synthesized using a batch method by mixing two aqueous solutions of $Na_4[Fe(CN)_6] \cdot 10H_2O$ (Wako Pure Chemical Ind., Ltd.) and $CoCl_2\ 6H_2O$ (special grade from Wako Pure Chemical Ind., Ltd.) with different molar concentration ratios (R_{mix} = 0.50, 0.75, 1.00, 1.50, and 2.00). Here, R_{mix} represents the mixing ratio of the concentration of $[Fe(CN)_6]^{4-}$ to that of Co^{2+}. The suspension was shaken using a multi shaker (SI-300C; AS One Corp.) for 3 min at 1700 rpm and room temperature. After shaking, the slurry solutions were centrifuged. The slurries were washed at least five times with Milli-Q water. They were dried under vacuum at 60 ℃ for 48 h.

For detailed studies conducted with a fixed composition, we prepared NaCoHCF-NP samples using a flow synthesis method to guarantee the homogeneity of the particle size and chemical composition [138]. The NaCoHCF-NPs, denoted Flow-1.00, was synthesized by mixing 0.4 mol/L solutions of the $Na_4[Fe(CN)_6] \cdot 10H_2O$ and $Co(NO_3)_2\ 6H_2O$ (special grade from Wako Pure Chemical Ind., Ltd.) in a Y-type micro-mixer with a hole of Φ250 μm, as shown schematically in Fig. 2-2. The mixed concentrations were the same as those for Batch-1.00. The flow rates of the two solutions were set to be equal. The total flow rate was 40 mL/min. The obtained slurries were washed using a hollow fiber rinse system (DBW-24; OCT Science Co., Ltd.) to remove the $NaNO_3$ byproduct. Then, the NaCoHCF-NPs were dried in vacuum at 60 ℃ for 72 h.

2.2.2 Characterization of NaCoHCF-NPs

The crystal structures of Flow-1.00 were studied before and after NH_4^+ adsorption using an X-ray diffractometer (D2 Phaser; Bruker Analytik GmbH, Germany) with Cu Kα (λ = 1.54 Å) radiation in the 2θ range of 5–60 ° at 30 kV and 10 mA. A Si (311) double-crystal monochromator was used to monochromatize the incident beam while reducing the high harmonics of the monochromatic beam. The XRD patterns were analyzed using the Pawley method to determine the space group and the lattice constants. For adsorption, a 500 mg/L NH_4^+ aqueous solution was used.

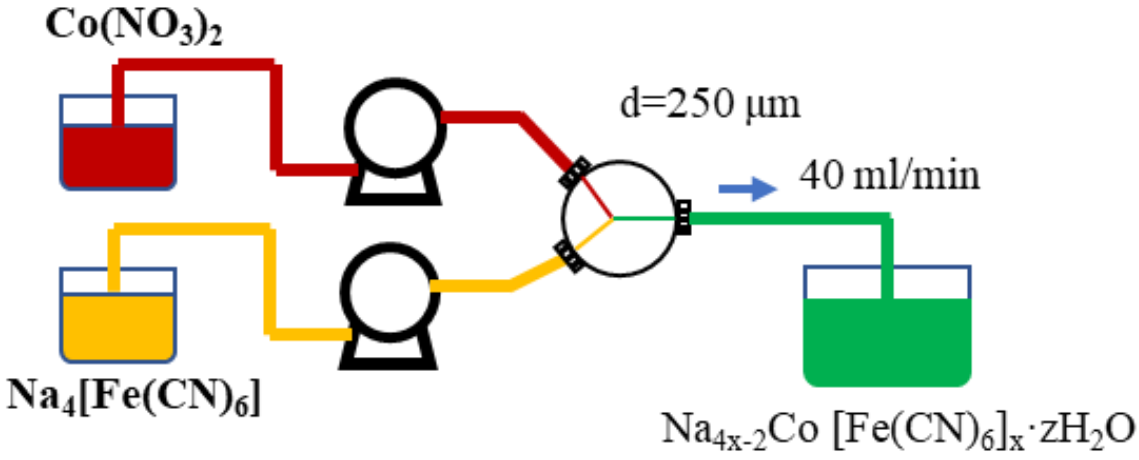

Fig. 2-2 Schematic view of the synthesis of NaCoHCF by a micromixer.

Other conditions are described in Section 2.3. The crystallite sizes were estimated using Scherrer analysis of the XRD patterns, assuming a Scherrer constant of 0.94 [145]. Sample images were obtained using a field-emission scanning electron microscope (FE-SEM, S-4800; Hitachi Hitec Corp.) with 5-kV accelerating voltage after Pt–Pd coating using an ion sputter coater (E-1030; Hitachi Ltd., Japan). The chemical compositions were determined using a Microwave Plasma-Atomic Emission Spectrometer (MP-AES, 4100; Agilent Technologies Inc., USA) with pre-decomposition using microwaves (MW, Multiwave 3000; PerkinElmer Inc., USA). The hydration numbers in each sample were ascertained through thermogravimetric analysis (Thermo Plus EVO2; Rigaku Corp.). The specific surface areas of Flow-1.00 was estimated by fitting the Brunauer, Emmett, and Teller (BET) equation to the N_2 adsorption isotherms obtained at 77 K. The pre-treatment condition was 100 °C for 24 h.

2.2.3 NH_4^+ adsorption test

To evaluate the composition dependence, a batch-shaking method was used to evaluate the NH_4^+ adsorption capacity of the NaCoHCF-NPs. The method was conducted as follows: 40 mg of an NaCoHCF sample (Batch-0.50, 0.75, 1.00, 1.50, and 2.00) was added to a 40 mL aqueous solution of NH_4Cl with a NH_4^+ concentration of 90 mg/L. The suspension was shaken using a multi shaker (SI-300C; AS One Corp.) at 600 rpm for 180 min at 30 ℃. After shaking, the supernatant was obtained via centrifuging and further separation using a 0.45-μm filter (MCE syringe filter; Membrane Solutions). The NH_4^+ concentration in the supernatant was evaluated using ion chromatography (IC, 883 Basic IC plus; Metrohm AG).

For a detailed study using a fixed composition, the conditions were the same except that the NH_4^+ concentration was changed to 1–1000 mg/L in the NH_4Cl aqueous solution and saline solution. The saline solution was prepared with 9350 mg/L of Na^+ ions (NaCl, special grade from Wako Pure Chemical Ind., Ltd.), where the Na^+ concentration was set to match that of Daigo's artificial seawater SP (Wako Pure Chemical Ind., Ltd.), 9348 mg/L.

For comparison, the NH_4^+ adsorption properties of synthetic zeolite (A-3, powder, through 75 μm, Wako Pure Chemical Industries Ltd.), sepiolite (Omi Mining Co., Ltd., Japan), and Amberlite IR-120 (H) (Alfa Aesar, UK) were also investigated. All samples were produced with no

pretreatment, such as drying, before the adsorption testing. The NH_4^+ concentrations in the aqueous NH_4Cl and in the saline solution were both set to 500 mg/L. To remove the effects of Na^+ from the NH_4^+ measurements, all saline solutions were diluted and distilled to trap only NH_4^+ ions before measurement by IC. When the concentration of NH_4^+ was higher than 150 mg/L after distillation, the solutions were diluted five times for IC measurement. Other solutions were measured directly by IC.

2.2.4 Evaluation of recyclability

The potential for recyclability was also investigated. The experimental setup is shown in Fig. 2-3. A membrane filter with NaCoHCF-NPs was prepared for the flow test. The Flow-1.00 powder was mixed with 2 mL Milli-Q (3.76 mg/mL) using an ultrasonic cleaner (W-113MK-II; Honda). Then, 100-μL solutions were dropped on the membrane filter (Φ25 mm, 0.45 μm pore size, JHWP01300; Merck), followed by drying at 60 ℃ for 2 min. Thus prepared, the solutions were set on a circular plastic plate of Φ25 mm with a hole of Φ5 mm in the middle. They were pasted on the film for effective adsorption–desorption. An FT-IR spectrometer (iD1 transmission iS5; Nicolet Biomedical Inc.) was used to confirm adsorption and desorption of NH_4^+. For the adsorption test, the NH_4^+ solution of 500 mg/L was flowed through the NaCoHCF-NP-dipped membrane for 30 min at the rate of 0.2 mL/min. For the desorption test, a NaCl solution of 5 mol/L was similarly flowed for 2 h at a rate of 1 mL/min.

2.3 Results and discussion

2.3.1 Composition dependence

The dependence of the chemical composition on the mixing ratio, R_{mix}, is presented in Table 2-1. For $R_{mix}<1.00$, x is an almost equal to R_{mix}. The value of y, the number of Na^+ ions in NaCoHCF, also increased. In contrast, when $R_{mix}>1.00$, the chemical composition was almost unchanged, demonstrating that the composition can be controlled by changing the reaction R_{mix} to $x < 1$.

The crystal structure of NaCoHCF depends on the chemical composition (see Fig. 2-4). When $R_{mix} \geq 1.00$, the crystal structure is rhombohedral ($R\bar{3}$), as reported [146, 147]. On the other hand, the structure for $R_{mix} = 0.50$ is unclear. Earlier reports described the space group as monoclinic ($P2/m$ or $P2_1/m$) [148] or cubic ($Pm\bar{3}m$) [149, 150]. In our case, the XRD pattern is explained as

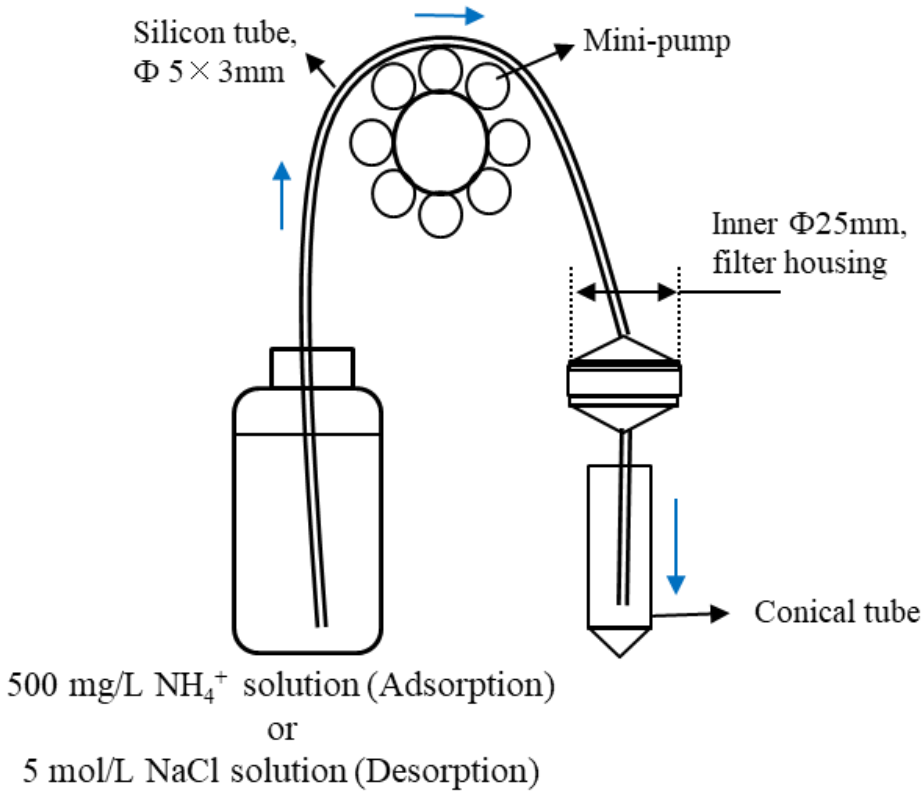

Fig. 2-3 Schematic view of the experimental setup for the investigation of the recyclability.

Table 2-1 The mixing ratio, R_{mix}, in synthesis and the chemical compositions and crystal structure of the NaCoHCF-NP samples.

Samples	R_{mix}	x	y	z	Chemical compositions	space group	a (Å)	b (Å)	c (Å)
Batch-0.50	0.50	0.57	0.49	3.64	$Na_{0.49}Co_{1.00}[Fe(CN)_6]_{0.57}$ $3.64H_2O$	$P2_1/m$	11.83	9.52	7.47
						$R\bar{3}c$	12.77	12.77	29.06
Batch-0.67	0.67	0.63	0.74	3.41	$Na_{0.74}Co_{1.00}[Fe(CN)_6]_{0.63}$ $3.41H_2O$	$P2_1/m$	11.66	9.27	7.28
						$R\bar{3}c$	12.97	12.97	25.77
Batch-1.00	1.00	0.87	1.65	2.84	$Na_{1.65}Co_{1.00}[Fe(CN)_6]_{0.87}$ $2.84H_2O$	$R\bar{3}c$	7.43	7.43	17.46
Batch-1.33	1.33	0.90	1.71	3.00	$Na_{1.71}Co_{1.00}[Fe(CN)_6]_{0.90}$ $3.00H_2O$	$R\bar{3}c$	7.45	7.45	17.45
Batch-2.00	2.00	0.90	1.75	3.36	$Na_{1.75}Co_{1.00}[Fe(CN)_6]_{0.90}$ $3.36H_2O$	$R\bar{3}c$	7.43	7.43	17.46
Flow-1.00	1.00	0.82	1.46	3.79	$Na_{1.46}Co_{1.00}[Fe(CN)_6]_{0.82}$ $3.79H_2O$	$R\bar{3}c$	7.39	7.39	17.55
Flow-1.00 after ads.	1.00					$Fm\bar{3}m$	10.16	10.16	10.16

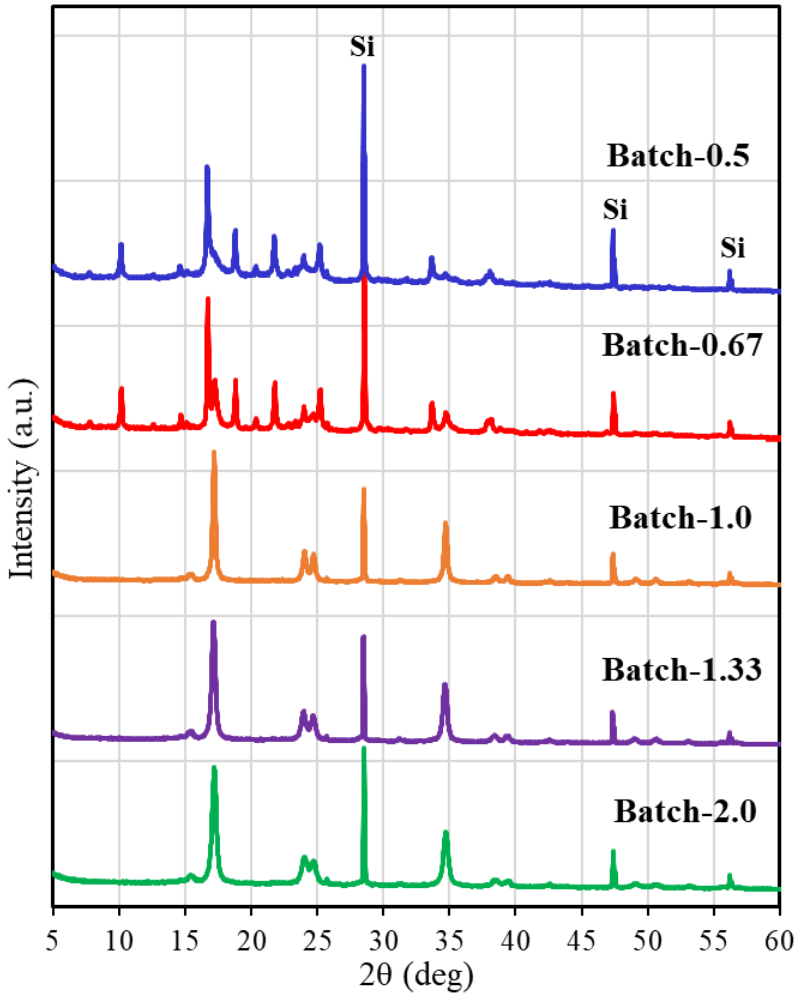

Fig. 2-4 XRD patterns for batch samples. “Si” represents the peak corresponding to the Si powder mixed to the sample for the angle standard.

a mixture of $R\bar{3}c$ and $P2_1/m$ structures, as shown in Table 2-1. The NaCoHCF with R_{mix} = 0.67 is also explainable as a mixture. Such a mixture could be the result of the batch synthesis because homogeneous synthesis is difficult using the batch method, resulting in the fluctuation of the chemical composition.

Fig. 2-5(a) shows that the NH_4^+ adsorption capacity improved with increasing R_{mix}. The amount of adsorbed ammonia of Batch-2.00 is about twice that of Batch-0.5. Fig. 2-5(b) shows that the amount of Na^+ from the adsorbent has an almost linear correlation with the NH_4^+ adsorption amount, indicating the NH_4^+ adsorption occurred through ion exchange with Na^+. These results demonstrate that the increase in the Na^+ composition in NaCoHCF enhances the NH_4^+ adsorption capacity, and that NaCoHCF retains its structure even after long-term shaking in water. However, for R_{mix} > 1.00, the adsorption capacity increased by only 2.9–3.9% from R_{mix} = 1.00 because the upper limit of x is 1.0.

2.3.2 Detailed study with flow-synthesized NaCoHCF with R_{mix}=1.00

Based on results of the composition dependence of the NH_4^+ capacity, we chose to conduct a detailed study of NaCoHCF-NPs with R_{mix} = 1.00 because we obtained the desired chemical composition by using this value of R_{mix} and because it showed sufficiently high capacity. For our detailed study, we used the flow-synthesized sample, Flow-1.00, to avoid the fluctuation of the chemical composition and particle size. Table 2-1 shows that the chemical composition of Flow-1.00 is almost identical to that of Batch-1.00. The adsorption kinetics was studied at an initial NH_4^+ concentration of 500 mg/L, 30 ℃, and at 600 rpm for 8 h (see Fig. 2-6). The results showed that the NH_4^+ adsorption was almost completed in 30 min. Such fast adsorption is similar to the case of KCuHCF [107].

Using BET analysis, we estimated the surface area to be 53 m^2/g, which is also comparable to that of Batch-1.00, 46 m^2/g. The N_2 isotherms are shown in Fig. 2-7. Both values are not very high because the interstitial sites of NaCoHCF are filled with Na^+, preventing the penetration of Na^+ into the porous network in the crystal. The average pore size was estimated to 31 nm for Flow-1.00, consistent with the size of the crystallites, as shown later.

After NH_4^+ adsorption, the crystal structure was maintained, except for a slight trigonal distortion. Fig. 2-8 shows the XRD patterns obtained before and after NH_4^+ adsorption. Some

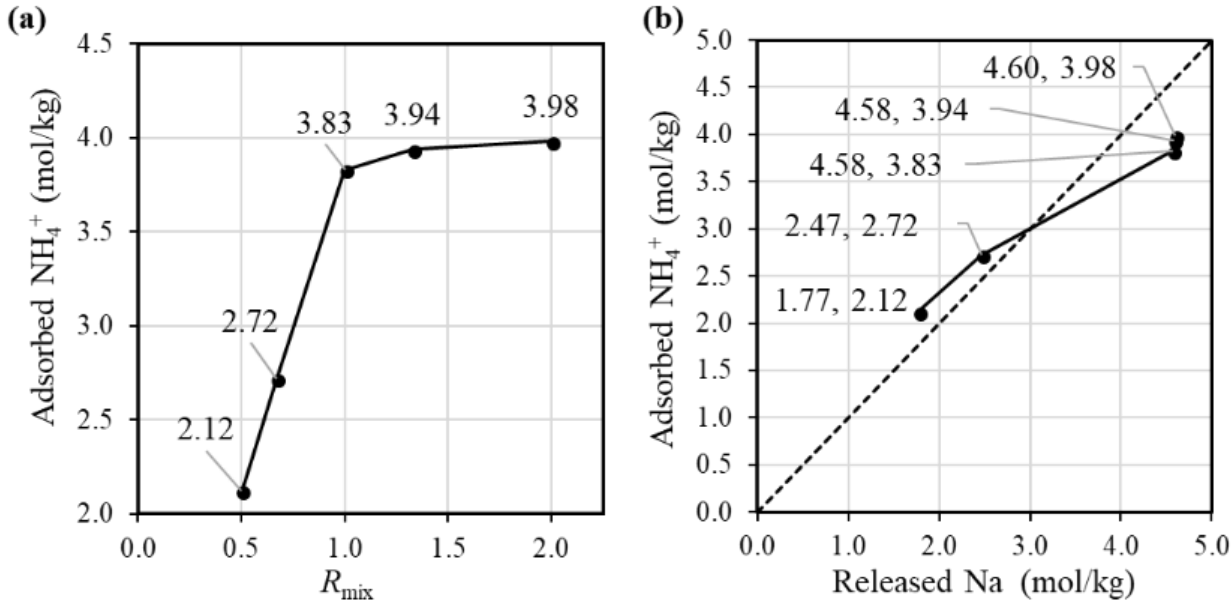

Fig. 2-5 (a) Amount of adsorbed NH_4^+ by the batch-synthesized NaCoHCF with different compositions. (b) The relationship between adsorbed NH_4^+ and released Na^+. The adsorption experiment was conducted at initial NH_4^+ of 90 mg/L, 30 ℃, and at 600 rpm for 3 h.

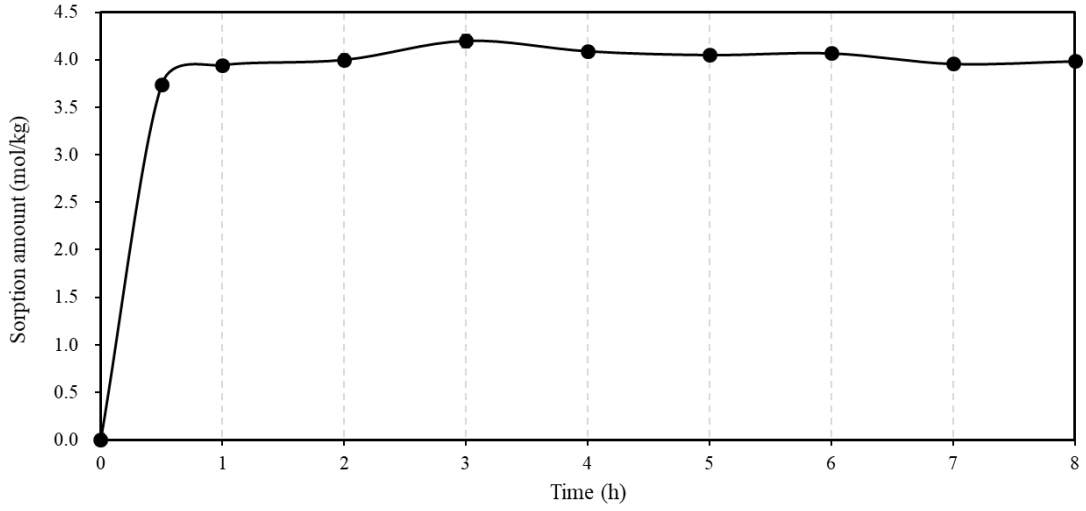

Fig. 2-6 Adsorption kinetics of ammonia onto Flow-1.00 at 30 ℃. Initial NH_4^+ = 500 mg/L, temperature = 30 ℃, solid/liquid =1:1000, 600 rpm. Dilution ×500. The standard deviation is so small that it lies within the mark.

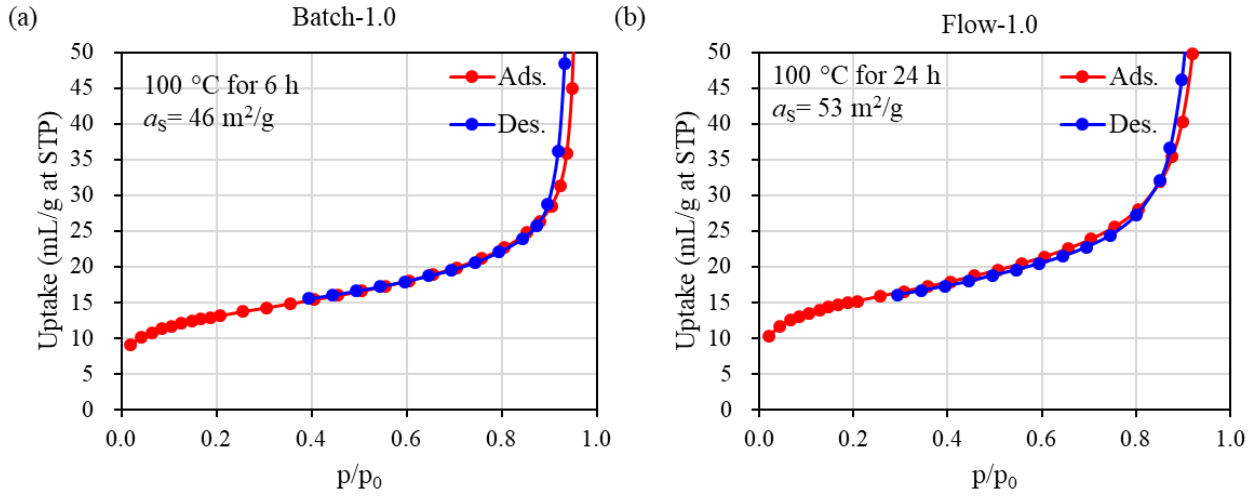

Fig. 2-7 N_2 isotherm of NaCoHCF at 77 K.

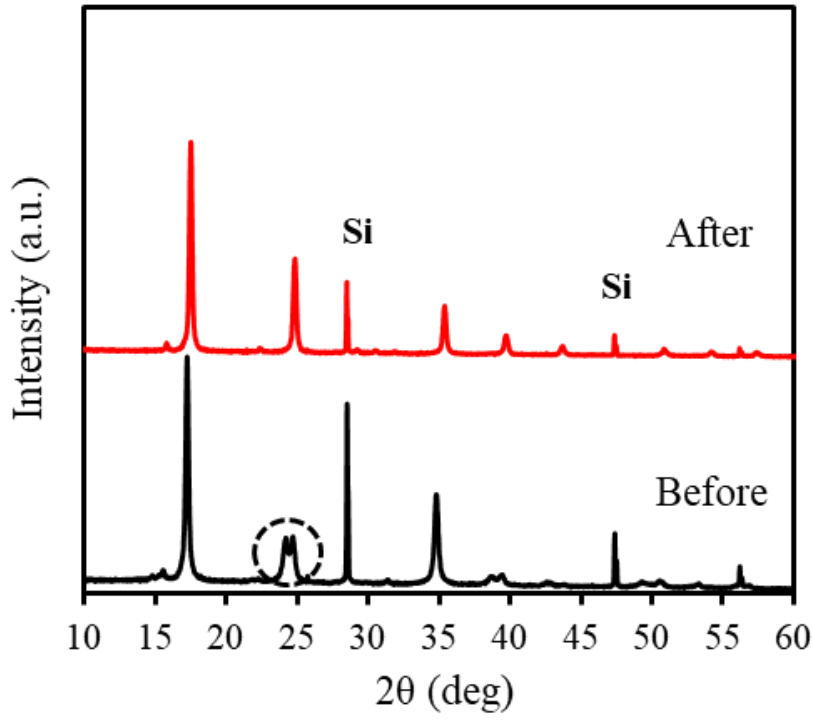

Fig. 2-8 XRD patterns of Flow-1.00 before and after adsorption with an aqueous NH_4Cl solution containing 500 mg/L of NH_4^+.

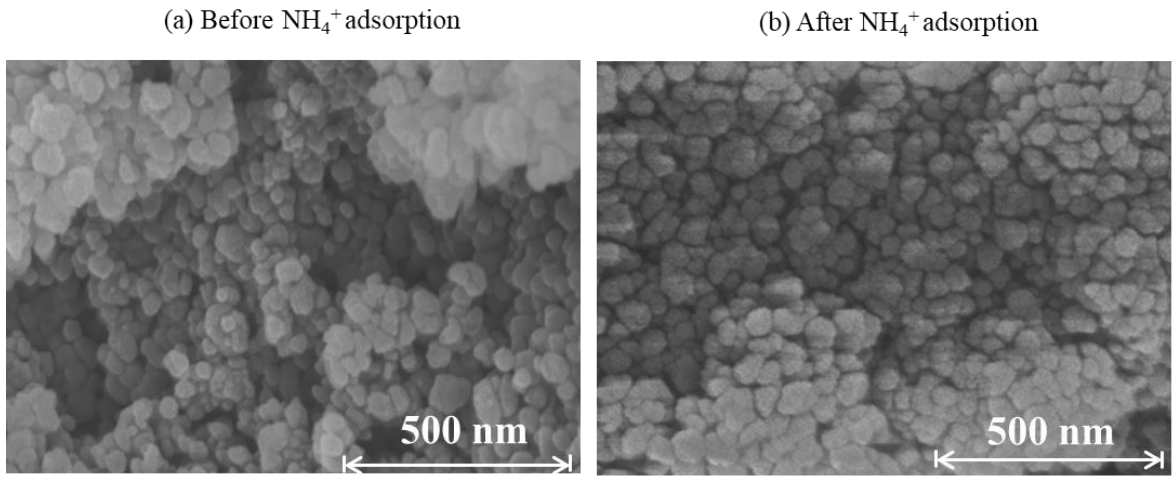

Fig. 2-9 SEM images of Flow-1.00 (a) before and (b) after adsorption of 500 mg/L NH_4^+ in pure water solution.

splitting of the Bragg peaks is apparent. The slight structural transformation observed is the same as that in the case of ion exchange between Na^+ and K^+ [147]. Before adsorption, NaCoHCF had a rhombohedral ($R\bar{3}c$) structure. However, after NH_4^+ adsorption, it changed to a cubic lattice ($Fm\bar{3}m$; Z = 4). Thus, the ion exchange reversibly changed the structure.

No nanoparticle degradation occurred during adsorption. The crystallite sizes estimated by Scherrer analysis of the XRD patterns (Fig. 2-8) before and after sorption were, respectively, 37.9 and 51.7 nm. This result is consistent with the SEM images in Fig. 2-9. The particle sizes estimated using SEM images were 33 ± 10 and 47 ± 13 nm. The data indicate no degradation, but there is a possibility of some particle growth. The reason for the growth remains unclear, but it could be due to the immobilization of the Co^{2+} and $[Fe(CN)_6]^{4-}$ ions eluted from the adsorbent onto the adsorbent. If so, the adsorbent would retain the eluted species. The surface morphology in SEM images shows no marked change after adsorption.

Fig. 2-10 shows the NH_4^+ adsorption isotherms in aqueous NH_4Cl solution and that in aqueous saline solution. In the saline solution, the concentration of the Na^+ solution was set to 9350 mg/L, the same as that of artificial seawater. The curves fit to the Langmuir, Freundlich, and Markham-Benton equations are also shown in Fig. 2-10. The fitting parameters for each equation are shown in Table 2-2.

The Langmuir equation is given by

$$\frac{C_\mathrm{e}}{q_\mathrm{e}} = \frac{1}{q_{max}} C_\mathrm{e} + \frac{1}{K q_\mathrm{max}}, \qquad (2\text{-}2)$$

where C_e, q_e, q_max, and K respectively represent the NH_4^+ concentration in solution at equilibrium, loaded NH_4^+ in the adsorbent, maximum adsorption capacity, and the equilibrium constant. The same data are also shown with other axes in Fig. 2-11, and the adsorption behavior fits the Langmuir equation well. We also carried out fitting to the Freundlich equation,

$$q_\mathrm{e} = K_\mathrm{f} \mathrm{C}^{1/n}. \qquad (2\text{-}3)$$

For the Freundlich equation, only the region where the loaded NH_4^+ concentration was less than 1.95 mol/kg, about a half the maximum capacity, was considered because the Freundlich equation is only suitable far from saturated loading. However, in this region, the Freundlich equation also well reproduced the experimental data.

For a more quantitative evaluation of the effect of the coexistent Na^+ ions, we also considered the Markham–Benton model for a solution with multi-alkali cations. As a type of extended

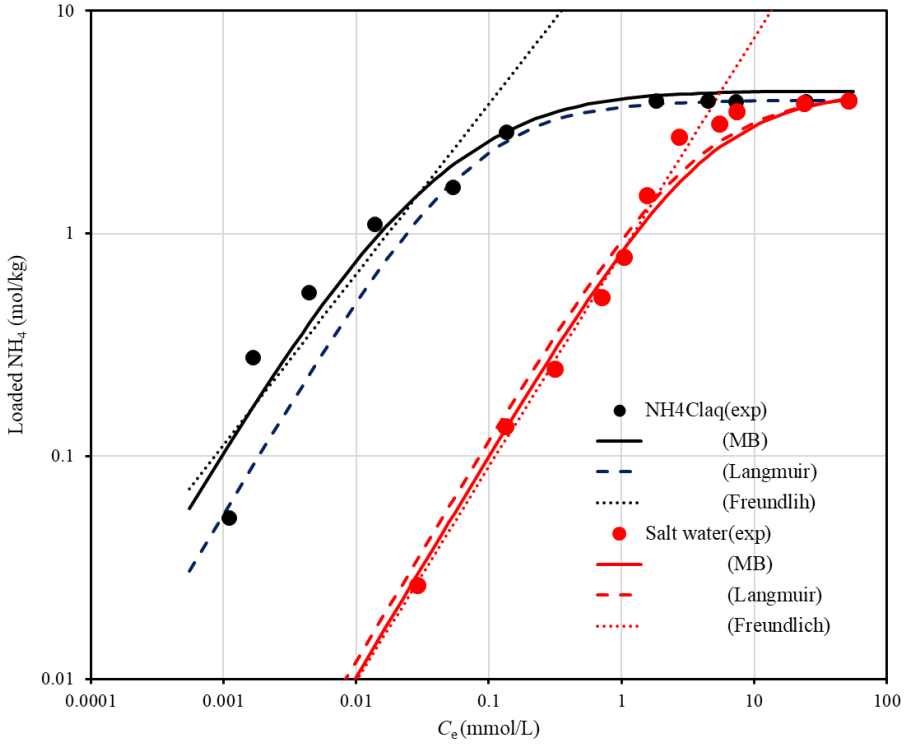

Fig. 2-10 Adsorption behaviour of NH_4^+ by the flow-synthesized NaCoHCF with R_{mix} = 1.00 with curves fit the Markham–Benton (solid lines), Langmuir (broken line), and Freundlich (dotted line) equations. The experimental points are represented by closed circles. Black and red symbols represent an NH_4Cl aqueous solution and salt water, respectively.

Table 2-2 The fitting parameters with the Langmuir, Freundlich, and the Markham–Benton equations for the NH_4^+ adsorption using the flow-synthesized NaCoHCF with R_{mix} = 1.00.

Langmuir				Freundlich				Markham–Benton		
NH_4Cl_{aq}		Salt water		NH_4Cl_{aq}		Salt water		NH_4Cl_{aq} & Salt water		
K	q_{max}	K	q_{max}	K_f	1/n	K_f	1/n	q_{max}	K	K’
(L/mol)	(mol/kg)	(L/mol)	(mol/kg)	(mol/kg)		(mol/kg)		(mol/kg)	(L/mol)	(L/mol)
13.99	3.97	0.28	4.28	22.27	0.77	0.82	0.96	4.36	24.84	0.26

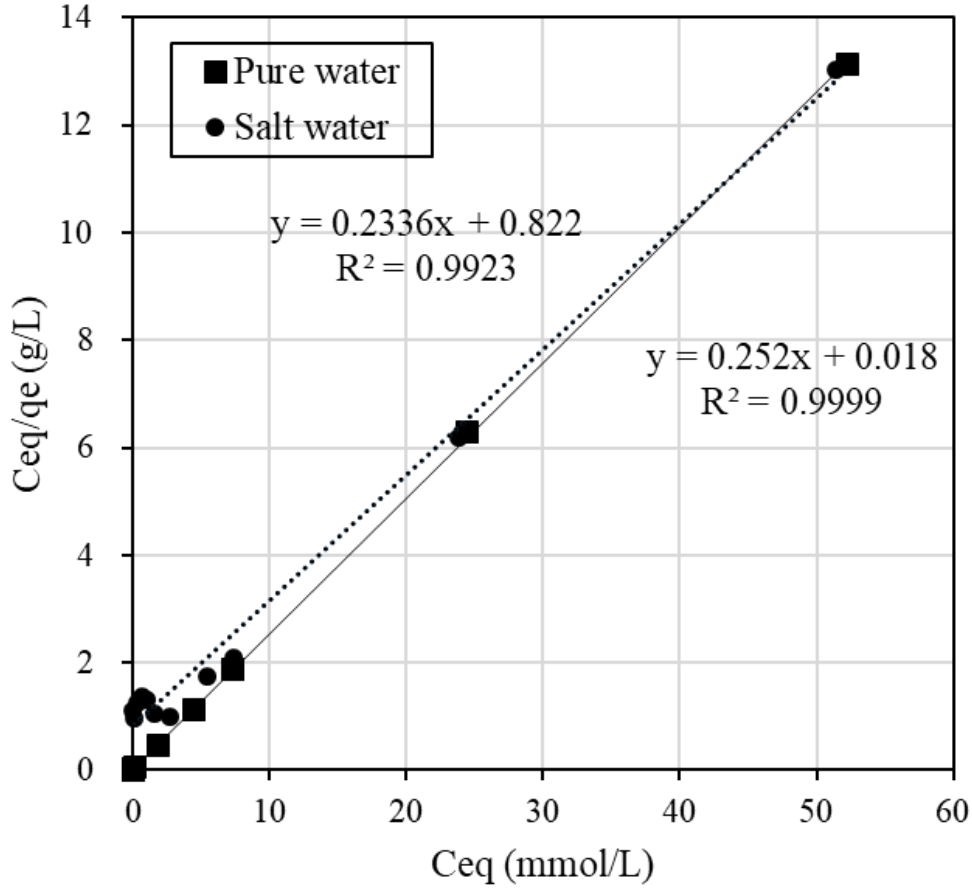

Fig. 2-11 Adsorption behaviour of NH_4^+ by flow-synthesized NaCoHCF at R_{mix}=1.00 in NH_4Cl aqueous solution and salty aqueous solution with the fitting curves by Langmuir liner model. The adsorption test was done under mixing for 3 hours with 600rpm at 30°C. The adsorbent was added to the solution at the concentration of 1-1,000 mg/L.

Langmuir equation, the Markham–Benton equation [151] was used to examine adsorption isotherms for multiple components to estimate the ease of desorption of the adsorbents. The results also provide some understanding of the selectivity of the sorbents for some ions. The Markham–Benton equation is

$$q_e = \frac{q_{max} K C_e}{1 + K C_e + K' C'_e}, \qquad (2\text{-}4)$$

where C_e, q_e, and K respectively represent the NH_4^+ ion concentration in equilibrium, the adsorption capacity, and the equilibrium constant. C'_e and K' respectively denote the Na^+ ion concentration in equilibrium and the equilibrium constant.

Considering the Na^+-ion exchange for NH_4^+ ions, i.e., even in NH_4Cl aqueous solution, an equal amount of Na^+ ions would be exchanged out, adversely affecting the adsorption capacity. When we consider both sources of Na^+ ions (those in NaCoHCF and that in the solution), the equation can be expressed by as

$$q_e = \frac{-(1 + K C_e + K' C'_0) + \sqrt{(1 + K C_e + K' C'_0)^2 + 4 K' \frac{m}{V} q_{max} K C_e}}{2 K' \frac{m}{V}}, \qquad (2\text{-}5)$$

where C'_0, m, and V respectively denote the initial Na^+ ion concentration in solutions, adsorbent mass, and solution volume.

The fitting parameters, q_{max}, K, and K', are shown in Table 2-2. Fig. 2-10 shows that the experimental data were well fitted using the Markham–Benton model. Again, with the Markham-Benton model, we use the same parameter set for $NH_4Cl_{(aq)}$ and the saline solutions. A selectivity factor, α, defined by the ratio of equilibrium constants for NH_4^+ to that for Na^+ was calculated to be $\alpha = 96.2$, indicating the high selectivity of NH_4^+ against Na^+.

Such high selectivity is expected to lead to extremely high capacity, even in an aqueous saline solution. To clarify the high capacity of NaCoHCF among the various adsorbents, we used two approaches. First, we surveyed and compared results with those of earlier studies, and we also conducted experimental investigations to assess the adsorption capacity of adsorbents in identical conditions. For the literature survey, we picked reports of adsorption tests carried out using a batch style because column-style tests generally report higher capacities, rendering a comparison of results difficult between batch-style tests and column tests.

Information from earlier studies is presented in Table 2-3 for the adsorption capacity of adsorbents for NH_4^+ from aqueous solution in batch style, indicating that the NaCoHCF (Flow-1.00)

capacity exceeds that of all earlier reports. However, as described above, SAC resins have been reported to have high capacities, although these values were achieved using the column method without coexistent cations. For comparison under the same conditions, we evaluated the respective adsorption capacities of a synthetic zeolite, Amberlite IR-120(H) as a representative SAC, sepiolite, and NaCoHCF (Flow-1.00). Even in the NH_4Cl aqueous solution (500 mg/L-NH_4), NaCoHCF exhibited the highest capacity, whereas Amberlite adsorbed only 1.29 mol kg^{-1}. This result is due to the difference between column and batch tests. In principle, in batch tests, a higher selectivity is required than in column tests because the cations are exchanged into the solution on the adsorption of NH_4^+ and remain in the system. The benefits of NaCoHCF were amplified in the case of aqueous saline solution with 9350 mg/L-Na and 500 mg/L-NH_4. Fig. 2-12 shows that NaCoHCF has an adsorption capacity that is almost identical to that of the case without Na^+, whereas the other adsorbents showed little adsorption.

Although our main aim, the preparation of an NH_4-adsorbent with high capacity and high selectivity, has been achieved, the recyclability of the adsorbent is also important for practical use. Therefore, finally, we demonstrate the potential for recyclability by attempting desorption tests. Fig. 2-13 shows that the adsorption–desorption–adsorption process was confirmed by measuring the infrared absorption corresponding to NH_4-vibration mode at around 1415 cm^{-1} [107]. Using the continuous flow of NaCl solution for desorption, the peak height was found to decrease to 28% the original value before flow, indicating the potential for NaCoHCF recyclability. Because perfect desorption was not achieved, the optimization of the desorption process is necessary to confirm recyclability.

2.4 Summary

$Na_yCo[Fe(CN)_6]_x \cdot zH_2O$ (NaCoHCF) were synthesized using a batch method with variation of the chemical composition. Synthesis was also done using a flow method with fixed composition. The adsorption capacity increased by decreasing $[Fe(CN)_6]$ vacancies with material stability in water. Such stability is a point that differs from copper hexacyanoferrate (KCuHCF). The NH_4^+ adsorption performance was compared with other high-capacity adsorbents in the same conditions: zeolites, ion exchange resin, and sepiolite. Results show that NaCoHCF exhibited the highest capacity in NH_4Cl aqueous solution. Using salty aqueous water with Na^+ concentration of 9,350 mg/L, the NaCoHCF benefits are enhanced drastically. The Markham–Benton model showed high

selectivity for NH_4^+ against co-existing Na^+. Finally, ammonium desorption from the adsorbent was demonstrated using NaCl aqueous solution.

Table 2-3 NH_4^+ adsorption capacities of adsorbents in aqueous solutions evaluated in batch experiments reported in the literature.

Adsorbent	Maximum capacity (mol kg^{-1})	Model	Ref.
Alkaline activated and lanthanum-impregnated zeolite	1.54	Langmuir	[33]
Sodium hydroxide modified zeolite mordenite	3.0		[68]
Natural zeolite	2.36		[118]
Modified natural zeolite	2.14		[118]
Dowex 50w-x8	2.64		[152]
Sepiolite	3.70		[153]
Carbon nanotubes	0.95		[154]
Poly ligand exchanger resin	2.51		[155]
Cation exchange resin	0.81		[156]
KCuHCF	1.94		[107]
NaCoHCF (Flow-1.00)	4.36	Markham-Benton	This study

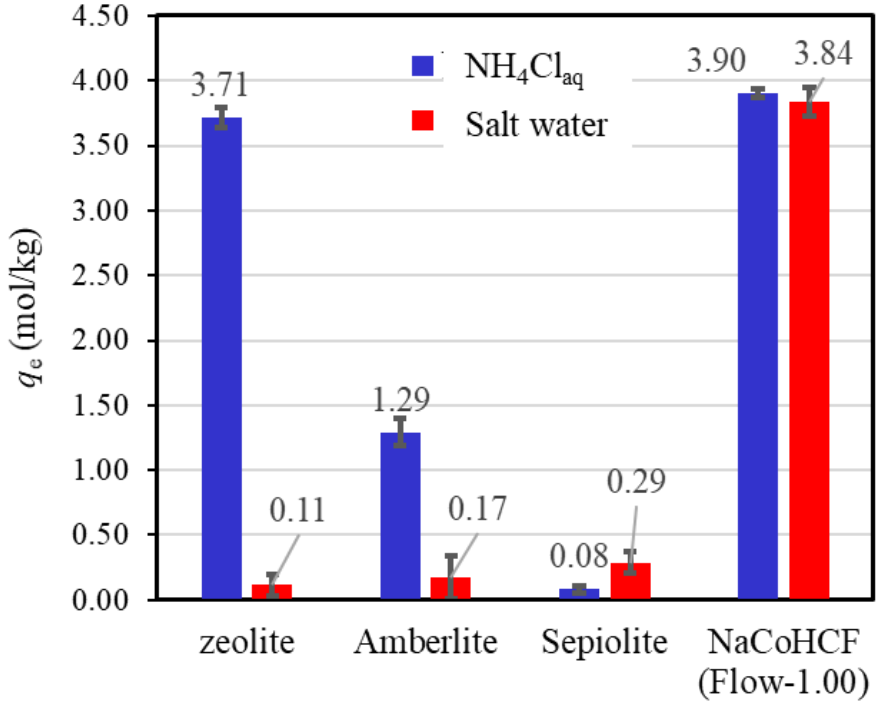

Fig. 2-12 Adsorption capacity of various adsorbents in NH_4Cl aqueous solution (500 mg NH_4^+/L) and saline solution with a concentration fixed at 9350 mg Na/L.

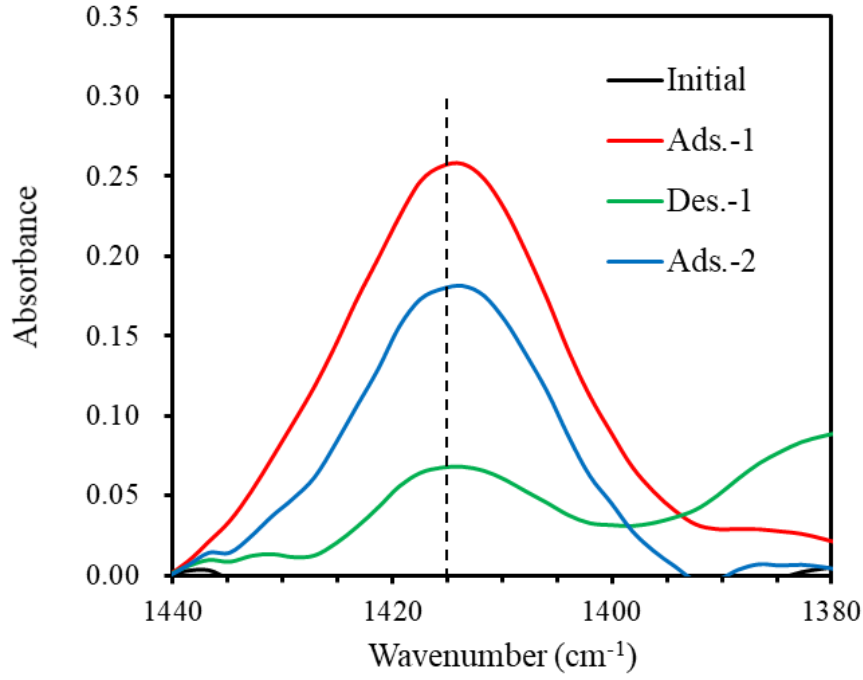

Fig. 2-13 FT-IR spectra showing the changes in the peak-height of NH_4^+ adsorbed onto Flow-1.00 after sorption and desorption.

Chapter 3 Adsorption and desorption of gaseous ammonia by Prussian Blue Analogue $Co_3[Co(CN)_6]_2$ at high working temperatures

3.1 Introduction

Ammonia, NH_3, in the atmosphere causes various issues, such as bad odour and corrosion in industry, agriculture, and museums. In particular, we are concerned with the small particulate matter, such as $PM_{2.5}$, in air, because NH_3 is known as a precursor of secondary inorganic aerosols, e.g., ammonium sulphate ($(NH_4)_2SO_4$) and ammonium nitrate (NH_4NO_3). NH_3 is considered to play an increasingly dominant role in $PM_{2.5}$ formation [157]. In order to solve and suppress these issues, the EU decided on a target of 19% reduction in NH_3 emissions by 2030 or later [158] in comparison with 2005. However, between 2014 and 2015, emissions increased by 1.8% [159]. On the other hand, China is the largest source of NH_3 emissions in the world, emitting over 15 Tg NH_3-N yr^{-1} in 2010, due to its low agricultural nitrogen use efficiency (NUE) in crop and livestock production [160, 161].

Hence, how to reduce NH_3 emission, i.e. how to effectively capture NH_3 under mild conditions, e.g., at room temperature (RT), has been getting considerable attention during the past few decades [110, 162–164]. Among these studies, the sorption method is widely accepted as an easy and cost-effective method to capture NH_3 gas with sorbents.

In recent years, sorption/desorption of NH_3 using sorbents at high temperatures has also attracted great attention from the viewpoint of practical applications and recycling, e.g. high-temperature removal of NH_3 from coal-derived gas [165], high-temperature removal of unburned NH_3 from diesel engines using selective catalytic reduction (SCR) in the temperature range of 150 to 400 ℃ [9], and removal of pollutants from diesel engines using the SCR in the temperature range of 60 to 300 ℃ [166]. In addition, in the field of hydrothermal conversion technology (HCT) to treat sewage sludge, ammonia can be generated under a relatively high temperature (in the range of 150 $^{\circ}$C to 250 $^{\circ}$C) in an autoclave process [167]. An NH_3 sorbent would be useful in the field of HCT.

For the utilisation of an NH_3 sorbent for such purposes, the following properties, even at high temperature, are necessary: sufficient capacity, stability during cycle use, and less volume change during the sorption-desorption process. Large volume change often brings difficulties in the design

of realistic systems. There are some reports of NH_3 adsorption at high temperatures, but there exists no sorbent that satisfies the requirements described above. For example, Y zeolites, H(85)Y was reported with a capacity at 150 °C of 9.37 mmol/g [168], but the sorption process was irreversible. Metal halide such as $CaCl_2$ also showed higher NH_3 capacity, but the volume change accompanying the adsorption and desorption is not negligible. The cell volume, 0.084 nm^3 per Ca atom in $CaCl_2$, drastically changed to 0.334 nm^3 [169, 170], i.e. about a 400 % expansion of the sorbent would occur.

Various materials as ammonia adsorbent have been investigated at RT, e.g. Prussian blue (PB) and its analogues [110], metal-organic frameworks [94, 105, 106, 171–173], covalent organic frameworks [174], graphene derivatives [175], Ion exchange resins [57, 176], as well as other traditional sorbents, such as zeolite, alumina, silica gel, and activated carbon [58]. Among them, to the best of our knowledge, cobalt hexacyanocobaltate (CoHCCo, Co^{II}_3 $[Co^{III}(CN)_6]_2$) , one of the PB analogues, exhibits a great NH_3 adsorption capacity, estimated to 21.9 mmol/g at RT [110], the highest among the recyclable porous adsorbents without a large volume change from sorption-desorption. The summary of the sorption capacity of ammonia in CoHCCo compared with series MOFs as shown in Table 3-1.

Accordingly, PB analogues including CoHCCo have been receiving considerable attention for their great gas adsorption and separation [110, 133, 177–179]. Because it has the simple cubic and nano-scale crystal structure as a well-known family of porous coordination polymers (PCPs) with liner bridging of the octahedral metal ions by cyanide anions, which defines nanopores within the framework to capture gas molecules [177]. The high sorption capacity of CoHCCo originates from the two kinds of sorption site with high density in the crystal [110]. The schematic view of the crystal structure is shown in Fig. 3-1. In the CoHCCo crystal, there two kinds of sorption sites for small molecules, i.e. interstitial sites and vacancy ones. The interstitial site is a cubic-confined pore, intrinsically existing in the crystal. On the other hand, the vacancy site is implemented by the introduction of the $[Co(CN)_6]$ vacancy. With these sorption sites, PB analogues show NH_3 sorption with high-density.

Here, NH_3 sorption and desorption performance of CoHCCo was reported, the composition of which is Co^{II} $[Co^{III}(CN)_6]_{0.60}$,[110] under heating conditions up to 260 °C for the first time, which

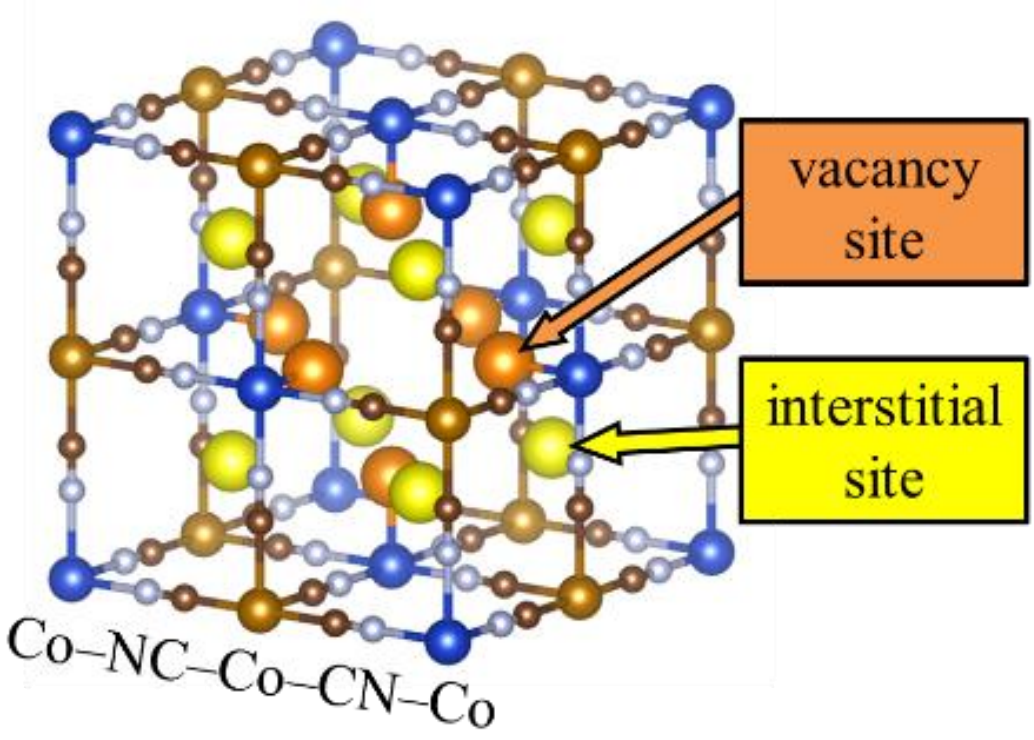

Fig. 3-1 Schematic view of the crystal structure of CoHCCo with a $[Fe(CN)_6]$ vacancy in the centre of the unit cell. The orange and yellow spheres represent vacancy sites and interstitial ones.

Table 3-1 Summary of adsorption equilibrium capacity of NH_3 at room temperature (RT) and 100 °C at around 1 bar compared with a class of MOFs.

Adsorbents	Capacity (mmol/g, RT)	Capacity (mmol/g, 100 °C)	BET Area (m^2/g)		Ref.
			before	after	
Cu_2Cl_2BBTA	19.79 [a]	×	1205	19	[182]
Zn-based MOF		×	367.1	×	[173]
BPP-5	17.7 [a]	×	700	×	[93]
Mn_2Cl_2(BTDD)	15.47 [a]	×	1917	×	[183]
UiO-66-C	7.78 [a]	×	800	×	[184]
HKUST-1	13.0 [a]	×	1460	×	[101]
Brønsted acidic porous polymers (P1-PO_3H_2)	18.7 [a]	× [d]	835	×	[185]
MOF-74(Mg)	14.11 [a]	×	×	×	[186]
ZIF-8	0.81 [a]	×	×	×	[186]
COF-10	15.2 [a]	×	×	×	[187]
CoHCCo	25.2 [22.3] [b], (21.9) [c]	18.6 [14.1] [e]	740 [f]	649 [g]	in this study

Note: ×: no data was found in the reference. ***a***: 25 °C. ***b***: 20 °C in this study, maximum capacity calculated by the dual-site Langmuir model (see Fig. 3-5), square brackets show the capacity at 1 bar. Round brackets show the capacity of our previous data at 1 bar. ***e***: maximum capacity calculated by the dual-site Langmuir model (see Fig. 3-5), square brackets show the capacity at 1 bar. ***f***: This value was relatively smaller than that of our previously published paper (***c***: ref [110]), 848 m^2/g. ***g***: After adsorption NH_3 using IR gas cell at 22 °C, and desorption at 200 °C in this case**.** ***d***: cf. as a similar acidic polymer, i.e., Amberlyst-15, its maximum capacity calculated by dual-site Langmuir model was 8.86 mmol/g at 100 °C, and the capacity at 1 bar.is 6.50 mmol/g at 100 °C in this study.

indicates quite high stability, large capacity, and recyclability in a wide range of ammonia concentrations.

3.2 Experimental section

3.2.1 Synthesis of CoHCCo

All reagents used in the synthetic studies were commercially available and used as supplied without further purification. $CoCl_2 \cdot 6H_2O$ was purchased from Wako Pure Chemical Industries Ltd. $K_3[Co(CN)_6]$ was purchased from Sigma-Aldrich Corporation.

In order to investigate the reproducibility and thermal stability, the new CoHCCo was synthesised. The synthesis method was slightly different from that in our previously published experimental study. [110] Briefly, 0.46 mol/L cobalt(II) chloride and 0.30 mol/L potassium hexacyanocobaltate(III) in a conical tube was mixed with shaking at a speed of 1,000 rpm for 24 h, followed by drying in vacuum for 2 days.

3.2.2 Characterization of CoHCCo

In-situ powder X-ray diffraction patterns (PXRD) were recorded with a D8 ADVANCE (Bruker AXS) at 40 kV and 40 mA using Cu K_α radiation (λ = 1.54 Å) with a scan speed of 0.10 s per step, step size of 0.02^o, and 2θ range of $5–60^o$. A Fourier-transform infrared (FT-IR) spectrometer (Nicolet Biomedical Inc.) equipped with a precision gas cell was used to confirm the cycle-ability of adsorption and desorption of NH_3 gas (NH_3 with a purity of 99.999% was mixed with room air at a volume ratio of ~8.0 vol%, measured by GASTEC Detector Tubes) under room air atmosphere with a humidity of ~41%. The other equipment used in this study can be referred to the subsection **2.2.2**.

3.2.3 Thermogravimetry

The reproducibility-control CoHCCo (~10 mg) was heated at 5 K min^{-1} from 25 °C to 500 °C in nitrogen, pure-air, and room-air (relative humidity (RH) of 27%) atmosphere with a flow rate of 200 ml/min.

3.2.4 In-situ XRD to determine the stability

An in-situ XRD analysis was performed in the NH_3 gas atmosphere (NH_3 with a purity of 99.999% was mixed with room air at a volume ratio of ~8.0 vol%, measured by GASTEC Detector Tubes) while increasing the temperature. The as-synthesised CoHCCo without pre-treatment was placed into a gas cell equipped for D8 ADVANCE. For evaluation of the dependence of the crystal structure on the temperature and ammonia sorption, two steps were employed. First, the temperature was increased from room temperature (RT) (21 ℃, RH = 66%) to 100 ℃, which was then maintained for 5 min in vacuum. This was followed by the injection of ammonia-containing air into the gas cell, which was maintained for 5 min. The second step was similar to the first, except for the different temperature of 250 ℃, instead of 100 °C. It is worth noting that before the heating, the room air condition was slightly different, i.e., 25.5 °C and RH = 54%.

3.2.5 Ammonia gas sorption measurement

Ammonia gas (purity: 99.999%) adsorption/desorption isotherms were measured at RT (20 °C) in a water bath with a temperature controller. The temperature was set to 100, 150, and 250 °C by a heater of an adsorption evaluation instrument, BELSORP-max (MicrotracBEL Corp.). Before the measurement, a 50-mg sample for each test was heated for dehydration at 150 ℃ for 24 h on a BELPREP-vac II.

3.2.6 Cycle-ability test in the NH_3-including atmosphere

The initial CoHCCo film before the NH_3 adsorption was prepared as follows. The CoHCCo powder was placed onto a BaF_2 plate, heated in a gas cell (Model S84, S.T. JAPAN Inc.) at 200 °C for 10 min in ambient atmosphere (RH = 40%), and then cooled down to RT in the N_2 atmosphere. The FT-IR measurement was performed in the transmission mode with a flowing NH_3 mixed with room air (RH=27%). The NH_3-containing atmosphere was prepared by mixing NH_3 gas with a purity of 99.999% and room air, at a volume ratio of ~8.0%. When NH_3-containing air was injected, the temperature was set to RT (22 °C). After adsorption, room air was flown into the gas cell as the atmosphere at a rate of 230 ml/min, and the temperature was adjusted to 250 °C. The flow rate of NH_3 gas was 130 ml/min. The flow of each gas was maintained for 3 min, immediately followed by an FT-IR measurement. During the cooling from 260 ℃ to RT, N_2 gas was flown at a rate of 200 ml/min.

3.3 Results and discussion

According to the TG results (see black lines in Fig. 3-2(a)), CoHCCo is quite stable under the atmosphere of flow nitrogen until around 400 °C. Additionally, stability in the presence of oxygen was also checked. The decomposition temperature, i.e., the combustion temperature of cyanide ligands in the case of CoHCCo under an atmosphere of pure air and room air is about the same, reach 297.9 °C and 301.8 °C, respectively. It is found that CoHCCo possesses relatively high thermal stability and durability against the oxidation reaction, i.e., higher temperature durability against burning until 300 °C, when compared to organic polymer materials such as polyethylene.

To confirm the stability of the crystal structure for CoHCCo, PXRD patterns under varying temperature were also recorded using a heating cell as shown in Fig. 3-2(b). It clearly shows that the crystal structure of CoHCCo is maintained at a high temperature up to 250 °C, even in the high-concentrated NH_3-including atmosphere, and the main peaks (17.4 °and 24.7 °) have a little shift to high angle after raising temperature. In connection with the little shift of the main peaks, the lattice constants under these conditions are shown in Fig. 3-2(b), indicating a rather small volume change during sorption-desorption, around 7% based on the initial stage at RT in air. The change would originate from the charge transfer between cobalt cations as described later. The position of the main peaks shifted to the high angle at 100 °C in a vacuum and returned to the original after being put into an NH_3 including atmosphere at 100 °C. However, the position of the peaks did not return to the original position at 250 °C, independent from the atmosphere. These results indicate that the small shrink of the crystal occurred with the desorption of the molecules, NH_3 or H_2O. Concerning the particle size, the crystallite size of CoHCCo estimated by Scherrer analysis of the PXRD patterns was 33.6 nm in RT. At 250 °C in a vacuum, the crystallite sizes of CoHCCo changed to a smaller 20.8 nm. At present, these changes of crystal may do not affect the sorption/desorption properties as shown in IR measurements. The morphology of CoHCCo was also checked by SEM, no obvious shape changes compared to the as-synthesized sample (see Fig. 3-2(c)).

Furthermore, CoHCCo was compared with well-known typical sorbents[58] for their NH_3 sorption capacity at high temperature (Fig. 3-3(a)). The preliminary sorption range of temperature was selected less than 300 °C based on TG measurements. For comparison, Amberlyst-15 was also investigated, a kind of polystyrene polymer with sulfonic acid moiety, which showed the large sorption capacity of NH_3 at RT in literature [176]. The isotherm measurements revealed that the

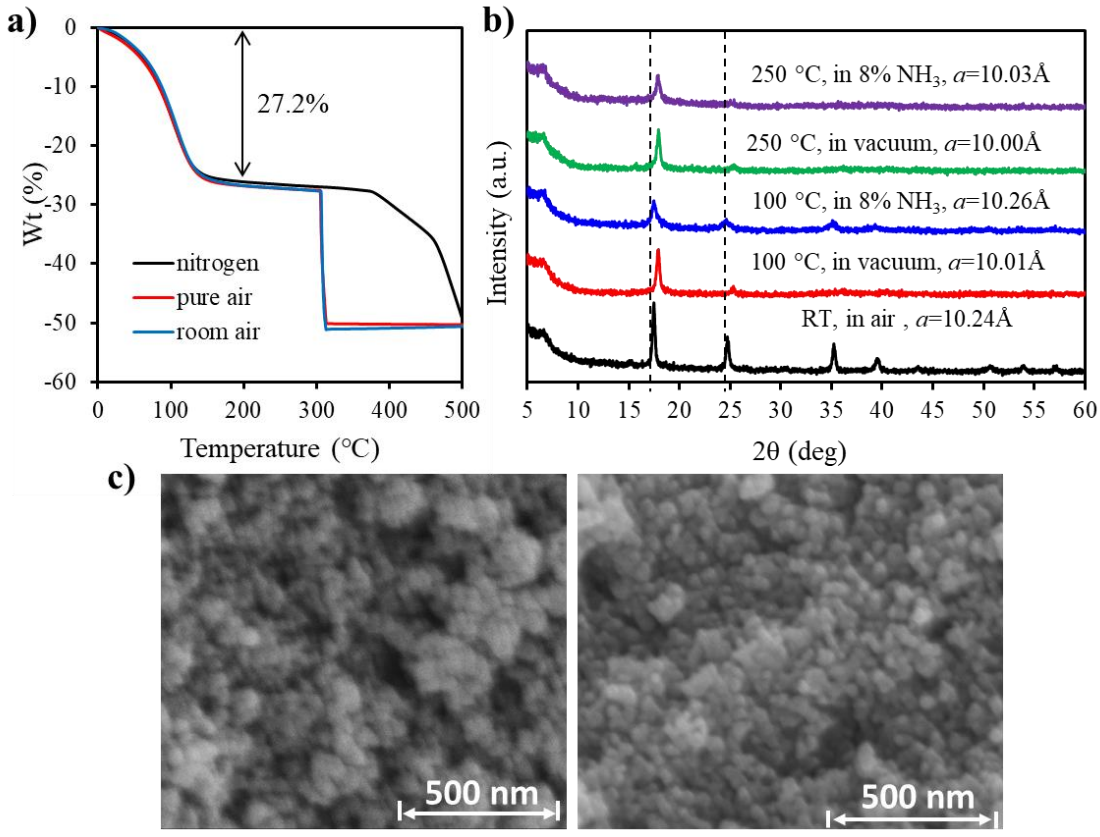

Fig. 3-2 Thermogravimetric analysis of CoHCCo, (a) Under the atmosphere of flowing N_2 (black line, reproducibility check), pure air (red line), and room air (blue line), respectively. (b) PXRD patterns of CoHCCo with variations of temperature and atmosphere. (c) Scanning electron microscopy (SEM) images showing the morphologies of the left: as-synthesised CoHCCo and right: sample after adsorption and desorption at 250 ℃ using the BELSORP-max through pressure swing.

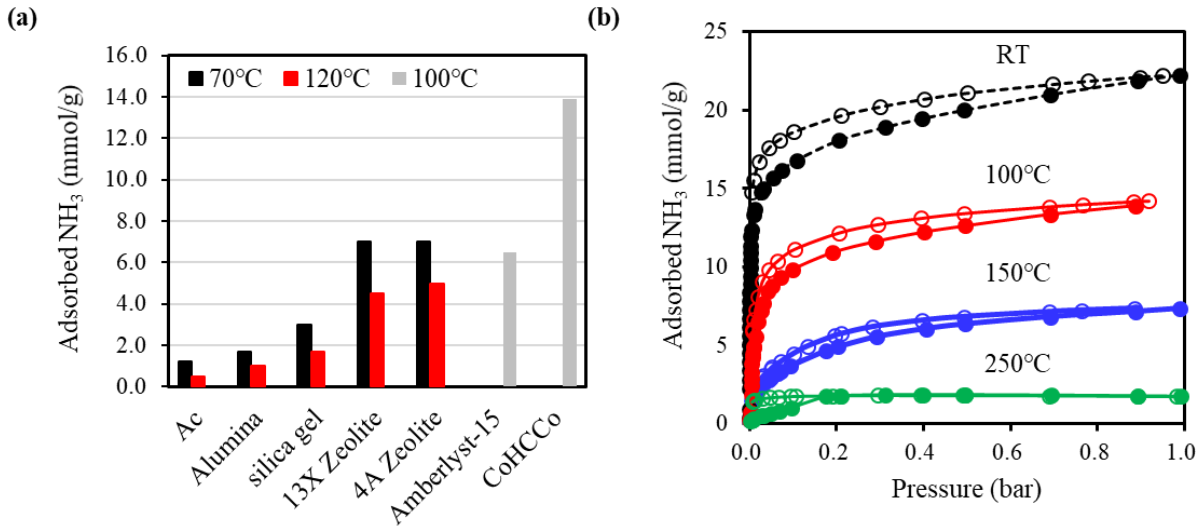

Fig. 3-3 (a) Comparison with other typical sorbents in the same or similar conditions, around 1 bar. [58] (b) Ammonia sorption (closed circles) and desorption (open circles) isotherm in CoHCCo at different heating temperatures. The sorption isotherm at RT (20 °C) is also given for comparison with that of others. The connecting lines are guides for the eyes.

sorption capacity of CoHCCo is about 2 times larger than that of Amberlyst-15 at 100 °C, with a pressure of ca. 1 bar (ca. 100 kPa, around ambient pressure) as shown in Fig. 3-3(a) and Fig. 3-4. Fig. 3-3(a) summarises adsorption amount in the comparison with other typical sorbents, indicating an apparently lower capacity than CoHCCo; According to these data, it indicates that the sorption capacity of NH_3 using CoHCCo clearly exceed other typical sorbents at higher temperatures in a wide range of ammonia concentrations, under relatively high concentration, from 1 (ca. 1% gas) to 100 kPa (pure gas) of ammonia as shown in Fig. 3-4 and Fig. 3-3(b).

The NH_3-sorption isotherms at various temperatures are shown in Fig. 3-3(b). It was found that the capacity of CoHCCo, even at 100 °C, was beyond that of Amberlyst-15 at RT, at 13.7 mmol/g [176]. The isotherms at RT, 100 °C and 150 °C are well fitted by a dual-site Langmuir model [180] as shown in Fig. 3-5, indicating it has two kinds of adsorption site. It is consistent with the existence of adsorption sites combined between the interstitial sites and the vacancy ones. For 250 °C analysed by dual-site Langmuir model, however, single-site Langmuir model is more dominant, implying only one kind of adsorption site works at 250 °C. The maximum capacity is evaluated 25.2, 18.6, 8.6, and 2.1 mmol/g at 20, 100 °C, 150 °C, and 250 °C, respectively (Table 3-2). Note that the capacity at RT was evaluated as 21.9 mmol/g in the previous report [110]. The difference comes from the change of the fitting model. Using the dual-site Langmuir model, the region at higher pressure can be better fitted than the single site Langmuir model, allowing the possibility of capacity re-evaluation.

From the viewpoint of practical applications under ambience, and to confirm the recyclability, the NH_3 adsorption/desorption was tested using CoHCCo by temperature swing under the atmosphere of moderately humid conditions in air (40%RH in this case). In this study, the cycle tests were done by in-situ FT-IR measurement with CoHCCo film on a barium fluoride substrate in a gas-flow cell. The temperature range was repeatedly changed between RT and 260 °C. As a result, CoHCCo seems to be perfectly reversible to adsorb-desorb NH_3 in the presence of oxygen and water molecules, as shown in Fig. 3-6(a); the sorption peaks in the range of 1,000-1,450 cm^{-1}, corresponding to NH_3 or NH_4^+ species, clearly appeared and disappeared with the elevation of the temperature.

The initial CoHCCo film, preheated at 200 °C, already had a peak around 1,260 cm^{-1} (NH_3(v), black line in Fig. 3-6(a)), indicating NH_3 coordinatingly sorbed in the vacancy site of CoHCCo.

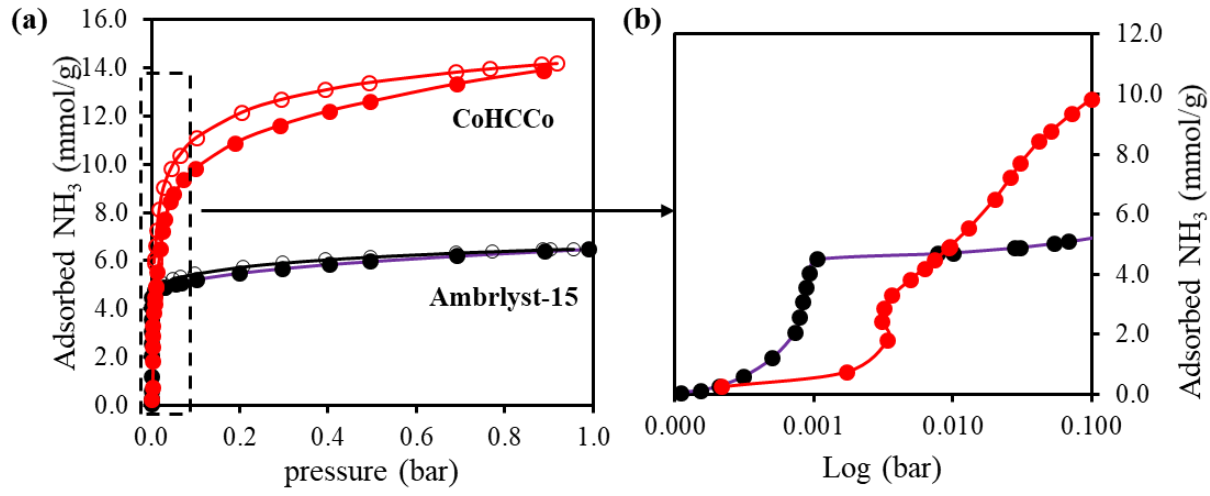

Fig. 3-4 a) Ammonia sorption (closed circles) and desorption (open circles) isotherms of CoHCCo and Amberlyst-15 at 100 °C. b) Sorption capacity of CoHCCo compared with that of Amberlyst-15 at low pressures below 0.1 bar. The connecting lines are shown as visual guides.

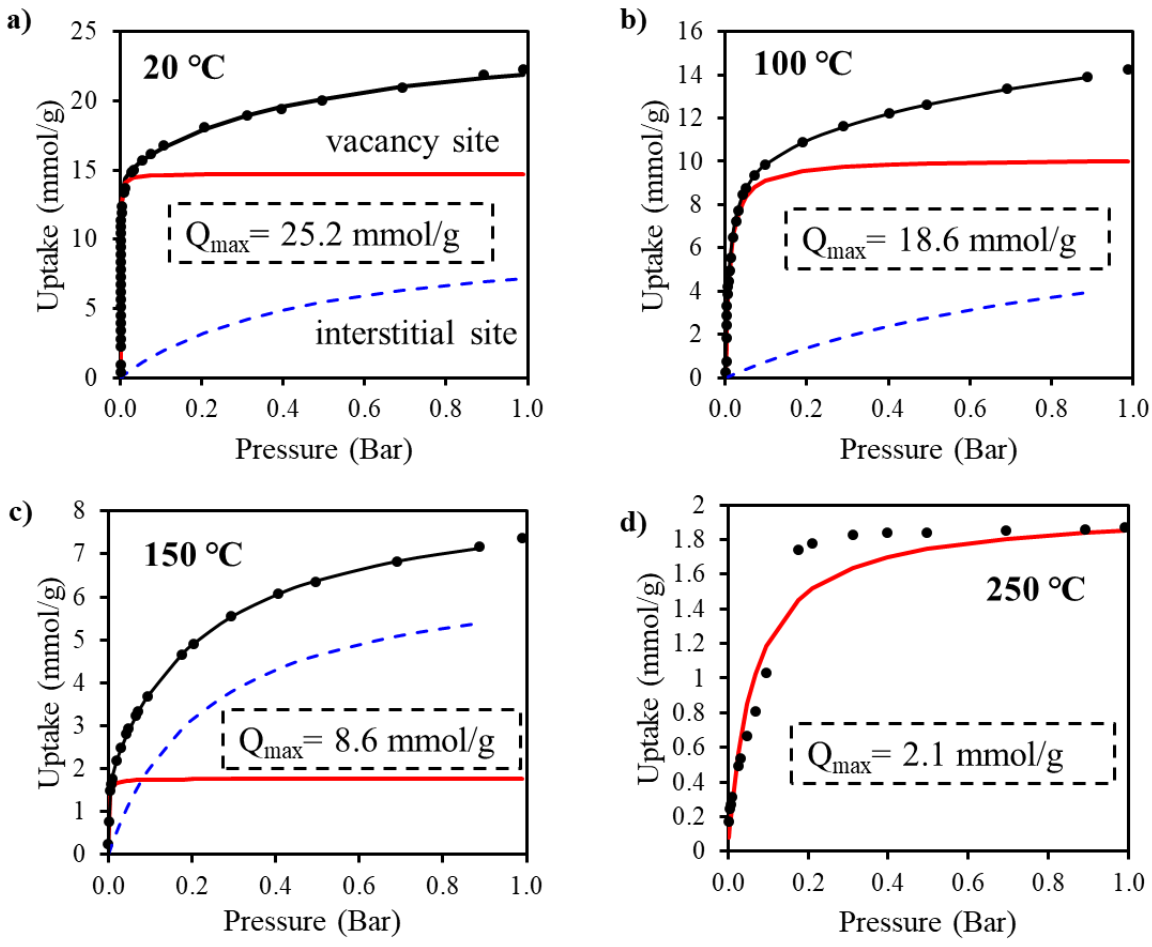

Fig. 3-5 Adsorption isotherms of CoHCCo for NH_3 at different heating temperatures. The black points represent the observed values. a, b, c) The black curves are the fitting curves obtained by the dual-site Langmuir model. The red and broken curves represent the contribution of each term in the dual-site Langmuir model. d) The red curve is the fitting curve obtained by the Langmuir model.

Table 3-2 Fitting parameters of the adsorption isotherms for CoHCCo powders obtained using the dual-site Langmuir model equation.

T (℃)	q_1^{m}	K_1	q_2^{m}	K_2	$Q_{sum.}$
20	14.7	1,712.3	10.5	2.2	25.2
100	10.1	94.5	8.5	1.0	18.6
150	1.8	857.0	6.8	4.3	8.6
250	0.0	0.0	2.1	13.8	2.1

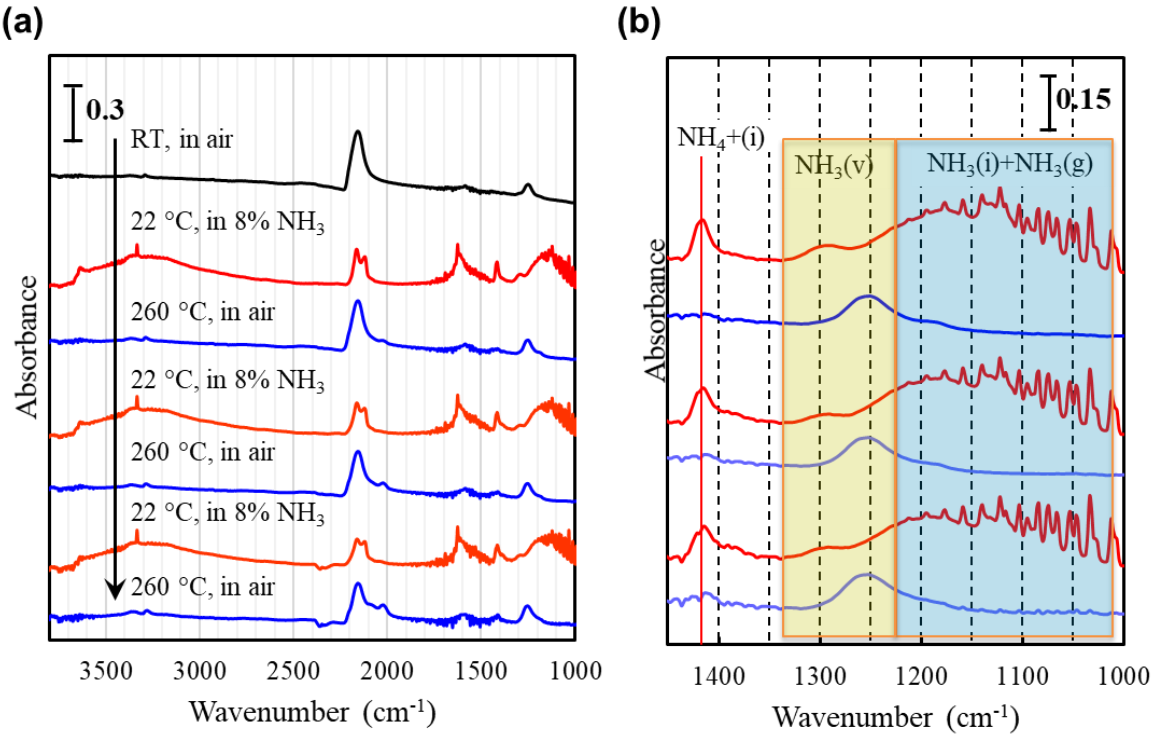

Fig. 3-6 (a) IR spectra for recyclability test (3 cycles) of ammonia adsorption and desorption of CoHCCo at the heating temperature, range changing between RT (22°C) and 260 °C (eye guide: Absorbance scale = 0.3). (b) Magnified view for the range of 1,000 – 1,450 cm^{-1} (eye guide: Absorbance scale = 0.15). The notation NH_4^+(i), NH_3(v), NH_3(i), and NH_3(g) represent the absorbance peaks corresponding to NH_4^+ in the interstitial site, NH_3 at the vacancy site, NH_3 at the interstitial site, and NH_3 in gas phase, respectively.

Similar adsorption of trace NH_3 in air was found with $K_{0.23}Fe[Fe(CN)_6]_{0.74}$, but in the case of PB, sorbed NH_3 is converted to NH_4^+ with protonation [110]. Because the coordination bonding could be stronger with Co than with Fe in PB framework, sorbed NH_3 would be kept as is. The coordinating sorption at the vacancy site seems quite strong because this peak remained even after heating at 260 °C. After the sorption-desorption cycles, almost the same profile is found in the air at RT, so the structure of CoHCCo framework and sorbed-NH_3 is concluded as returning to the initial state.

For the condition of CoHCCo in NH_3-atmosphere at 22 °C, the situation is rather complicated. The IR absorption in the range of 1,000-1,450 cm^{-1} is decomposed into 4 components as follows, where the abbreviation in parentheses represents the peak position indicated in Fig. 3-6(b). ***(1).*** oscillating peaks at 1,000-1,200 cm^{-1} (NH_3(g)) were brought from the gaseous NH_3 without adsorption (see Fig. 3-7), ***(2).*** the broad peak at 1,000-1,250 cm^{-1} (NH_3(i)) would be from NH_3 weakly sorbed in interstitial sites, ***(3).*** the narrow peak at 1,300 cm^{-1} (NH_3(v)), RT after the sorption, corresponds to the NH_3 at the vacancy site with the coordination bonding to Co, but 40 cm^{-1} of shift was found at 260 °C from that in the air at RT, and ***(4).*** the narrow peak at 1,410 cm^{-1} (NH_4^+(i)) shows the converted species to NH_4^+ from NH_3. The conversion to NH_4^+ was also found with $K_{0.23}Fe[Fe(CN)_6]_{0.74}$, considered to be caused by the protonation by crystal water [110]. From these assignments, NH_3 and NH_4^+ sorbed in the interstitial site would be desorbed in the air at 260 °C. The result is consistent with the isotherm analysis at 250 °C, where only one adsorption site, maybe the vacancy site, seems to work.

Note that waiting only three minutes for the FT-IR measurement after the target temperature was achieved, indicating that the sorption and desorption proceeded sufficiently in a short amount of time. On the other hand, it is necessary for the evaluation of the persistence of the NH_3 at vacancy site with the coordination bonding to investigate the time dependence of the corresponding peak.

For the peak shift corresponding to NH_3(v), some possibilities from the result of IR spectra in another wavelength region and the PXRD patterns was speculated. In the IR chart at 2,000-2,150 cm^{-1}, the peak splitting into two suggests a change in the electronic state of the Co atoms in NH_3-atmosphere. The change would be associated with the colour change before and after adsorption at 100 °C (Fig. 3-8). One possible cause of the change is the partial charge transfer, Co^{II}

$[Co^{III}(CN)_6]_{0.60}$ to $Co^{II}_{0.4}$ $Co^{III}_{0.6}$ $[Co^{II}(CN)_6]_{0.60}$. Because from the change of the crystal structure evaluated from PXRD analysis shown in Fig. 3-2(b), about 0.2 Å of lattice constant decrease was found, consistent with the charge transfer accompanied by the spin state change, $Co^{II\text{-}HS}$ – $Co^{III\text{-}LS}$ to $Co^{III\text{-}LS}$ – $Co^{II\text{-}LS}$. Since the ionic radii of the $Co^{II\text{-}HS}$ and $Co^{II\text{-}LS}$ in octahedral bondings are 0.745 Å and 0.65 Å, respectively [181], from these radii, the difference in the lattice constant is estimated to 0.19 Å, which is in good agreement with our result.

3.4 Summary

CoHCCo is able to sorb great volumes of ammonia molecules reversibly at heating temperatures below 1 bar. The structure of CoHCCo was kept stable after sorbing/desorbing the NH_3 gas, even under moderately humid conditions at high temperatures, to 250 °C. The temperature swing adsorption (TSA) process is expected to be employed using CoHCCo to adsorb/desorb NH_3 gas for practical applications in the field of ammonia collection.

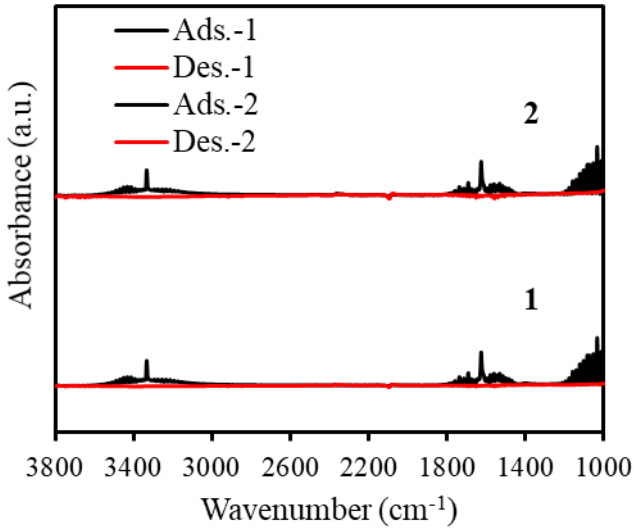

Fig. 3-7 IR spectra for two-cycle blank tests using the gas cell without CoHCCo, for adsorption and desorption process of ammonia with humidity. The black lines represent the adsorption process at RT, while the red lines represent the desorption process at 250 °C.

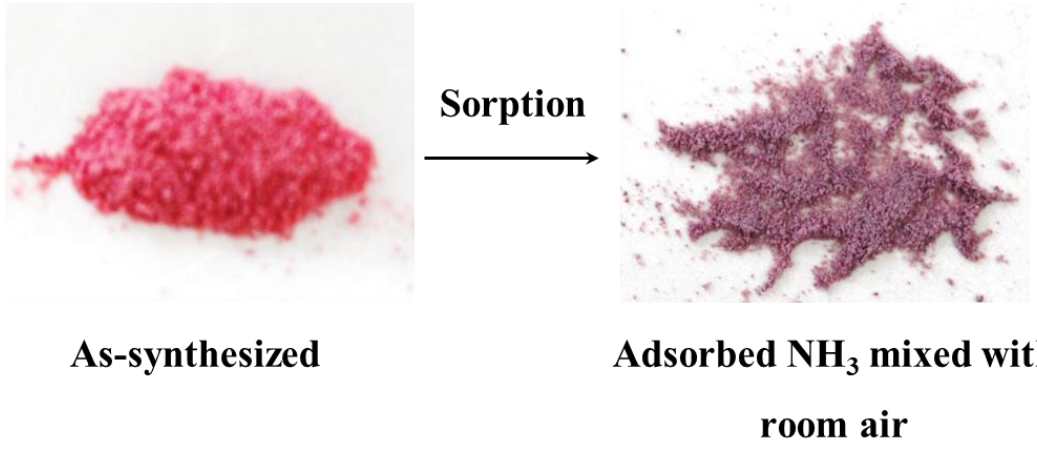

Fig. 3-8 Colour change after ammonia gas with a moderate humidity adsorbed at 100 °C.

Chapter 4 Unique gaseous ammonia adsorption and desorption behaviour of Prussian Blue Analogue $Zn_3[Co(CN)_6]_2$ at moderate working temperature

4.1 Introduction

Ammonia, which represents one of the most widely used in chemicals, nevertheless, chemical processes utilizing ammonia produce ammonia-containing gas mixtures, and ammonia-gas separation is highly necessary and desirable [58]. Not only because it has a severe irritant, has been identified as a major air quality concern by the National Research Council (NRC) [188], which is harmful to people health [189]. But also in the field of integrated circuits industries, volatile NH_3 can make the silicon wafer useless [190, 191]. Besides, it has the potential to be used as the H_2 alternative energy [62, 192–194] and green fuels [195].

In EU, USA, and China, increased NH_3 emissions driven by an increase in the consumption of synthetic nitrogen fertilisers and increase in the numbers of livestock (mainly are cattle and pigs), has been aroused many attentions [159, 196, 197]. Moreover, the manufacturing industry (ammonia and coke), refrigeration systems, or sewage treatment plants—require purification systems also contribute to the NH_3 gas emission [198]. Several adsorbents, such as zeolite, alumina, silica gel, and activated carbon [59, 80, 81], are related to the separation of ammonia from the gas streams in the ammonia manufacturing process. Besides, powdered or granulated activated carbons, are already being used at an industrial scale [199]. Nevertheless, there is still a need for adsorbents to be able to have higher sorption capacity for NH_3 and to be easily regenerated after use.

Considering all of these, many attempts have been employed to find an efficient adsorbent for ammonia. One kind of the materials, recently, as it has nanosized porous, Lewis acidic unsaturated metal centres, Brønsted acid groups and easily modify for the structure, already received many attentions, called metal-organic frameworks (MOFs), such as HKUST-1 [200–202], MOF-5 [198], Zn-MOF [203], and Brønsted acid MOFs (aka. MOF-205 [204], BPP-5 [93]). Nevertheless, there is still a need for adsorbents to be able to strongly retain even higher amounts of NH_3, stable ability to ammonia exposure, especially to humid conditions**,** as the sorption process is always employed at ambient conditions, i.e. the omnipresence of moisture, where the competitive behaviour between water and ammonia to bind to a polar adsorbent weakens the ability of the adsorbent for selectively capturing ammonia from humid air [203, 205]. Hence, the competitive behaviour between

ammonia and water to bind to an adsorbent weakens the ability of the adsorbent for selectively capturing ammonia from the humid air should be considered.

$M_3^{II}[Co^{III}(CN)_6]_2$ (M is transition metals, water is omitted), one kind of PB analogues, is a well-known family member of porous coordination polymers (PCPs), which features a simple cubic framework, with liner bridging of the octahedral metal ions by cyanide anions which defines pores within the framework [177], have been aroused many concerns in the fields of gases adsorption and separation [110, 133, 178], catalyst [206, 207], molecular sensing [109]. The presence of different inorganic metal nods in cubic framework shows different sorption properties including interactions forces, regenerate, and stability, which are important features in gas sorption. Additionally, it has reported that the greater sorption ability of $M_3^{II}[Co^{III}(CN)_6]_2$ is based on the mechanism which two kinds of sorption site with high density in the crystal [110].

In the previous studies, PCP has been studied for sorption NH_3 (99.999% purity) gas at room temperature (RT) and high temperature (HT) below 1 bar, among them cobalt hexacyanocobaltate (CoHCCo) shows the maximum sorption capacity 21.9 mmol/g (RT), 18.6 mmol/g (100 °C) compared to other reported recyclable porous sorbents without a large volume change during the sorption-desorption process [110]. Zinc hexacynanocobaltate (ZnHCCo), as it has dimorphic characteristics, i.e. cubic phase (*Fm-3m*) at RT, while hexagonal one (*R-3C*) can be formed from hot solutions synthesis (>60 °C) or dehydrating the cubic phase by heating [208, 209], corresponding to different properties, has been demonstrated to apply in the field of gas sorption, such as capture H_2 [133], CO_2 [60, 208, 210] , SO_2, H_2S, NO and water at RT and desorb each gas at a slightly higher temperature (~70 °C) [64]. However, some studies indicated that in the case of hexagonal one (*R-3C*), the Zn atom is found tetrahedrally coordinated to the N ends, without available coordination sites [208, 211].

Up to now, except the CoHCCo, there is no report on sorption ammonia gas at a moderate temperature, especially on the performance of sorption ammonia gas with humidity using ZnHCCo. As it is known, the successful ammonia storage material must have high capacity under 40–60 kPa of ammonia at ambient temperature, and must release ammonia easily by a mild operation such as evacuation to 10 kPa (pressure swing adsorption: PSA) or heating to 200 °C (temperature swing adsorption: TSA) [162]. In this study, the sorption performance of ZnHCCo on ammonia gas at a

moderate temperature below 1 bar, moreover the recyclability and the effect of moderate humidity on the ammonia sorption performance are also discussed.

4.2 Experimental section

4.2.1 Synthesis of ZnHCCo

All reagents used in synthetic studies were commercially available and used as supplied without further purification. $ZnCl_2$ was purchased from Wako Pure Chemical Industries Ltd. $K_3[Co(CN)_6]$ were purchased from Sigma-Aldrich Corporation.

Synthesis of Zn_3(II) $[Co(III)(CN)_6]_2$: Mix of $ZnCl_2$ (0.317 g, 2.28 mmol), $K_3[Co(CN)_6]$ (0.521 g, 1.52 mmol) using 50 mL conical tube at RT. The suspension was shaken using a multi shaker (SI-300C; AS One Corp.) for 24h with 1,000 rpm at room temperature. After shaking, the slurry solutions were centrifuged. The slurries were washed at least three times with milli-Q water. Then dried in vacuum at RT for 48 h.

4.2.2 Characterization of ZnHCCo

This part can be referred to the subsection **3.2.2**.

4.2.3 Thermogravimetry

This part can be referred to the subsection **3.2.3.**

4.2.4 In-situ XRD to determine the stability

This part can be referred to the subsection **3.2.4**. In addition, for evaluation of the dependence of the crystal structure on the temperature and ammonia sorption, the temperature was increased from RT (31 ℃, RH = 45%) to 100 ℃, and maintained for 5 min in vacuum at 100 ℃, followed by injection of ammonia-containing air into the gas cell, which was also maintained for 5 min. Then tried to desorb the NH_3 at 200 °C by maintaining 5 min.

Furthermore, to check the structural change by adsorbing NH_3 gas (NH_3 including atmosphere) at RT, a film gas cell with gas inlet and outlet was also used to test the sorption and desorption process for ZnHCCo. The first step, to simulate sorption process in IR test (discussed in later), the NH_3 gas was flowed through the film gas cell from gas inlet by a syringe (200 ml) with 2 times and

outflowed from gas outlet (see Fig.4-1(a)), then the second step, a vacuum pump for the desorption process was employed for 5 h. The structure of each step was detected using D8 ADVANCE.

4.2.5 Nitrogen/Ammonia gas sorption measurement

This part can be referred to the subsection **3.2.5**.

4.2.6 FT-IR measurement in the NH_3-including atmosphere

This part can be referred to the subsection **3.2.6**.

In addition, to avoid the NH_3 signal impact coming from the window (discussed in Chapter 3), and better understand the desorption property of ZnHCCo at 100 °C. We put the BaF_2 plate loaded ZnHCCo powders into a plastic bag, then the NH_3 gas atmosphere was injected into the plastic bag, sealed fast and wait for 3 min. After that, the adsorbed sample was moved to the gas cell equipped for the IR, to observe the TSA process. The first step, heating to 100 °C then keep the time for 5 min. The second step injected the dry N_2 gas with a flow rate of 200 ml/min at the constant temperature of 100 °C (RT: 23 °C, RH: 34%).

4.2.7 Effect of moderate humidity on the sorption performance

Wet suspensions of as-synthesized ZnHCCo powders were placed onto a silicon substrate and then was dried at 60 ℃ for 3 min in the oven. The adsorption process was that the silicon substrate loaded ZnHCCo film was exposed in the ambient (RT: 23 ℃, RH: 35%), then NH_3 including atmosphere with a flow rate 200 ml/min was blown onto the surface of the film for 2 min. After overnight, it was moved into a desiccator, then flowing a stream of room air with moderate humidity (RH: ~76%, Fig. 4-2) for 10 min at the rate of 200 ml/min into the desiccator, to find the effect of moderate humidity on the sorption affinity of ZnHCCo against NH_3 gas molecular. The test has used the package (iD1 transmission iS5; Nicolet Biomedical Inc.) to confirm the stability of adsorbed NH_3 gas molecular.

4.3 Results and discussion

4.3.1 Characterization of ZnHCCo

The composition of ZnHCCo measured by MP-AES and TG is $K_{0.19}Zn_{1.00}[Co(CN)_6]_{0.63}$ $3.01H_2O$. In view of the excess of Zn^{2+} in the synthesis mixture and in the

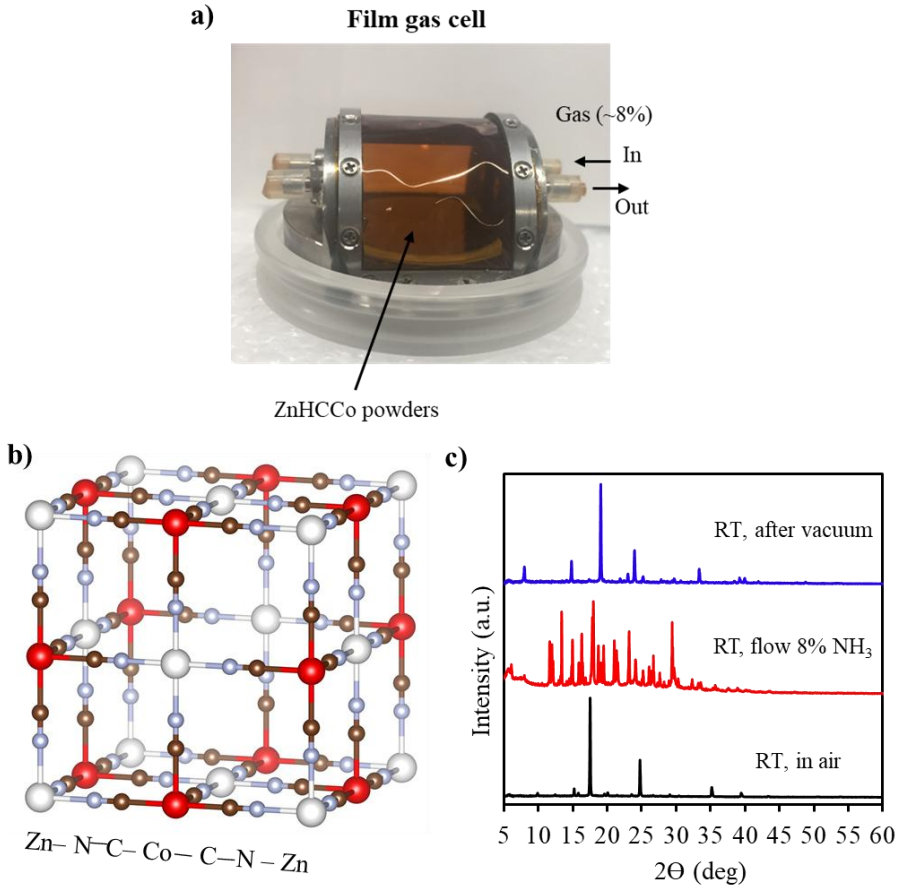

Fig. 4-1 (a) A film gas cell used by checking the structural change, (b) Schematic view of the crystal structure of ZnHCCo with a $[Co(CN)_6]$ vacancy in the centre of the unit cell. (c) PXRD patterns of ZnHCCo with variations atmosphere at RT. The notation for atmosphere "in air" and "in 8% NH_3" represent using laboratory air, and a mixed atmosphere of laboratory air and NH_3 air to make 8 vol% of the NH_3 concentration.

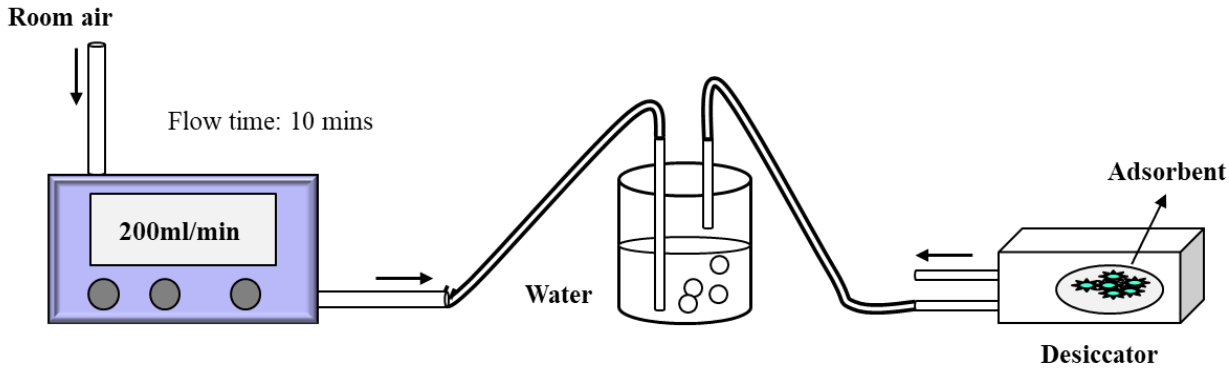

Fig. 4-2 The schematic of room air flowing process with high humidity

structure, it is expected that zinc terminates the crystals and is abundant on the outer surface [207], and the schematic view of the crystal structure is shown Fig. 4-1(b). The Brunauer–Emmer–Teller (BET) surface area measurement was performed using nitrogen adsorption at 77 K (Fig. 4-3). A typical Type I isotherm was observed for ZnHCCo with surface areas 693 m^2/g, lower than that of CoHCCo 848 m^2/g [110], consistent with the result of crystal size estimated by Scherrer analysis 59.0, and 20.8nm, respectively, also in good agreement with reported literature [133]. Fig. 4-1(c) shows the structure of ZnHCCo is a typical microporous coordination solid with the structure of the cubic phase (*Fm-3m*) [133, 208]. In addition, the little rhombohedral phase is also detected, resulting from K^+ located in the framework cavities, resulting in little isomorphous phase is formed with the same to the high-temperature phase of ZnHCCo (*R-3C*) [208, 209].

4.3.2 Stability at high temperature

Fig. 4-4 shows decomposition temperature of cyanide ligand in the case of ZnHCCo is ~400 °C under nitrogen, however, a little decrease to ~350 °C under pure air and room air (RH 27%) flow with the same flow rate, which shows higher than the decomposition temperature of CoHCCo, ~300 °C, at the same conditions under pure air and room air atmosphere. A sharp weight loss of 21% between RT to 130 °C illustrate the loss of water molecules from the porous structure, which also shows lower than that of CoHCCo, ~150 °C, indicating the stronger affinity of CoHCCo to the H_2O molecular. After dehydrated in a vacuum at 100 °C, even the phase structure was kept the cubic structure, however, the crystallite sizes of ZnHCCo estimated by Scherrer analysis became smaller, from 120.0 reaches to 77.9 nm, as the crystal structure shrink after dehydrating, a similar phenomenon as that of CoHCCo. Here, the results showed different with other studies, i.e. other reports indicated that phase would change to *R-3C* when heating above 60 °C or in the presence of a low chemical potential of water [208, 209].

4.3.3 NH_3 sorption properties

Unique adsorption and desorption behaviour for ammonia gas under varying temperature conditions are shown in Fig. 4-5. Especially at the conditions of RT and 100 °C, the sorption isotherm of ZnHCCo becomes steeper when the pressure over 0.5 bar at 20 °C, indicating the sorption capacity increases faster than that of the pressure lower than 0.5 bar. It may be caused by

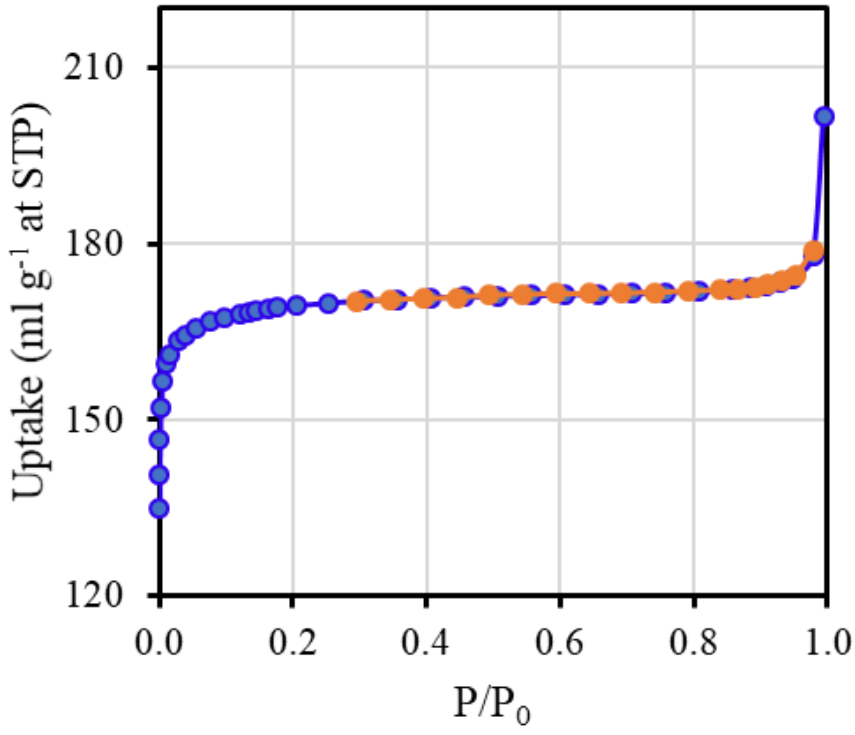

Fig. 4-3 N_2 adsorption isotherm at 77K.

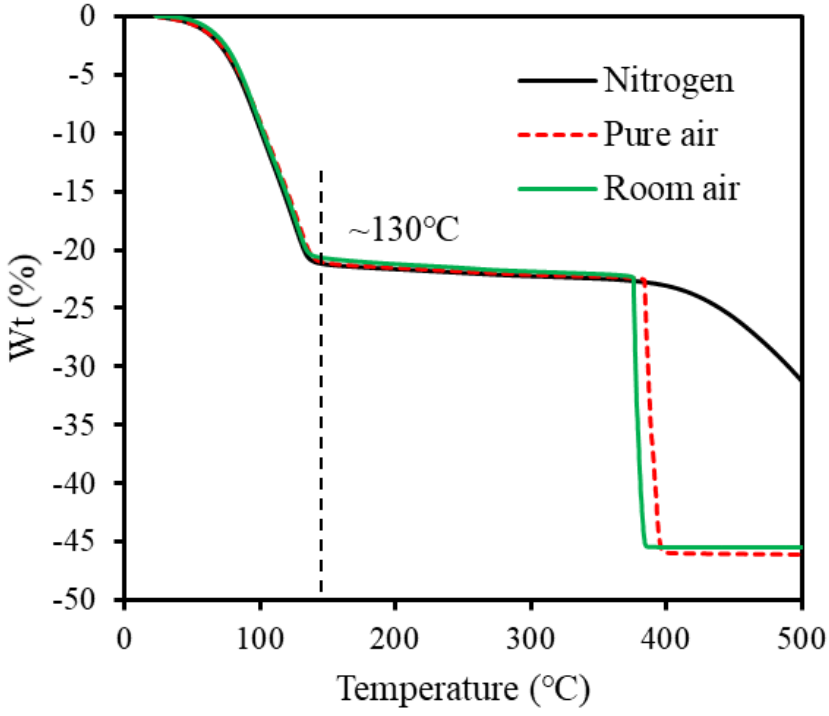

Fig. 4-4 Thermal analysis of ZnHCCo between RT to 500 °C.

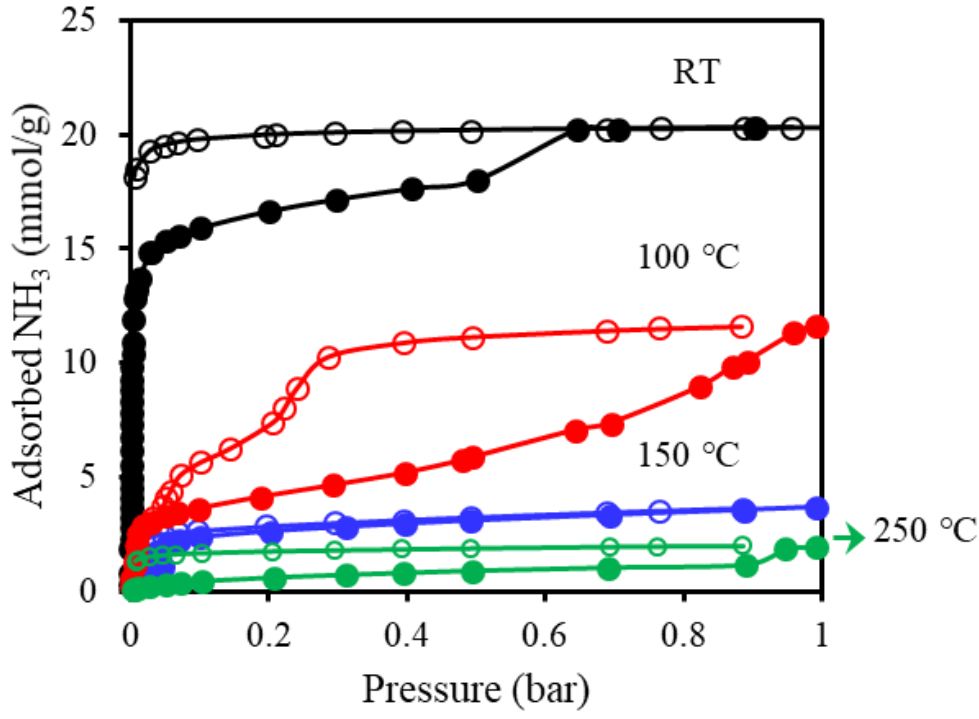

Fig. 4-5 Ammonia sorption (closed circles) and desorption (open circles) isotherm in ZnHCCo at different heating temperatures. The sorption isotherm at RT (20 °C) is also given for comparison with that of others. The connecting lines are guides for the eyes.

a phase change, resulted in there were no available sorption sites over 0.6 bar, which the structural change has been demonstrated by the PXRD patterns with sorption result using the film gas cell, see Fig. 4-1(c). It clearly shows the structure changed after sorption NH_3 gas compared with the as-synthesized sample at RT, and most of the NH_3 gas and H_2O molecular are removed by vacuum in 5 h, but not completely recover to the original phase, *Fm-3m.* The reason is unclear now. Moreover, the sorption atmosphere also has some effect on the structure change, i.e. the structure changed after adsorbing NH_3 including atmosphere (8 vol%), however, in the case of the pure NH_3 atmosphere, the change happened when the equilibrium pressure over 0.5 bar, i.e. exceed of ~50 vol% NH_3. Furthermore, compared to isotherm results of CoHCCo, ZnHCCo presents relative higher sorption capacity and easier desorption ability by pressure swing in the case of 100 $^{\circ}$C, reach to 11.62 mmol/kg at equilibrium pressure ~1 bar, and can desorb most of adsorbed NH_3 gas at the pressure of 0.1 bar. This unique sorption property was also ascribed to the structural change and has been demonstrated by the PXRD patterns, see Fig. 4-6. It clearly shows the structure changed after adsorbed NH_3 including atmosphere at 100 $^{\circ}$C, and the structure not recover to the original at 200 $^{\circ}$C in vacuum for 5 min, shows no clear change according to the XRD patterns compared to sorption and desorption at a higher temperature. Maybe the desorption time was too short. Although it needs a further study about the desorption time, it is possible to develop adsorbents which can be applied in the TSA or PSA process only by metal substitution in PB analogues was found.

In the case of 150 $^{\circ}$C, ZnHCCo also shows good desorption ability, overlapped with the sorption curve, so difference with other conditions. The sorption capacity is also relative higher, reach to 3.67 mmol/g at equilibrium around 1 bar. Interestingly, the sorption isotherm presents similar the same shape with RT at 250 $^{\circ}$C, however, the structure change happened when the equilibrium pressure over 0.9 bar, i.e. exceed of ~90 vol% NH_3. After the isotherm test, the morphology of ZnHCCo was also checked by SEM, no obvious shape changes compared to the as-synthesized sample (see Fig. 4-7), even the structure changed after adsorption.

According to the sorption results, the sorption capacity of ZnHCCo was compared to other typical ammonia sorbents at similar the same conditions. Fig. 4-8(a) illustrates the sorption capacity of other typical sorbents except for CoHCCo apparently lower than that of ZnHCCo at RT. Furthermore, according to the study of Chapter 3, Amberlyst-15 showed a large capacity of

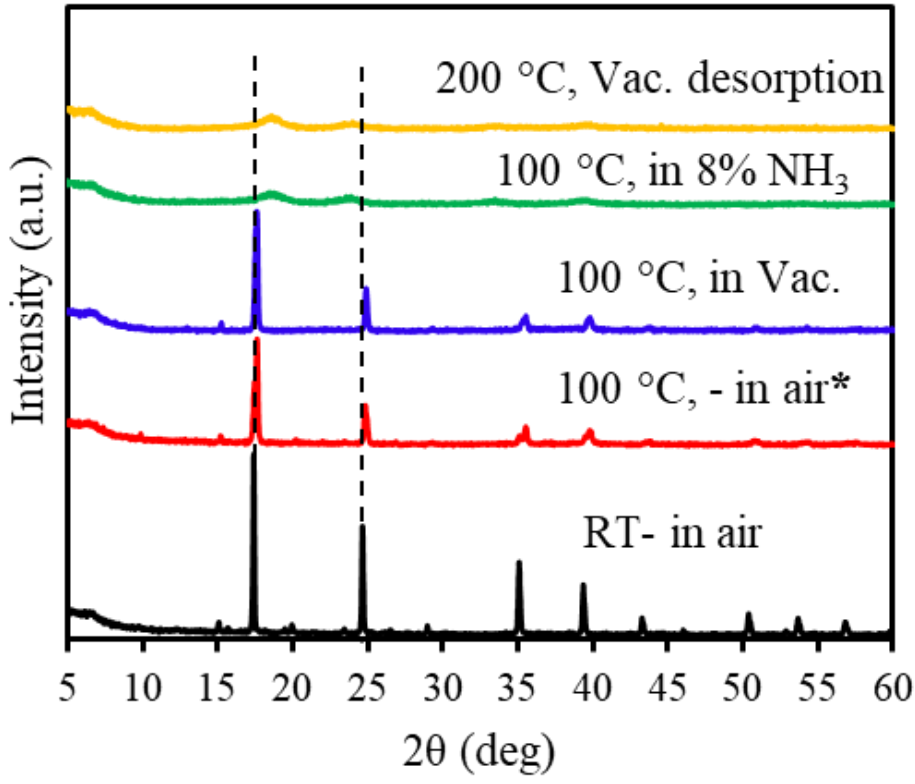

Fig. 4-6 PXRD patterns of ZnHCCo with variations of temperature and atmosphere. The notation for atmosphere "in air" and "in 8% NH_3" represent using laboratory air, and a mixed atmosphere of laboratory air and NH_3 air to make 8 v% of the NH_3 concentration. The broken lines represent the peak positions at room temperature in air.

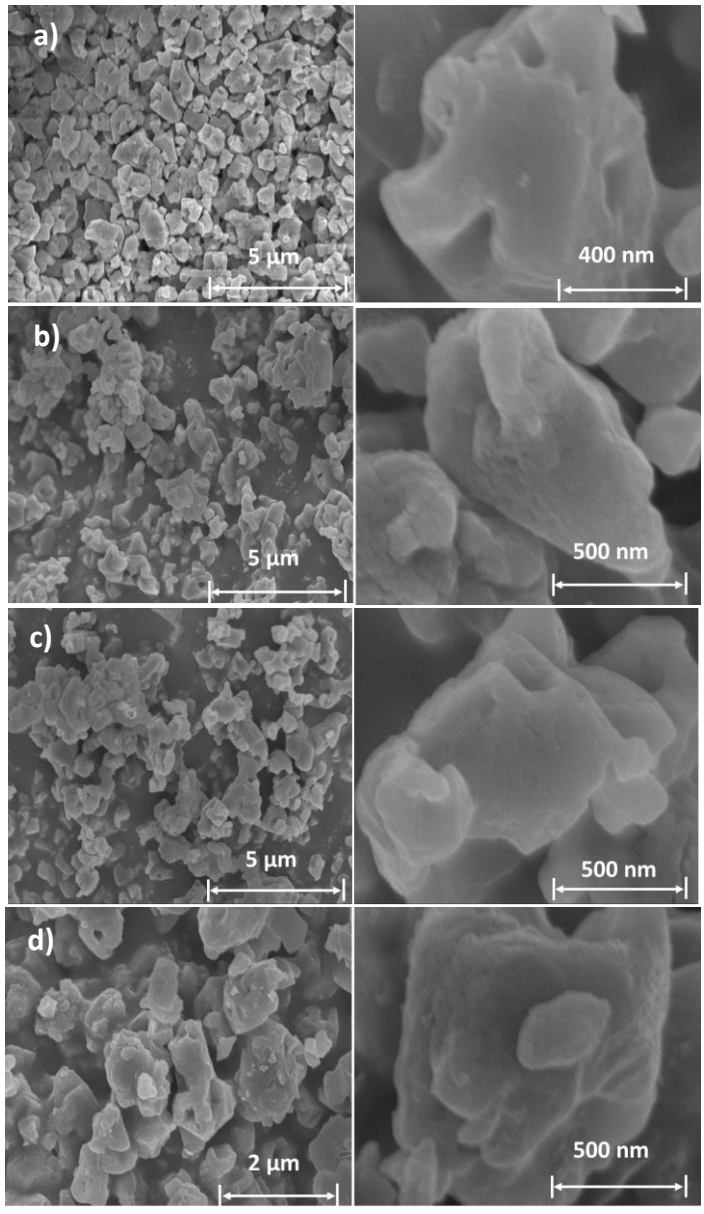

Fig. 4-7 SEM morphology of ZnHCCo. a) as synthesized, b) after adsorption & desorption at 100 °C, c) after adsorption and desorption at 150 °C, d) after adsorption and desorption at 250 °C using the BELSORP-max.

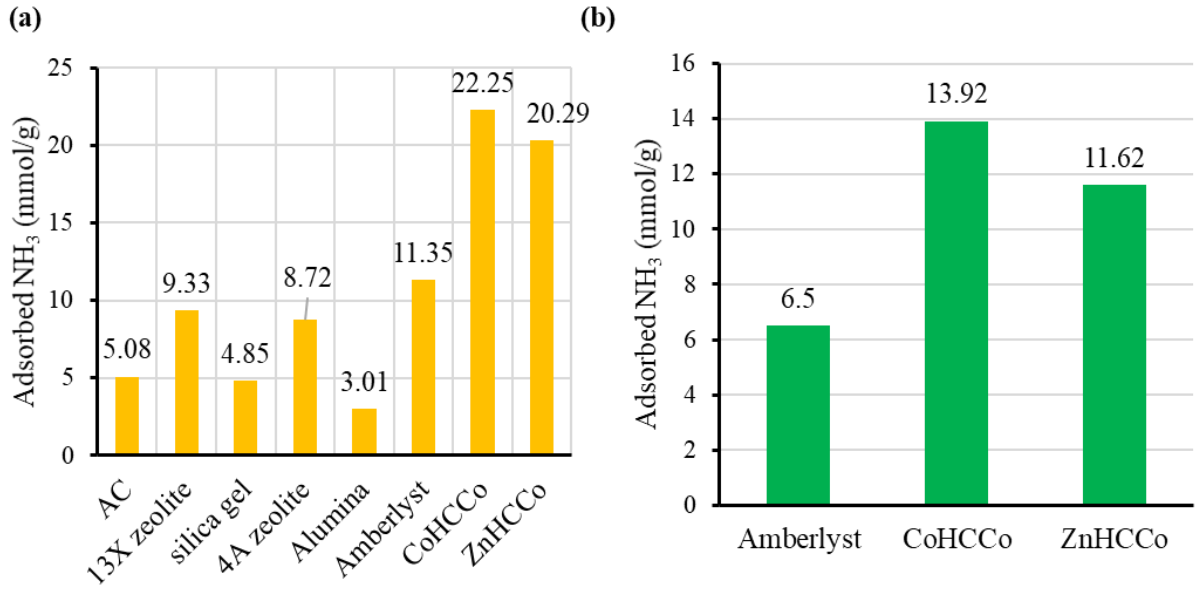

Fig. 4-8 a) Compare with the ammonia adsorption capacity of other typical sorbents at RT (ZnHCCo and CoHCCo was set at 20 °C, others[176] was 25 °C). b) Compare with the ammonia adsorption capacity of other typical sorbents at 100 °C. All data was measured around the equilibrium pressure 1 bar.

ammonia at 100 °C, hence, ZnHCCo was only compared to the Amberlyst-15 and CoHCCo at 100 °C around 1 bar (Fig. 4-8(b)), combined the result at RT, both presenting the ammonia sorption capacity of ZnHCCo just shows a little lower than that of CoHCCo, and clearly outstrips other typical adsorbents in a wide range of working temperatures.

4.3.4 Recyclability evaluation

Fig. 4-9 shows ammonia gas can be desorbed well in adsorbed ZnHCCo at 250 °C and ZnHCCo has similar good performance to the recyclability of CoHCCo, i.e. most of the adsorbed ammonia gas could be desorbed at higher temperature in air, 250 °C, however, a little was left maybe the vacancy site, also seems to work as the same property to CoHCCo. The difference coming from the structure change after adsorbing NH_3 gas (NH_3 including atmosphere), consistent with the results of PXRD measurement (See Fig. 4-1(c)), as the position of CN^- peak changed from 2173 cm^{-1} (before) to 2121 cm^{-1} (after) adsorption, and the shape is also changed largely compared to before, furthermore, the structure is not recovered to the same before, also consistent with the results of PXRD measurement (See Fig. 4-5 and 4-6). In addition, Fig. 4-9 also shows two kinds of adsorption sites for NH_3 gas molecular in ZnHCCo, similar with CoHCCo, i.e. NH_3 gas molecules can be adsorbed at vacancy site (NH_3(v)) and interstitial site (NH_3(i)), and the adsorbed ammonia at the vacancy sites cannot be desorbed effectively even at the HT 250 °C.

Fig. 4-10 shows there are also two peaks appeared clearly after sorption ammonia gas (NH_3 including atmosphere), consistent with the result of FT-IR test in Fig. 4-9 by flowing ammonia gas stream, and illustrates the part 2 (NH_3(i)) of ammonia gas can be absolutely desorbed at 100 °C by flowing dry N_2, however, most of part 1 (NH_3(v)) is also left, indicating there are also two sorption sites existing, maybe vacancy and interstitial sites, even the structure changed after ammonia sorption. Furthermore, compared with the IR result of CoHCCo, it clearly shows there is almost no the form of NH_4^+(i) after sorption ammonia gas stream, indicating the interaction force between Zn (II) and NH_3 molecules is stronger than that of between Co (II) and NH_3 molecules. R. Gilson et al. also indicated the pK_a value of $[Co(OH_2)_6]^{3+}$ 2.9 is less than that of $[Zn(OH_2)_6]^{2+}$ 9.5 [212], meaning water ligands in CoHCCo are easier to release proton H^+, which lead to the adsorbed NH_3 gas molecules always transform to the form of NH_4^+.

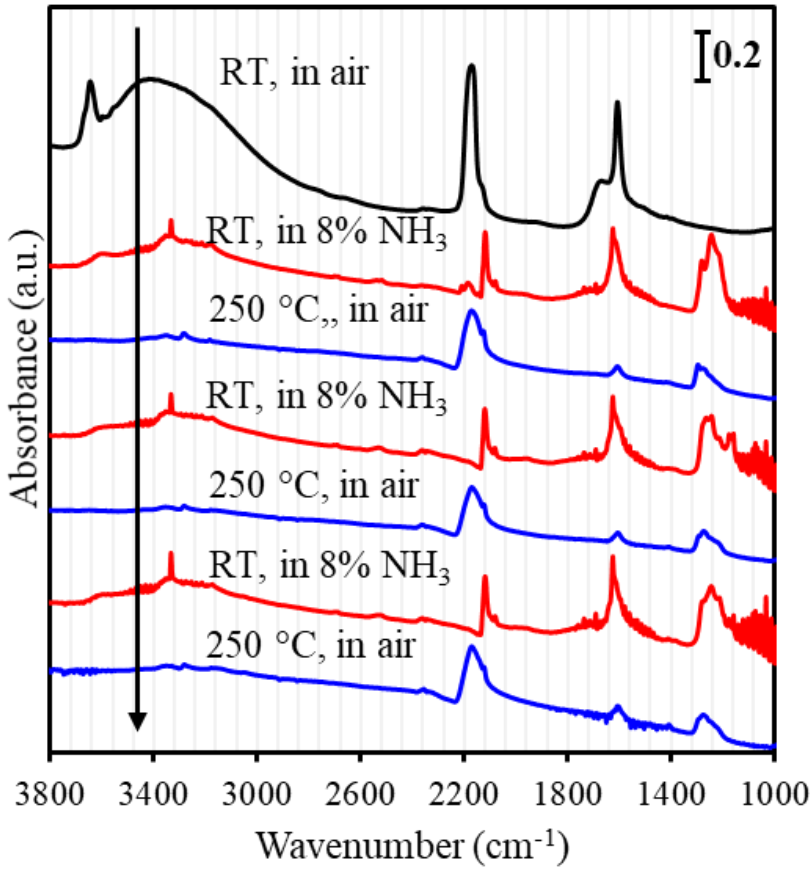

Fig. 4-9 IR spectra for recyclability test (3 cycles) of ammonia adsorption and desorption of ZnHCCo at the heating temperature range changing between ambient temperature (23°C) and 250 °C (RH: ~ϟ0% in Lab., eye-guide: Absorbance scale = 0.2).

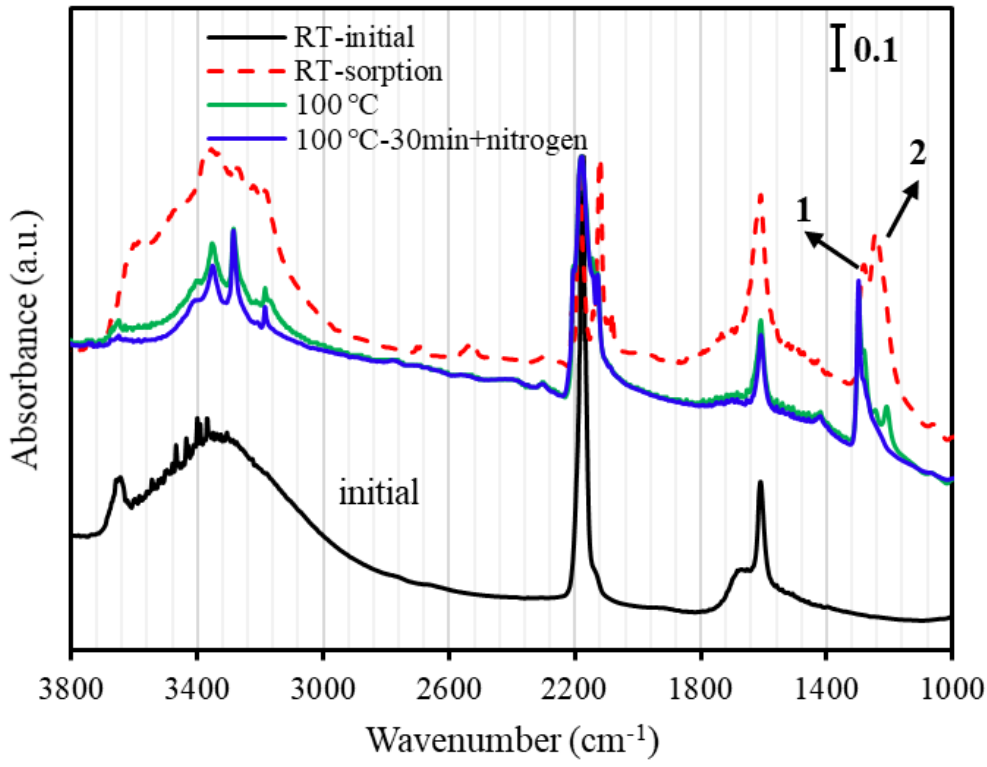

Fig. 4-10 IR spectra for ZnHCCo with ammonia adsorption at ambient temperature (RT: 23 °C, RH: 34%), and desorbed NH_3 gas by heating and flowing dry N_2 at 100 °C (eye guide: Absorbance scale = 0.1).

In addition, it also demonstrated that with increasing the heating temperature, the desorption efficiency can be improved combined with the result of desorption process using IR at 250 °C, i.e. the temperature swing adsorption (TSA) can also be employed using ZnHCCo to adsorb/desorb NH_3 gas for practical applications in the field of ammonia recovery. More importantly, we know the desorption can also be realized at moderate working temperature (100 °C) accompanied by flowing dry N_2 in short time, compared to desorb NH_3 gas at 250 °C, it can save more energy.

4.3.5 Humidity

Fig. 4-11 (a) shows ZnHCCo has a strong affinity to NH_3 even exposed in a high humid atmosphere (RH=~76%), even though exposure in air overnight, the adsorbed NH_3 gas was not transformed to the form of NH_4^+. In contrast, in the case of CoHCCo, the IR test result as shown in Fig. 4-11 (b), all of sorbed NH_3 is converted to NH_4^+, similar the same to the NH_3 adsorbed PB in ambient air, showed that NH_3 transform to the form of NH_4^+ even experienced 15 minutes when exposure in the ambient atmosphere [110]. Furthermore, the shape of the NH_3 peak is nearly no change even after flowing moderate humidity, indicating ZnHCCo has good selectivity to NH_3 gas molecule under the atmosphere with moderate humidity, which is also consistent with the ammonia gas stream sorption results by IR test (see Fig. 4-9 and 4-10). However, the structure change cannot clearly see after adsorption the same ammonia atmosphere using different sorption method as above described. The difference property in NH_3 gas sorption with moderate humidity reflected by IR test between CoHCCo and ZnHCCo at RT, indicating ZnHCCo with dimorphic characteristics has unique gaseous ammonia adsorption behaviour, i.e. ZnHCCo have stronger interreact force with NH_3 gas molecules under the conditions of moderate humid atmosphere, but desorption can be realized according to the isotherm measurement and IR test, especially desorption at 100 °C by pressure swing or companied by flowing dry N_2.

4.4 Summary

In this study, isotherms and IR test for ammonia gas sorption and desorption using ZnHCCo in the temperature range from 20 °C to 250 °C below 1 bar were discussed. Compared to our previous study on CoHCCo, ZnHCCo showed special characteristics in ammonia sorption and desorption processes at moderate working temperatures, in particular, at 100 °C. Moreover, the effect of

moderate humidity (RH=~76%) on the state of adsorbed ammonia in ZnHCCo illustrated ammonia adsorbed ZnHCCo is more durable to humidity atmosphere than that of CoHCCo at the same working conditions. In addition, as a cost-effective element Zn compared to Co, hence ZnHCCo can be one good potential candidate for recover ammonia gas under the atmosphere with moderate humidity at moderate working temperatures. In future work, PAS process using ZnHCCo at different humid and ammonia concentration conditions will be systematically studied.

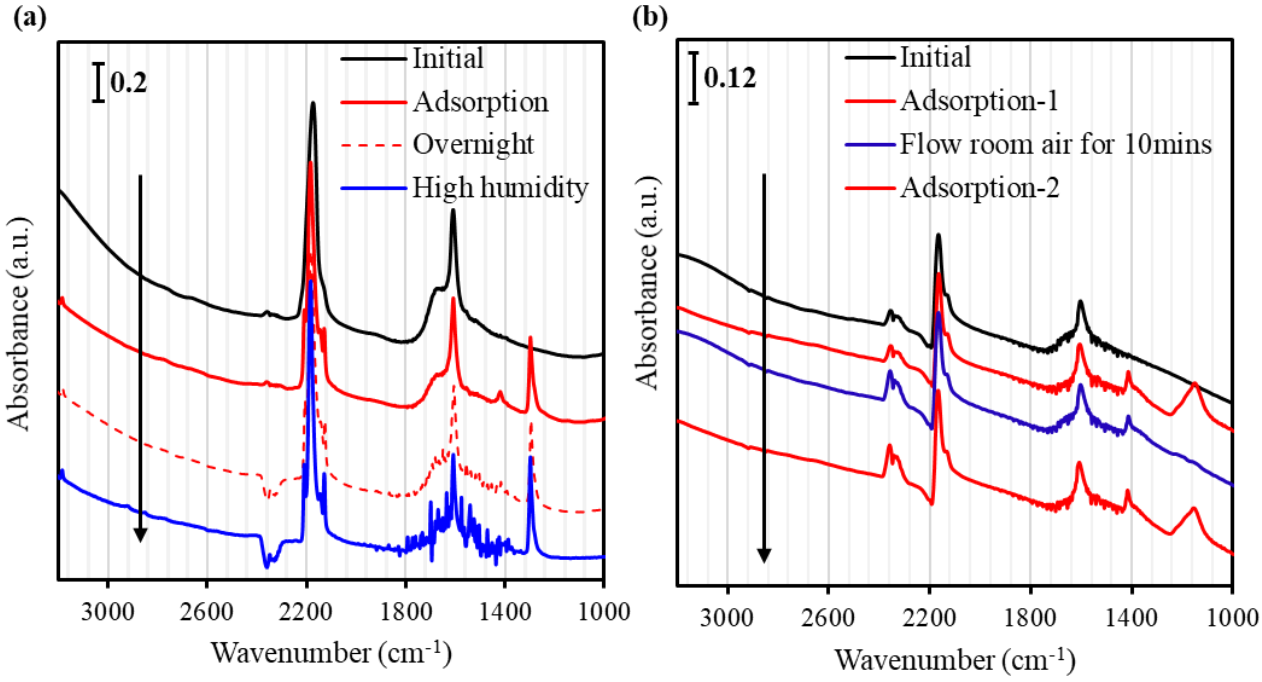

Fig. 4-11 IR spectra for ammonia adsorption and flow room air with high humidity on the NH_3 adsorbed ZnHCCo a) and CoHCCo b) at RT (RT: 23 °C, RH: ~76%).

.

Chapter 5 Conclusions

In this study, PB-based adsorbents were developed targeting ammonia removal/recovery from wastewater and NH_3-containing atmosphere. The results from the effect of high sodium salt concentration on dissolved ammonia sorption indicated the developed adsorbent NaCoHCF has the highest sorption capacity (q_{max}) of 4.36 mol/kg compared to other commercial adsorbents, especially about 40 times higher than zeolite under the aqueous solutions with high sodium salt concentration (9,350 mg/L) which the sodium salt concentration was set as the same to the artificial seawater. The high sorption capacity is attributable to its higher selectivity to NH_4^+, providing important references for NH_4^+ removal/recovery from the sea water. CoHCCo and ZnHCCo were also developed and evaluated for gaseous NH_3 capture/recovery from 8 vol% NH_3 atmosphere when operation temperature varied from 20 to 250 °C. The highest NH_3 sorption capacities of CoHCCo were 25.2, 18.6, 8.6, and 2.1 mmol/g at 20, 100, 150, and 250 °C, respectively. The decomposition temperature of CoHCCo and ZnHCCo can reach around 300 and 350 °C, respectively, even under pure air and room air conditions, and both have similar the same sorption capacity under the same working conditions. However, other typical sorbents, such as mostly MOFs would be corrupted after NH_3 sorption at a high working temperature under the atmosphere of pure air or room air. Also, CoHCCo could keep its stable structure even after adsorbing 8 vol% NH_3 atmosphere at a wide working temperature (~250 °C). CoHCCo and ZnHCCo have good recyclability during the sorption-desorption process by TSA. Besides, ZnHCCo can also be recycled by PSA at high working temperature (100 °C), indicating ZnHCCo has unique sorption properties at moderate high working temperature. Furthermore, ZnHCCo can keep NH_3 form well under a moderate humid atmosphere (RH=~76%). It is very meaningful to utilize TSA or PSA process to desorb the adsorbed NH_3 as the desorbed NH_3 can be easily used as fuels or clean energy H_2 carrier.

Results from this study imply that the new adsorbents, PB analogues, could provide an effective solution for NH_4^+ removal from wastewater or for ammonia recovery from exhaust gas containing NH_3 due to their much higher sorption capacity and selectivity, and for NH_3 capture/recovery in the field of wastewater treatment and air pollution control. As NH_3 can be used as fuels and H_2 carrier, the developed adsorbents can be very promising in the hydrogen energy

field. This study also provides a cost-effective method to alleviate ammonia pollution caused by excessive use of fertilizer and large-scale ammonia production. Further research efforts are still necessary for recycling and re-utilization of the adsorbents and confirmation of NH_3 recovery efficiency in the presence of other trace gases and humidity.

References

[1] S.D. Hafner, J.J. Bisogni, W.J. Jewell, Measurement of un-ionized ammonia in complex mixtures, Environ. Sci. Technol. 40 (2006) 1597–1602. doi:10.1021/es051638j.

[2] A.M. Fan, V.E. Steinberg, Health implications of nitrate and nitrite in drinking water: An update on methemoglobinemia occurrence and reproductive and developmental toxicity, Regul. Toxicol. Pharmacol. 23 (1996) 35–43. doi:10.1006/rtph.1996.0006.

[3] J.N. Galloway, F.J. Dentener, D.G. Capone, E.W. Boyer, R.W. Howarth, S.P. Seitzinger, G.P. Asner, C.C. Cleveland, P.A. Green, E.A. Holland, D.M. Karl, A.F. Michaels, J.H. Porter, A.R. Townsend, C.J. Vörösmarty, Nitrogen cycles : past , present , and future, Biogeochemistry 70 (2004) 153–226. doi:10.1007/s10533-004-0370-0.

[4] R.W. Howarth, Coastal nitrogen pollution: A review of sources and trends globally and regionally, Harmful Algae 8 (2008) 14–20. doi:10.1016/J.HAL.2008.08.015.

[5] L. Olsen, M. Holmer, Y. Olsen, Perspectives of nutrient emission from fish aquaculture in coastal waters. Literature review with evaluated state of knowledge, 66FHF Project No. 542014, FHF–Fishery and Aquaculture Industry Research Fund, 2008.

[6] European Environment Agency, Ammonia (NH_3) emissions, 2010. https://www.eea.europa.eu/data-and-maps/indicators/eea-32-ammonia-nh3-emissions-1 (accessed January 7, 2019).

[7] O. Elishav, G. Tvil, B. Mosevitzky, D. Lewin, G.E. Shter, G.S. Grader, The nitrogen economy: The feasibility of using nitrogen-based alternative fuels, Energy Procedia 135 (2017) 3–13. doi:10.1016/j.egypro.2017.09.482.

[8] C. Zamfirescu, I. Dincer, Ammonia as a green fuel and hydrogen source for vehicular applications, Fuel Process. Technol. 90 (2009) 729–737. doi:10.1016/J.FUPROC.2009.02.004.

[9] W. Wang, J.M. Herreros, A. Tsolakis, A.P.E. York, Ammonia as hydrogen carrier for transportation; Investigation of the ammonia exhaust gas fuel reforming, Int. J. Hydrogen Energy 38 (2013) 9907–9917. doi:10.1016/j.ijhydene.2013.05.144.

[10] J.O. Jensen, A.P. Vestbø, Q. Li, N.J. Bjerrum, The energy efficiency of onboard hydrogen storage, J. Alloys Compd. 446–447 (2007) 723–728. doi:10.1016/J.JALLCOM.2007.04.051.

[11] S.F. Yin, B.Q. Xu, X.P. Zhou, C.T. Au, A mini-review on ammonia decomposition catalysts for on-site generation of hydrogen for fuel cell applications, Appl. Catal. A Gen. 277 (2004) 1–9. doi:10.1016/J.APCATA.2004.09.020.

[12] V.K. Gupta, H. Sadegh, M. Yari, R. Shahryari Ghoshekandi, B. Maazinejad, M. Chahardori, Removal of ammonium ions from wastewater: A short review in development of efficient methods, Glob. J. Environ. Sci. Manag. 1 (2015) 149–158. doi:10.7508/gjesm.2015.02.007.

[13] G. Tchobanoglous, F.L. Franklin L. Burton, H.D. Stensel, Metcalf & Eddy., Wastewater engineering : treatment and reuse, McGraw-Hill, 2003. https://books.google.co.jp/books/about/Wastewater_Engineering_Treatment_and_Reu.html?id=L1MAXTAkL-QC&redir_esc=y (accessed August 23, 2018).

[14] NiraliKansara, L. Bhati, M. Narang, R.Vaishnavi, Wastewater treatment by ion exchange method: a review of past and recent researches, Environ. Sci. An Indian J. 12 (n.d.). http://www.tsijournals.com/abstract/wastewater-treatment-by-ion-exchange-method-a-review-of-past-and-recent-researches-3001.html (accessed September 4, 2018).

[15] A. Amini, The sustainability of ion exchange water treatment technology [D], University of South Florida, 2017. http://scholarcommons.usf.edu/etdhttp://scholarcommons.usf.edu/etd/6640 (accessed October 9, 2018).

[16] A.G. Capodaglio, P. Hlavńek, M. Raboni, A.G. Capodaglio, P. Hlavńek, M. Raboni, Physico-chemical technologies for nitrogen removal from wastewaters: a review, Ambient. e Agua - An Interdiscip. J. Appl. Sci. 10 (2015) 481–498. doi:10.4136/ambi-agua.1618.

[17] P.Y. Yang, Z. Zhang, Nitrification and denitrification in the wastewater treatment system. In Proceedings of the UNESCO—University of Tsukuba International Seminar on Traditional

Technology for Environmental Conservation and Sustainable Development in the Asian-Pacific Region, Tsukuba Science City, Japan, 11–14 December 1995.

[18] S. B, K. Beebi. Sk, Bioremediation of ammonia from polluted waste waters- A review, Am. J. Microbiol. Res. 2 (2014) 201–210. doi:10.12691/ajmr-2-6-6.

[19] K.A. Third, A.O. Sliekers, J.G. Kuenen, M.S.M. Jetten, The CANON system (Completely Autotrophic Nitrogen-removal over nitrite) under ammonium limitation: Interaction and competition between three groups of bacteria, Syst. Appl. Microbiol. 24 (2001) 588–596. doi:10.1078/0723-2020-00077.

[20] W.R.L. van der Star, W.R. Abma, D. Blommers, J.-W. Mulder, T. Tokutomi, M. Strous, C. Picioreanu, M.C.M. van Loosdrecht, Startup of reactors for anoxic ammonium oxidation: Experiences from the first full-scale anammox reactor in Rotterdam, Water Res. 41 (2007) 4149–4163. doi:10.1016/J.WATRES.2007.03.044.

[21] A. Mosquera-Corral, F. González, J.L. Campos, R. Méndez, Partial nitrification in a SHARON reactor in the presence of salts and organic carbon compounds, Process Biochem. 40 (2005) 3109–3118. doi:10.1016/j.procbio.2005.03.042.

[22] J. van de Vossenberg, J.E. Rattray, W. Geerts, B. Kartal, L. van Niftrik, E.G. van Donselaar, J.S. Sinninghe Damsté, M. Strous, M.S.M. Jetten, Enrichment and characterization of marine anammox bacteria associated with global nitrogen gas production, Environ. Microbiol. 10 (2008) 3120–3129. doi:10.1111/j.1462-2920.2008.01643.x.

[23] J. Nakajima, M. Sakka, T. Kimura, K. Furukawa, K. Sakka, Enrichment of anammox bacteria from marine environment for the construction of a bioremediation reactor, Appl. Microbiol. Biotechnol. 77 (2008) 1159–1166. doi:10.1007/s00253-007-1247-7.

[24] P. Cannavo, A. Richaume, F. Lafolie, Fate of nitrogen and carbon in the vadose zone: in situ and laboratory measurements of seasonal variations in aerobic respiratory and denitrifying activities, Soil Biol. Biochem. 36 (2004) 463–478. doi:10.1016/j.soilbio.2003.10.023.

[25] J. Dosta, I. Fernández, J.R. Vázquez-Padín, A. Mosquera-Corral, J.L. Campos, J. Mata-Álvarez, R. Méndez, Short- and long-term effects of temperature on the Anammox process, J. Hazard. Mater. 154 (2008) 688–693. doi:10.1016/j.jhazmat.2007.10.082.

[26] Z. Salem, H. Lebik, W.K. Cherafa, K. Allia, Valorisation of olive pits using biological denitrification, Desalination. 204 (2007) 72–78. doi:10.1016/J.DESAL.2006.04.025.

[27] J. Shen, R. He, W. Han, X. Sun, J. Li, L. Wang, Biological denitrification of high-nitrate wastewater in a modified anoxic/oxic-membrane bioreactor (A/O-MBR), J. Hazard. Mater. 172 (2009) 595–600. doi:10.1016/j.jhazmat.2009.07.045.

[28] O. Moradi, The removal of ions by functionalized carbon nanotube: Equilibrium, isotherms and thermodynamic studies, Chem. Biochem. Eng. Q. 25 (2011) 229–240.

[29] M.A.A. Nasehir Khan E M Yahaya, Ismail Abustan, Muhamad Faizal Pakir Mohamed Latiff, Olugbenga Solomon Bello, Fixed-bed column study for Cu (II) removal from aqueous solutions using rice husk based activated carbon, Int. J. Eng. Technol. 11 (2011) 186–190. https://www.researchgate.net/publication/285169739 (accessed September 1, 2018).

[30] S. Balci, Y. Dinçel, Ammonium ion adsorption with sepiolite: Use of transient uptake method, Chem. Eng. Process. 41 (2002) 79–85. doi:10.1016/S0255-2701(01)00104-0.

[31] P. Vassileva, P. Tzvetkova, R. Nickolov, Removal of ammonium ions from aqueous solutions with coal-based activated carbons modified by oxidation, Fuel. 88 (2009) 387–390. doi:10.1016/J.FUEL.2008.08.016.

[32] H. Huang, X. Xiao, B. Yan, L. Yang, Ammonium removal from aqueous solutions by using natural Chinese (Chende) zeolite as adsorbent, J. Hazard. Mater. 175 (2010) 247–252. doi:10.1016/J.JHAZMAT.2009.09.156.

[33] Y. He, H. Lin, Y. Dong, Q. Liu, L. Wang, Simultaneous removal of ammonium and phosphate by alkaline-activated and lanthanum-impregnated zeolite, Chemosphere. 164 (2016) 387–395. doi:10.1016/j.chemosphere.2016.08.110.

[34] E. Otal, L.F. Vilches, Y. Luna, R. Poblete, J.M. García-Maya, C. Fernández-Pereira, Ammonium ion adsorption and settleability improvement achieved in a synthetic zeolite-amended activated sludge, Chinese J. Chem. Eng. 21 (2013) 1062–1068. doi:10.1016/S1004-9541(13)60566-2.

[35] X. Cui, H. Hao, C. Zhang, Z. He, X. Yang, Capacity and mechanisms of ammonium and cadmium sorption on different wetland-plant derived biochars, Sci. Total Environ. 539 (2016) 566–575. doi:10.1016/J.SCITOTENV.2015.09.022.

[36] Y. Zheng, Y. Liu, A. Wang, Fast removal of ammonium ion using a hydrogel optimized with response surface methodology, Chem. Eng. J. 171 (2011) 1201–1208. doi:10.1016/J.CEJ.2011.05.026.

[37] J.P. Bassin, M. Pronk, R. Kraan, R. Kleerebezem, M.C.M. van Loosdrecht, Ammonium adsorption in aerobic granular sludge, activated sludge and anammox granules, Water Res. 45 (2011) 5257–5265. doi:10.1016/j.watres.2011.07.034.

[38] X. Yu, C. Wan, Z. Lei, X. Liu, Y. Zhang, J.H. Tay, D.-J. Lee, Use of aerobic granules for treating synthetic high-strength ammonium wastewaters, Environ. Technol. 35 (2014) 1785–1790. doi:10.1080/09593330.2014.882992.

[39] M. Suneetha, K. Ravindhranath, Removal of ammonia from polluted waters using biosorbents derived from powders of leaves, stems or barks of some plants, Der Pharma Chem. 4 (2012) 214–227. www.derpharmachemica.com (accessed September 1, 2018).

[40] Z.Z. Ismail, U. Tezel, S.G. Pavlostathis, Sorption of quaternary ammonium compounds to municipal sludge, Water Res. 44 (2010) 2303–2313. doi:10.1016/J.WATRES.2009.12.029.

[41] J.K. Rosenjeld, Ammonium adsorption in nearshore anoxic sediments, Ltmnol. Ocean. 24 (1979) 356–364. https://aslopubs.onlinelibrary.wiley.com/doi/pdf/10.4319/lo.1979.24.2.0356 (accessed September 1, 2018).

[42] R.I. Masel, Principles of adsorption and reaction on solid surfaces, Wiley Interscience., 1996. https://cds.cern.ch/record/643993/files/0471303925_TOC.pdf (accessed September 4, 2018).

[43] H. Freundlich, Die Bedeutung der Kapillarchemie für technische und physiologische Fragen, Zeitschrift Für Angew. Chemie. 22 (1909) 1393–1395. doi:10.1002/ange.19090222802.

[44] P.R.H. Paul R. Haddad, Chapter 2 An introduction to ion-exchange methods, in: J. Chromatogr. Libr., Elsevier, 1990: pp. 15–27. doi:10.1016/S0301-4770(08)61134-3.

[45] J. Wang, K. Wu, The design for ion exchange column, 2015. https://www.oasen.nl/files/imported-ion-exchange-research-project (accessed September 4, 2018).

[46] F.G. Helfferich, Ion exchange, Dover Publications, 1995. https://books.google.com/books?id=F9OQMEA88CAC (accessed September 5, 2018).

[47] T.C. Jorgensen, Removal of ammonia from wastewater by ion exchange in the presence of organic compounds, University of Canterbury Christchurch, New Zealand, 2000. http://citeseerx.ist.psu.edu/viewdoc/download?doi=10.1.1.1029.2183&rep=rep1&type=pdf (accessed August 22, 2018).

[48] S.J. Juutilainen, P.A. Simell, A.O.I. Krause, Zirconia: Selective oxidation catalyst for removal of tar and ammonia from biomass gasification gas, Appl. Catal. B Environ. 62 (2006) 86–92. doi:10.1016/j.apcatb.2005.05.009.

[49] W. Wang, N. Padban, Z. Ye, A. Andersson, I. Bjerle, Kinetics of ammonia decomposition in hot gas ceaning, Ind. Eng. Chem. Res. 38 (1999) 4175–4182. doi:10.1021/ie990337d.

[50] C. Petit, T.J. Bandosz, Exploring the coordination chemistry of MOF–graphite oxide composites and their applications as adsorbents, Dalt. Trans. 41 (2012) 4027. doi:10.1039/c2dt12017h.

[51] G. Leson, A.M. Winer, Biofiltration: An innovative air pollution control technology for voc emissions, J. Air Waste Manag. Assoc. 41 (1991) 1045–1054. doi:10.1080/10473289.1991.10466898.

[52] E. Smet, H. Van Langenhove, K. Maes, Abatement of high concentrated ammonia loaded waste gases in compost biofilters, Water. Air. Soil Pollut. 119 (2000) 177–190. doi:10.1023/A:1005186327201.

[53] Y.C. Chung, Y.Y. Lin, C.P. Tseng, Removal of high concentration of NH_3 and coexistent H_2S by biological activated carbon (BAC) biotrickling filter, Bioresour. Technol. 96 (2005) 1812–1820. doi:10.1016/j.biortech.2005.01.003.

[54] Wei-Hsin Chen, Atmospheric ammonia scavenging mechanisms around a liquid droplet in convective flow, Atmos. Environ. 38 (2004) 1107–1116. https://works.bepress.com/wei-hsin_chen/35/ (accessed October 9, 2018).

[55] K. Terasaka, J. Oka, H. Tsuge, Ammonia absorption from a bubble expanding at a submerged orifice into water, Chem. Eng. Sci. 57 (2002) 3757–3765. doi:10.1016/S0009-2509(02)00308-1.

[56] X. Guo, J. Tak, R.L. Johnson, Ammonia removal from air stream and biogas by a H_2SO_4 impregnated adsorbent originating from waste wood-shavings and biosolids, J. Hazard. Mater. 166 (2009) 372–376. doi:10.1016/j.jhazmat.2008.11.028.

[57] P.F. Siril, H.E. Cross, D.R. Brown, New polystyrene sulfonic acid resin catalysts with enhanced acidic and catalytic properties, J. Mol. Catal. A Chem. 279 (2008) 63–68. doi:10.1016/j.molcata.2007.10.001.

[58] J. Helminen, J. Helenius, E. Paatero, I. Turunen, Comparison of sorbents and isotherm models for NH_3-gas separation by adsorption, AIChE J. 46 (2000) 1541–1555. doi:10.1002/aic.690460807.

[59] Ram Lavie, Process for the manufacture of ammonia, 1985. https://patents.google.com/patent/US4537760 (accessed September 6, 2018).

[60] C. Zamfirescu, I. Dincer, Ammonia as a green fuel and hydrogen source for vehicular applications, Fuel Process. Technol. 90 (2009) 729–737. doi:10.1016/j.fuproc.2009.02.004.

[61] Z. Tamainot-Telto, S.J. Metcalf, R.E. Critoph, Y. Zhong, R. Thorpe, Carbon–ammonia pairs for adsorption refrigeration applications: ice making, air conditioning and heat pumping, Int. J. Refrig. 32 (2009) 1212–1229. doi:10.1016/J.IJREFRIG.2009.01.008.

[62] M.E.E. Abashar, Ultra-clean hydrogen production by ammonia decomposition, J. King Saud Univ. - Eng. Sci. 30 (2018) 2–11. doi:10.1016/j.jksues.2016.01.002.

[63] S. Choi, J.H. Drese, C.W. Jones, Adsorbent materials for carbon dioxide capture from large anthropogenic point sources, ChemSusChem. 2 (2009) 796–854. doi:10.1002/cssc.200900036.

[64] P.K. Thallapally, R.K. Motkuri, C.A. Fernandez, B.P. McGrail, G.S. Behrooz, Prussian blue analogues for CO_2 and SO_2 capture and separation applications, Inorg. Chem. 49 (2010) 4909–4915. doi:10.1021/ic902397w.

[65] S. Choi, J.H. Drese, C.W. Jones, Adsorbent materials for carbon dioxide capture fromlarge anthropogenic point sources, ChemSusChem. 2 (2009) 796–854. doi:10.1002/cssc.200900036.

[66] A. Arslan, S. Veli, Zeolite 13X for adsorption of ammonium ions from aqueous solutions and hen slaughterhouse wastewaters, J. Taiwan Inst. Chem. Eng. 43 (2012) 393–398. doi:10.1016/j.jtice.2011.11.003.

[67] M.P. Bernal, J.M. Lopez-Real, Natural zeolites and sepiolite as ammonium and ammonia adsorbent materials, Bioresour. Technol. 43 (1993) 27–33. doi:10.1016/0960-8524(93)90078-P.

[68] J.P. Soetardji, J.C. Claudia, Y.-H. Ju, J.A. Hriljac, T.-Y. Chen, F.E. Soetaredjo, S.P. Santoso, A. Kurniawan, S. Ismadji, Ammonia removal from water using sodium hydroxide modified zeolite mordenite, RSC Adv. 5 (2015) 83689–83699. doi:10.1039/C5RA15419G.

[69] L. Lin, Z. Lei, L. Wang, X. Liu, Y. Zhang, C. Wan, D.-J. Lee, J.H. Tay, Adsorption mechanisms of high-levels of ammonium onto natural and NaCl-modified zeolites, Sep. Purif. Technol. 103 (2013) 15–20. doi:10.1016/j.seppur.2012.10.005.

[70] P. Singer, F. Salamanca-Buentello, A. Daar, A. Daar, Harnessing nanotechnology to improve global equity, Issues Sci. Technol. XXI (2005) 57–64.. http://ethics.iit.edu/eelibrary/node/13117 (accessed September 11, 2018).

[71] S. Kilpimaa, H. Runtti, T. Kangas, U. Lassi, T. Kuokkanen, Removal of phosphate and nitrate over a modified carbon residue from biomass gasification, Chem. Eng. Res. Des. 92 (2014) 1923–1933. doi:10.1016/J.CHERD.2014.03.019.

[72] Y. Wang, D. Sun, Phosphate removal from aqueous solutions on fly ash with medium calcium content, Korean J. Chem. Eng. 32 (2015) 1323–1326. doi:10.1007/s11814-014-0342-6.

[73] X. Liu, L. Zhang, Removal of phosphate anions using the modified chitosan beads: Adsorption kinetic, isotherm and mechanism studies, Powder Technol. 277 (2015) 112–119. doi:10.1016/J.POWTEC.2015.02.055.

[74] K.M. Dontsova, L.D. Norton, C.T. Johnston, Calcium and magnesium effects on ammonia adsorption by soil clays, Soil Sci. Soc. Am. J. 69 (2005) 1225–1232. doi:10.2136/sssaj2004.0335.

[75] J. Wu, Y. Chang, H. Gao, R. Yu, Impacts of ammonia on zinc oxide nanoparticle toxicity to *Nitrosomonas europaea*, IOP Conf. Ser. Earth Environ. Sci. 64 (2017) 012114. doi:10.1088/1755-1315/64/1/012114.

[76] H.-L. Lien, Y.-S. Jhuo, L.-H. Chen, Effect of heavy metals on dechlorination of carbon tetrachloride by iron nanoparticles, Environ. Eng. Sci. 24 (2007) 21–30. doi:10.1089/ees.2007.24.21.

[77] A. Chianese, L. Di Palma, E. Petrucci, M. Stoller, G.G. Muradova, S.R. Gadjieva, L. Di Palma, G. Vilardi, Nitrates removal by bimetallic nanoparticles in water, Chem. Eng. Trans. 47 (2016) 205–210. doi:10.3303/CET1647035.

[78] A. Hedström, Ion exchange of ammonium in zeolites: A literature review, J. Environ. Eng. 127 (2001) 673–681. doi:10.1061/(ASCE)0733-9372(2001)127:8(673).

[79] E. Pagans, X. Font, A. Sánchez, Adsorption, absorption, and biological degradation of ammonia in different biofilter organic media, Biotechnol. Bioeng. 97 (2007) 515–525. doi:10.1002/bit.21246.

[80] Kent S. Knaebel, pressure swing adsorption system for ammonia synthesis, 5711926A, 1996. https://patentimages.storage.googleapis.com/63/02/61/40a19a70115eea/US5711926.pdf (accessed August 9, 2018).

[81] Alan A. HaslamWieslaw H. IsalskiTerence R. Tomlinson, Recovery of hydrogen from ammonia synthesis purge gas, 1983. https://patents.google.com/patent/US4380461 (accessed August 12, 2018).

[82] V.I. Isaeva, L.M. Kustov, The application of metal-organic frameworks in catalysis (Review), Pet. Chem. 50 (2010) 167–180. doi:10.1134/S0965544110030011.

[83] S. Ketrat, T. Maihom, S. Wannakao, M. Probst, S. Nokbin, J. Limtrakul, Coordinatively unsaturated Metal–Organic Frameworks $M_3(btc)_2$ (M = Cr, Fe, Co, Ni, Cu, and Zn) catalyzing the oxidation of CO by N_2O: Insight from DFT calculations, Inorg. Chem. 56 (2017) 14005–14012. doi:10.1021/acs.inorgchem.7b02143.

[84] B. Van de Voorde, B. Bueken, J. Denayer, D. De Vos, Adsorptive separation on metal–organic frameworks in the liquid phase, Chem. Soc. Rev. 43 (2014) 5766–5788. doi:10.1039/C4CS00006D.

[85] Y. He, W. Zhou, G. Qian, B. Chen, Methane storage in metal–organic frameworks, Chem. Soc. Rev. 43 (2014) 5657–5678. doi:10.1039/C4CS00032C.

[86] E. Barea, C. Montoro, J.A.R. Navarro, Toxic gas removal – metal–organic frameworks for the capture and degradation of toxic gases and vapours, Chem. Soc. Rev. 43 (2014) 5419–5430. doi:10.1039/C3CS60475F.

[87] Y. Lin, C. Kong, Q. Zhang, L. Chen, Metal-Organic Frameworks for carbon dioxide capture and methane storage, Adv. Energy Mater. 7 (2017) 1601296. doi:10.1002/aenm.201601296.

[88] C.A. Trickett, A. Helal, B.A. Al-Maythalony, Z.H. Yamani, K.E. Cordova, O.M. Yaghi, The chemistry of metal–organic frameworks for CO_2 capture, regeneration and conversion, Nat. Rev. Mater. 2 (2017) 17045. doi:10.1038/natrevmats.2017.45.

[89] M. Ranocchiari, J.A. van Bokhoven, Catalysis by metal–organic frameworks: fundamentals and opportunities, Phys. Chem. Chem. Phys. 13 (2011) 6388. doi:10.1039/c0cp02394a.

[90] A. Dhakshinamoorthy, M. Alvaro, H. Garcia, Metal–organic frameworks as heterogeneous catalysts for oxidation reactions, Catal. Sci. Technol. 1 (2011) 856. doi:10.1039/c1cy00068c.

[91] P. Ghosh, K.C. Kim, R.Q. Snurr, Modeling water and ammonia adsorption in hydrophobic Metal–Organic Frameworks: Single components and mixtures, J. Phys. Chem. C. 118 (2014) 1102–1110. doi:10.1021/jp410758t.

[92] B. Tan, C. Chen, L.-X. Cai, Y.-J. Zhang, X.-Y. Huang, J. Zhang, Introduction of Lewis acidic and Redox-active sites into a porous framework for ammonia capture with visual color response, Inorg. Chem. 54 (2015) 3456–3461. doi:10.1021/acs.inorgchem.5b00023.

[93] J.F. Van Humbeck, T.M. McDonald, X. Jing, B.M. Wiers, G. Zhu, J.R. Long, Ammonia capture in porous organic polymers densely functionalized with Brønsted acid groups, J. Am. Chem. Soc. 136 (2014) 2432–2440. doi:10.1021/ja4105478.

[94] A.J. Rieth, Y. Tulchinsky, M. Dincă, High and reversible ammonia uptake in mesoporous azolate Metal-Organic Frameworks with open Mn, Co, and Ni sites, J. Am. Chem. Soc. 138 (2016) 9401–9404. doi:10.1021/jacs.6b05723.

[95] L. Liu, Y. Zhou, S. Liu, M. Xu, The applications of Metal−Organic Frameworks in electrochemical sensors, ChemElectroChem. 5 (2018) 6–19. doi:10.1002/celc.201700931.

[96] K.S. Park, Z. Ni, A.P. Côté, J.Y. Choi, R. Huang, F.J. Uribe-Romo, H.K. Chae, M. O'Keeffe, O.M. Yaghi, Exceptional chemical and thermal stability of zeolitic imidazolate frameworks., Proc. Natl. Acad. Sci. U. S. A. 103 (2006) 10186–10191. doi:10.1073/pnas.0602439103.

[97] H.K. Chae, D.Y. Siberio-Pérez, J. Kim, Y. Go, M. Eddaoudi, A.J. Matzger, M. O'Keeffe, O.M. Yaghi, A route to high surface area, porosity and inclusion of large molecules in crystals, Nature. 427 (2004) 523–527. doi:10.1038/nature02311.

[98] H. Li, M. Eddaoudi, M. O'Keeffe, O.M. Yaghi, Design and synthesis of an exceptionally stable and highly porous metal-organic framework, Nature. 402 (1999) 276–279. doi:10.1038/46248.

[99] S.S.-Y. Chui, S.M.-F. Lo, J.P.H. Charmant, A.G. Orpen, I.D. Williams, A chemically functionalizable nanoporous material, Science. 283 (1999) 1148–50. doi:10.1126/SCIENCE.283.5405.1148.

[100] D. Saha, S. Deng, Ammonia adsorption and its effects on framework stability of MOF-5 and MOF-177., J. Colloid Interface Sci. 348 (2010) 615–20. doi:10.1016/j.jcis.2010.04.078.

[101] G.W. Peterson, G.W. Wagner, A. Balboa, J. Mahle, T. Sewell, C.J. Karwacki, Ammonia vapor removal by $Cu_3(BTC)_2$ and its characterization by MAS NMR, J. Phys. Chem. C. 113 (2009) 13906–13917. doi:10.1021/jp902736z.

[102] I. Spanopoulos, P. Xydias, C.D. Malliakas, P.N. Trikalitis, A straight forward route for the development of Metal–Organic Frameworks functionalized with aromatic −OH groups: Synthesis, characterization, and gas (N_2, Ar, H_2, CO_2, CH_4, NH_3) sorption properties, Inorg. Chem. 52 (2013) 855–862. doi:10.1021/ic302010e.

[103] C. Petit, T.J. Bandosz, Synthesis, characterization, and ammonia adsorption properties of mesoporous Metal-Organic Framework (MIL(Fe))-graphite oxide composites: Exploring the limits of materials fabrication, Adv. Funct. Mater. 21 (2011) 2108–2117. doi:10.1002/adfm.201002517.

[104] T. Kajiwara, M. Higuchi, A. Yuasa, H. Higashimura, S. Kitagawa, One-dimensional alignment of strong Lewis acid sites in a porous coordination polymer, Chem. Commun. 49 (2013) 10459. doi:10.1039/c3cc43384f.

[105] T. Kajiwara, M. Higuchi, D. Watanabe, H. Higashimura, T. Yamada, H. Kitagawa, A systematic study on the stability of porous coordination polymers against ammonia, Chem. - A Eur. J. 20 (2014) 15611–15617. doi:10.1002/chem.201403542.

[106] A.J. Rieth, M. Dincă, Controlled gas uptake in Metal–Organic Frameworks with record ammonia sorption, J. Am. Chem. Soc. 140 (2018) 3461–3466. doi:10.1021/jacs.8b00313.

[107] D. Parajuli, H. Noguchi, A. Takahashi, H. Tanaka, T. Kawamoto, Prospective application of copper hexacyanoferrate for capturing dissolved ammonia, Ind. Eng. Chem. Res. 55 (2016) 6708–6715. doi:10.1021/acs.iecr.6b00748.

[108] J. Balmaseda, E. Reguera, J. Fernández, A. Gordillo, H. Yee-Madeira, Behavior of Prussian blue-based materials in presence of ammonia, J. Phys. Chem. Solids. 64 (2003) 685–693. doi:10.1016/S0022-3697(02)00378-5.

[109] S. Manakasettharn, A. Takahashi, T. Kawamoto, K. Noda, Y. Sugiyama, T. Nakamura, Highly sensitive and exceptionally wide dynamic range detection of ammonia gas by indium

hexacyanoferrate nanoparticles using FTIR spectroscopy, Anal. Chem. 90 (2018) 4856–4862. doi:10.1021/acs.analchem.8b00359.

[110] A. Takahashi, H. Tanaka, D. Parajuli, T. Nakamura, K. Minami, Y. Sugiyama, Y. Hakuta, S. Ohkoshi, T. Kawamoto, Historical pigment exhibiting ammonia gas capture beyond standard adsorbents with adsorption sites of two kinds, J. Am. Chem. Soc. 138 (2016) 6376–6379. doi:10.1021/jacs.6b02721.

[111] J.N. Galloway, J.D. Aber, J.W. Erisman, S.P. Seitzinger, R.W. Howarth, E.B. Cowling, B.J. Cosby, The nitrogen cascade, Bioscience. 53 (2003) 341–356. doi:10.1641/0006-3568(2003)053[0341:tnc]2.0.co;2.

[112] Aquatic life ambient water quality criteria for ammonia - Freshwater (2013) Fact Sheet, US Environ. Prot. Agency. (2013). https://www.epa.gov/sites/production/files/2015-08/documents/fact_sheet_aquatic-life-ambient-water-quality-criteria-for-ammonia-freshwater-2013.pdf (accessed May 1, 2018).

[113] The environment protection rules, (1986). http://cpcb.nic.in/GeneralStandards.pdf (accessed May 1, 2018).

[114] Maximum allowable discharge concentrations for other pollutants in China. https://chinawaterrisk.org/wp-content/uploads/2011/05/Maximum-Allowable-Discharge-Concentrations-For-Other-Pollutants-in-China.pdf (accessed May 1, 2018).

[115] H. Chen, W. Wang, L. Xue, C. Chen, G. Liu, R. Zhang, Effects of ammonia on anaerobic digestion of food waste: Process performance and microbial community, Energy & Fuels. 30 (2016) 5749–5757. doi:10.1021/acs.energyfuels.6b00715.

[116] O. Yenigün, B. Demirel, Ammonia inhibition in anaerobic digestion: A review, Process Biochem. 48 (2013) 901–911. doi:10.1016/j.procbio.2013.04.012.

[117] A. Malovanyy, H. Sakalova, Y. Yatchyshyn, E. Plaza, M. Malovanyy, Concentration of ammonium from municipal wastewater using ion exchange process, Desalination. 329 (2013) 93–102. doi:10.1016/j.desal.2013.09.009.

[118] D. Guaya, C. Valderrama, A. Farran, C. Armijos, J.L. Cortina, Simultaneous phosphate and ammonium removal from aqueous solution by a hydrated aluminum oxide modified natural zeolite, Chem. Eng. J. 271 (2015) 204–213. doi:10.1016/j.cej.2015.03.003.

[119] X. Li, J. Wang, A.I. Rykov, V.K. Sharma, H. Wei, C. Jin, X. Liu, M. Li, S. Yu, C. Sun, D.D. Dionysiou, Prussian blue/TiO_2 nanocomposites as a heterogeneous photo-Fenton catalyst for degradation of organic pollutants in water, Catal. Sci. Technol. 5 (2015) 504–514. doi:10.1039/C4CY00947A.

[120] X. Li, A.I. Rykov, B. Zhang, Y. Zhang, J. Wang, Graphene encapsulated Fe_xCo_y nanocages derived from metal–organic frameworks as efficient activators for peroxymonosulfate, Catal. Sci. Technol. 6 (2016) 7486–7494. doi:10.1039/C6CY01479H.

[121] X. Li, A.I. Rykov, J. Wang, Hydrazine drastically promoted Fenton oxidation of bisphenol A catalysed by a Fe^{III}–Co Prussian blue analogue, Catal. Commun. 77 (2016) 32–36. doi:10.1016/j.catcom.2016.01.004.

[122] V.D. Neff, Some performance characteristics of a Prussian blue battery, J. Electrochem. Soc. 132 (1985) 1382. doi:10.1149/1.2114121.

[123] M. Okubo, D. Asakura, Y. Mizuno, J.-D. Kim, T. Mizokawa, T. Kudo, I. Honma, Switching Redox-active sites by valence tautomerism in Prussian blue analogues A_x Mn_y $[Fe(CN)_6] \cdot n$ H_2O (A: K, Rb): Robust frameworks for reversible Li storage, J. Phys. Chem. Lett. 1 (2010) 2063–2071. doi:10.1021/jz100708b.

[124] M. Takachi, T. Matsuda, Y. Moritomo, Cobalt hexacyanoferrate as cathode material for na+ secondary battery, Appl. Phys. Express. 6 (2013) 4–7. doi:10.7567/APEX.6.025802.

[125] M. Pasta, R.Y. Wang, R. Ruffo, R. Qiao, H.-W. Lee, B. Shyam, M. Guo, Y. Wang, L.A. Wray, W. Yang, M.F. Toney, Y. Cui, Manganese–cobalt hexacyanoferrate cathodes for sodium-ion batteries, J. Mater. Chem. A. 4 (2016) 4211–4223. doi:10.1039/C5TA10571D.

[126] V.D. Neff, Electrochemical oxidation and reduction of thin films of Prussian blue, J. Electrochem. Soc. 125 (1978) 886–887. doi:10.1149/1.2131575.

[127] L.-C. Chen, Y.-H. Huang, K.-C. Ho, A complementary electrochromic system based on Prussian blue and indium hexacyanoferrate, J. Solid State Electrochem. 7 (2002) 6–10. doi:10.1007/s10008-002-0272-9.

[128] R.J. Kulesza, M.A. Malik, K. Miecznikowski, A. Wolkiewicz, P.J. Kulesza, Countercation-sensitive electrochromism of cobalt hexacyanoferrate films, J. Electrochem. Soc. 143 (1996) L10. doi:10.1149/1.1836374.

[129] T.-C.C. Liao, W.-H.H. Chen, H.-Y.Y. Liao, L.-C.C. Chen, Multicolor electrochromic thin films and devices based on the Prussian blue family nanoparticles, Sol. Energy Mater. Sol. Cells. 145 (2016) 26–34. doi:10.1016/j.solmat.2015.08.004.

[130] E. Kholoud, H. Watanabe, A. Takahashi, M.M. Emara, B.A. Abd-El-Nabey, M. Kurihara, K. Tajima, T. Kawamoto, Cobalt hexacyanoferrate nanoparticles for wet-processed brown–bleached electrochromic devices with hybridization of high-spin/low-spin phases, J. Mater. Chem. C. 5 (2017) 8921–8926. doi:10.1039/C7TC02576A.

[131] W.-R. Cai, G.-Y. Zhang, T. Song, X.-J. Zhang, D. Shan, Cobalt hexacyanoferrate electrodeposited on electrode with the assistance of laponite: The enhanced electrochemical sensing of captopril, Electrochim. Acta. 198 (2016) 32–39. doi:10.1016/j.electacta.2016.03.080.

[132] R. Pauliukaite, M. Florescu, C.M.A. Brett, Characterization of cobalt- and copper hexacyanoferrate-modified carbon film electrodes for redox-mediated biosensors, J. Solid State Electrochem. 9 (2005) 354–362. doi:10.1007/s10008-004-0632-8.

[133] S.S. Kaye, J.R. Long, Hydrogen storage in the dehydrated Prussian blue analogues $M_3[Co(CN)_6]_2$ (M = Mn, Fe, Co, Ni, Cu, Zn), J. Am. Chem. Soc. 127 (2005) 6506–6507. doi:10.1021/ja051168t.

[134] L. Hu, P. Zhang, Q.-W. Chen, J.-Y. Mei, N. Yan, Room-temperature synthesis of Prussian blue analogue $Co_3[Co(CN)_6]_2$ porous nanostructures and their CO_2 storage properties, RSC Adv. 1 (2011) 1574. doi:10.1039/c1ra00624j.

[135] O. Sato, T. Iyoda, A. Fujishima, K. Hashimoto, Photoinduced magnetization of a cobalt-iron cyanide, Science. 272 (1996) 704–705. doi:10.1126/science.272.5262.704.

[136] S.I. Ohkoshi, K. Hashimoto, Design of a novel magnet exhibiting photoinduced magnetic pole inversion based on molecular field theory, J. Am. Chem. Soc. 121 (1999) 10591–10597. doi:10.1021/ja991473c.

[137] V. Escax, a. Bleuzen, C. Cartier dit Moulin, F. Villain, a. Goujon, F. Varret, M. Verdaguer, Photoinduced ferrimagnetic systems in Prussian blue analogues $CI_xCo_4[Fe(CN)_6]_y$ (CI = Alkali Cation). 3. Control of the photo- and thermally induced electron transfer by the $[Fe(CN)_6]$ vacancies in cesium derivatives, J. Am. Chem. Soc. 123 (2001) 12536–12543. doi:10.1021/ja011296r.

[138] A. Takahashi, N. Minami, H. Tanaka, K. Sue, K. Minami, D. Parajuli, K.-M. Lee, S. Ohkoshi, M. Kurihara, T. Kawamoto, Efficient synthesis of size-controlled open-framework nanoparticles fabricated with a micro-mixer: route to the improvement of Cs adsorption performance, Green Chem. 17 (2015) 4228–4233. doi:10.1039/C5GC00757G.

[139] D. Parajuli, A. Kitajima, A. Takahashi, H. Tanaka, H. Ogawa, Y. Hakuta, K. Yoshino, T. Funahashi, M. Yamaguchi, M. Osada, T. Kawamoto, Application of Prussian blue nanoparticles for the radioactive Cs decontamination in Fukushima region, J. Environ. Radioact. 151P1 (2015) 233–237. doi:10.1016/j.jenvrad.2015.10.014.

[140] A. Nilchi, R. Saberi, M. Moradi, H. Azizpour, R. Zarghami, Adsorption of cesium on copper hexacyanoferrate-PAN composite ion exchanger from aqueous solution, Chem. Eng. J. 172 (2011) 572–580. doi:10.1016/j.cej.2011.06.011.

[141] J. Causse, A. Tokarev, J. Ravaux, M. Moloney, Y. Barré, A. Grandjean, Facile one-pot synthesis of copper hexacyanoferrate nanoparticle functionalised silica monoliths for the selective entrapment of 137Cs, J. Mater. Chem. A. 2 (2014) 9461. doi:10.1039/c4ta01266f.

[142] M. Ishizaki, S. Akiba, A. Ohtani, Y. Hoshi, K. Ono, M. Matsuba, T. Togashi, K. Kananizuka, M. Sakamoto, A. Takahashi, T. Kawamoto, H. Tanaka, M. Watanabe, M. Arisaka, T. Nankawa, M. Kurihara, Proton-exchange mechanism of specific Cs+ adsorption via lattice defect sites of Prussian blue filled with coordination and crystallization water molecules, Dalt. Trans. 42 (2013) 16049–55. doi:10.1039/c3dt51637g.

[143] E.R. Nightingale, Phenomenological theory of ion solvation. Effective radii of hydrated ions, J. Phys. Chem. 63 (1959) 1381–1387. doi:10.1021/j150579a011.

[144] A. Takahashi, H. Tanaka, K. Minami, K. Noda, M. Ishizaki, M. Kurihara, H. Ogawa, T. Kawamoto, Unveiling Cs-adsorption mechanism of Prussian blue analogs: Cs+-percolation via vacancies to complete dehydrated state, Subnmitted to J. Phys. Chem. C. (n.d.).

[145] P. Scherrer, No Title, Nachr. Ges. Wiss. Göttingen. 26 (1918) 98.

[146] Y. Moritomo, K. Igarashi, T. Matsuda, J. Kim, Doping-induced structural phasetransition in $Na_{1.6-x}Co[Fe(CN)_6]_{0.90}\cdot 2.9H_2O$, J. Phys. Soc. Japan. 78 (2009) 074602. doi:10.1143/JPSJ.78.074602.

[147] T. Matsuda, J. Kim, Y. Moritomo, Symmetry switch of cobalt ferrocyanideframework by alkaline cation exchange, J. Am. Chem. Soc. 132 (2010) 12206–12207. doi:10.1021/ja105482k.

[148] M. Avila, L. Reguera, J. Rodríguez-Hernández, J. Balmaseda, E. Reguera, Porous framework of $T_2[Fe(CN)_6]\cdot xH_2O$ with T=Co, Ni, Cu, Zn, and H_2 storage, J. Solid State Chem. 181 (2008) 2899–2907. doi:10.1016/j.jssc.2008.07.030.high

[149] S. Adak, L.L. Daemen, M. Hartl, D. Williams, J. Summerhill, H. Nakotte, Thermal expansion in 3d-metal Prussian Blue Analogs—A survey study, J. Solid State Chem. 184 (2011) 2854–2861. doi:10.1016/j.jssc.2011.08.030.

[150] S. Adak, M. Hartl, L. Daemen, E. Fohtung, H. Nakotte, Study of oxidation states of the transition metals in a series of Prussian blue analogs using x-ray absorption near edge structure (XANES) spectroscopy, J. Electron Spectros. Relat. Phenomena. 214 (2017) 8–19. doi:10.1016/j.elspec.2016.11.011.

[151] E.C. Markham, A.F. Benton, The adsorption of gas mixtures by silica, J. Am. Chem. Soc. 53 (1931) 497–507. doi:10.1021/ja01353a013.

[152] T.C. Jorgensen, L.R. Weatherley, Ammonia removal from wastewater by ion exchange in the presence of organic contaminants, Water Res. 37 (2003) 1723–1728. doi:10.1016/S0043-1354(02)00571-7.

[153] S. Balci, Nature of ammonium ion adsorption by sepiolite: analysis of equilibrium data with several isotherms, Water Res. 38 (2004) 1129–1138. doi:10.1016/j.watres.2003.12.005.

[154] O. Moradi, K. Zare, Adsorption of ammonium ion by multi-walled carbon nanotube: Kinetics and thermodynamic studies, Fullerenes, Nanotubs and Carbon Nanostructures. 21 (2013) 449–459. doi:10.1080/1536383X.2011.613538.

[155] Q. Chen, K. Zhou, Y. Chen, A. Wang, F. Liu, Removal of ammonia from aqueous solutions by ligand exchange onto a Cu(II)-loaded chelating resin: kinetics, equilibrium and thermodynamics, RSC Adv. 7 (2017) 12812–12823. doi:10.1039/C6RA28287C.

[156] N. Imchuen, Y. Lubphoo, J.-M. Chyan, S. Padungthon, C.-H. Liao, Using cation exchange resin for ammonium removal as part of sequential process for nitrate reduction by nanoiron, Sustain. Environ. Res. 26 (2016) 156–160. doi:10.1016/j.serj.2016.01.002.

[157] R.-J. Huang, Y. Zhang, C. Bozzetti, K.-F. Ho, J.-J. Cao, Y. Han, K.R. Daellenbach, J.G. Slowik, S.M. Platt, F. Canonaco, P. Zotter, R. Wolf, S.M. Pieber, E.A. Bruns, M. Crippa, G. Ciarelli, A. Piazzalunga, M. Schwikowski, G. Abbaszade, J. Schnelle-Kreis, R. Zimmermann, Z. An, S. Szidat, U. Baltensperger, I. El Haddad, A.S.H. Prévôt, High secondary aerosol contribution to particulate pollution during haze events in China, Nature 514 (2014) 218–222. doi:10.1038/nature13774.

[158] DG Agriculture and Rural Development and European Commission, Eco-innovation for air quality, Sofia, 2018. http://ec.europa.eu/environment/ecoinnovation2018/1st_forum/material/presentations/Session 3.1_Angelo Innamorati_EC_ECOAP Sofia forum.pdf (accessed November 23, 2018).

[159] European Environment Agency, European Union emission inventory report 1990–2015 under the UNECE convention on long-range transboundary air pollution (LRTAP), 2017. doi:10.2800/18374.

[160] X. Liu, Y. Zhang, W. Han, A. Tang, J. Shen, Z. Cui, P. Vitousek, J.W. Erisman, K. Goulding, P. Christie, A. Fangmeier, F. Zhang, Enhanced nitrogen deposition over China, Nature. 494 (2013) 459–462. doi:10.1038/nature11917.

[161] B. Gu, X. Ju, J. Chang, Y. Ge, P.M. Vitousek, Integrated reactive nitrogen budgets and future trends in China., Proc. Natl. Acad. Sci. U. S. A. 112 (2015) 8792–7. doi:10.1073/pnas.1510211112.

[162] C.Y. Liu, K. Aika, Absorption and desorption behavior of ammonia with alkali earth halide and mixed halide, Chem. Lett. 31 (2002) 798–799. doi:10.1246/cl.2002.798.

[163] A. Klerke, C.H. Christensen, J.K. Nørskov, T. Vegge, Ammonia for hydrogen storage: challenges and opportunities, J. Mater. Chem. 18 (2008) 2304. doi:10.1039/b720020j.

[164] R.Z. Sørensen, J.S. Hummelshøj, A. Klerke, J.B. Reves, T. Vegge, J.K. Nørskov, C.H. Christensen, Indirect, reversible high-density hydrogen storage in compact metal ammine salts, J. Am. Chem. Soc. 130 (2008) 8660–8668. doi:10.1021/ja076762c.

[165] B. Dou, M. Zhang, J. Gao, W. Shen, X. Sha, High-temperature removal of NH_3, organic sulfur, HCl, and Tar component from coal-derived gas, Ind. Eng. Chem. Res. 41 (2002) 4195–4200. doi:10.1021/ie010913h.

[166] Y. Peng, H. Chang, Y. Dai, J. Li, Structural and surface effect of MnO_2 for low temperature selective catalytic reduction of NO with NH_3, Procedia Environ. Sci. 18 (2013) 384–390. doi:10.1016/j.proenv.2013.04.051.

[167] G.H. Teletzke, W.B. Gitchel, D.G. Diddams, C.A. Hoffman, Components of sludge and its wet air oxidation products, Water Pollut. Control Fed. 39 (1967) 994–1005. doi:10.2307/25035949.

[168] V.. Shiralkar, S.. Kulkarni, Sorption of ammonia in cation-exchanged Y zeolites: Isotherms and state of sorbed molecules, J. Colloid Interface Sci. 108 (1985) 1–10. doi:10.1016/0021-9797(85)90230-9.

[169] M. Olejak-Chodan, H.A. Eick, Characterization of the $CaCl_2$-$EuCl_2$ and $CaCl_2$-$SrCl_2$ systems by X-ray powder diffraction, J. Solid State Chem. 69 (1987) 274–279. doi:10.1016/0022-4596(87)90084-3.

[170] S. Westman, P.-E. Werner, T. Schuler, W. Raldow, P.H. Nielsen, X-ray investigations of ammines of alkaline earth metal halides. I. The structures of $CaCl_2(NH_3)_8$, $CaCl_2(NH_3)_2$ and

the decomposition product CaClOH., Acta Chem. Scand. 35a (2016) 467–472. doi:10.3891/acta.chem.scand.35a-0467.

[171] E. Article, K.A. Colwell, A. Nandy, A. Reimer, S. Bordiga, R. Long, Highly effective ammonia removal in a series of Brønsted acidic porous polymers: investigation of chemical and structural variations, Chem. Sci. 8 (2017) 4399–4409. doi:10.1039/C6SC05079D.

[172] J.B. DeCoste, M.S. Denny, G.W. Peterson, J.J. Mahle, S.M. Cohen, Enhanced aging properties of HKUST-1 in hydrophobic mixed-matrix membranes for ammonia adsorption, Chem. Sci. 7 (2016) 2711–2716. doi:10.1039/c5sc04368a.

[173] B. Tan, C. Chen, L.X. Cai, Y.J. Zhang, X.Y. Huang, J. Zhang, Introduction of Lewis acidic and redox-active sites into a porous framework for ammonia capture with visual color response, Inorg. Chem. 54 (2015) 3456–3461. doi:10.1021/acs.inorgchem.5b00023.

[174] J.F. Van Humbeck, T.M. McDonald, X. Jing, B.M. Wiers, G. Zhu, J.R. Long, Ammonia capture in porous organic polymers densely functionalized with Brønsted acid groups, J. Am. Chem. Soc. 136 (2014) 2432–2440. doi:10.1021/ja4105478.

[175] H. Yang, H. Bae, M. Park, S. Lee, K.C. Kim, H. Lee, Fe–Porphyrin-like nanostructures for selective ammonia capture under humid conditions, J. Phys. Chem. C. 122 (2018) 2046–2052. doi:10.1021/acs.jpcc.7b11991.

[176] J. Helminen, J. Helenius, E.P. Turunen, E. Paatero, Adsorption equilibria of ammonia gas on inorganic and organic sorbents at 298.15 K, J. Chem. Eng. Data. 46 (2001) 391–399. doi:10.1021/je000273.

[177] K.W. Chapman, P.D. Southon, C.L. Weeks, C.J. Kepert, Reversible hydrogen gas uptake in nanoporous Prussian Blue analogues, Chem. Commun. (2005) 3322. doi:10.1039/b502850g.

[178] G. Autie-Castro, M. Autie, E. Reguera, R. Moreno-Tost, E. Rodríguez-Castellón, A. Jiménez-López, J. Santamaría-González, Adsorption and separation of propane and propylene by porous hexacyanometallates, Appl. Surf. Sci. 257 (2011) 2461–2466. doi:10.1016/j.apsusc.2010.10.003.

[179] C.P. Krap, J. Balmaseda, L.F. del Castillo, B. Zamora, E. Reguera, Hydrogen storage in Prussian blue analogues: H_2 interaction with the metal found at the cavity surface, Energy & Fuels. 24 (2010) 581–589. doi:10.1021/ef900823s.

[180] M. Asai, A. Takahashi, Y. Jiang, M. Ishizaki, M. Kurihara, T. Kawamoto, Trace alcohol adsorption by metal hexacyanocobaltate nanoparticles and the adsorption mechanism, J. Phys. Chem. C. (2018) acs.jpcc.8b03015. doi:10.1021/acs.jpcc.8b03015.

[181] R.D. Shannon, Revised effective ionic radii and systematic studies of interatomic distances in halides and chalcogenides, Acta Crystallogr. Sect. A. 32 (1976) 751–767. doi:10.1107/S0567739476001551.

[182] A.J. Rieth, M. Dincă, Controlled gas uptake in Metal–Organic Frameworks with record ammonia sorption, J. Am. Chem. Soc. 140 (2018) 3461–3466. doi:10.1021/jacs.8b00313.

[183] A.J. Rieth, Y. Tulchinsky, M. Dincã, M. Dincă, High and reversible ammonia uptake in mesoporous azolate Metal-Organic Frameworks with open Mn, Co, and Ni sites, J. Am. Chem. Soc. 138 (2016) 9401–9404. doi:10.1021/jacs.6b05723.

[184] W. Morris, C.J. Doonan, O.M. Yaghi, Postsynthetic modification of a metal-organic framework for stabilization of a hemiaminal and ammonia uptake, Inorg. Chem. 50 (2011) 6853–6855. doi:10.1021/ic200744y.

[185] G. Barin, G.W. Peterson, V. Crocellà, J. Xu, K.A. Colwell, A. Nandy, J.A. Reimer, S. Bordiga, J.R. Long, Highly effective ammonia removal in a series of Brønsted acidic porous polymers: investigation of chemical and structural variations, Chem. Sci. 8 (2017) 4399–4409. doi:10.1039/C6SC05079D.

[186] T. Kajiwara, M. Higuchi, D. Watanabe, H. Higashimura, T. Yamada, H. Kitagawa, A systematic study on the stability of Porous Coordination Polymers against ammonia, Chem. - A Eur. J. 20 (2014) 15611–15617. doi:10.1002/chem.201403542.

[187] C.J. Doonan, D.J. Tranchemontagne, T.G. Glover, J.R. Hunt, O.M. Yaghi, Exceptional ammonia uptake by a covalent organic framework., Nat. Chem. 2 (2010) 235–8. doi:10.1038/nchem.548.

[188] N.R. Council, Air emissions from animal feeding operations, National Academies Press, Washington, D.C., 2003. doi:10.17226/10586.

[189] F. Paulot, D.J. Jacob, Hidden Cost of U.S. Agricultural exports: Particulate matter from ammonia emissions, Environ. Sci. Technol. 48 (2014) 903–8. doi:10.1021/es4034793.

[190] S.A. MacDonald, W.D. Hinsberg, H.R. Wendt, N.J. Clecak, C.G. Willson, C.D. Snyder, Airborne contamination of a chemically amplified resist. 1. Identification of problem, Chem. Mater. 5 (1993) 348–356. doi:10.1021/cm00027a018.

[191] I.-K. Lin, H. Bai, B.-J. Wu, Analysis of relationship between inorganic gases and fine particles in cleanroom environment, Aerosol Air Qual. Res. 10 (2010) 245–254. doi:10.4209/aaqr.2009.10.0065.

[192] M.R. Rahimpour, A. Asgari, Production of hydrogen from purge gases of ammonia plants in a catalytic hydrogen-permselective membrane reactor, Int. J. Hydrogen Energy. 34 (2009) 5795–5802. doi:10.1016/j.ijhydene.2009.05.013.

[193] A.K. Hill, L. Torrente-Murciano, In-situ H_2 production via low temperature decomposition of ammonia: Insights into the role of cesium as a promoter, Int. J. Hydrogen Energy. 39 (2014) 7646–7654. doi:10.1016/j.ijhydene.2014.03.043.

[194] S. Mukherjee, S. V. Devaguptapu, A. Sviripa, C.R.F. Lund, G. Wu, Low-temperature ammonia decomposition catalysts for hydrogen generation, Appl. Catal. B Environ. 226 (2018) 162–181. doi:10.1016/J.APCATB.2017.12.039.

[195] D.W. Kang, J.H. Holbrook, Use of NH_3 fuel to achieve deep greenhouse gas reductions from US transportation, Energy Reports. 1 (2015) 164–168. doi:10.1016/j.egyr.2015.08.001.

[196] B.E. Erickson, Manure emissions up in the air, ACS Chem. Life. (2018) 28. https://cen.acs.org/magazine/96/09614.html (accessed June 13, 2018).

[197] B. Gu, X. Ju, J. Chang, Y. Ge, P.M. Vitousek, Integrated reactive nitrogen budgets and future trends in China, Proc. Natl. Acad. Sci. 112 (2015) 8792–8797. doi:10.1073/pnas.1510211112.

[198] C. Petit, T.J. Bandosz, Enhanced adsorption of ammonia on metal-organic framework/graphite oxide composites: Analysis of surface interactions, Adv. Funct. Mater. 20 (2010) 111–118. doi:10.1002/adfm.200900880.

[199] T.J. Bandosz, Activated carbon surfaces in environmental remediation, Elsevier, 2006.

[200] G.W. Peterson, G.W. Wagner, A. Balboa, J. Mahle, T. Sewell, C.J. Karwacki, Ammonia vapor removal by $Cu_3(BTC)_2$ and its characterization by MAS NMR, J. Phys. Chem. C. 113 (2009) 13906–13917. doi:10.1021/jp902736z.

[201] T. Watanabe, D.S. Sholl, Molecular chemisorption on open metal sites in Cu(3)(benzenetricarboxylate)(2): A spatially periodic density functional theory study, J. Chem. Phys. 133 (2010) 094509. doi:10.1063/1.3479041.

[202] J.B. Decoste, G.W. Peterson, B.J. Schindler, K.L. Killops, M.A. Browe, J.J. Mahle, The effect of water adsorption on the structure of the carboxylate containing metal-organic frameworks Cu-BTC, Mg-MOF-74, and UiO-66, J. Mater. Chem. A. 1 (2013) 11922–11932. doi:10.1039/c3ta12497e.

[203] B. Tan, C. Chen, L.-X. Cai, Y.-J. Zhang, X.-Y. Huang, J. Zhang, Introduction of lewis acidic and redox-active sites into a porous framework for ammonia capture with visual color response, Inorg. Chem. 54 (2015) 3456–3461. doi:10.1021/acs.inorgchem.5b00023.

[204] H. Furukawa, N. Ko, Y.B. Go, N. Aratani, S.B. Choi, E. Choi, A.O. Yazaydin, R.Q. Snurr, M. O'Keeffe, J. Kim, O.M. Yaghi, Ultrahigh porosity in Metal-Organic Frameworks, Science. 329 (2010) 424–428. doi:10.1126/science.1192160.

[205] B.J. Murray, E.C. Walter, R.M. Penner, Amine vapor sensing with silver mesowires, Nano Lett. 4 (2004) 665–670. doi:10.1021/nl049841k.

[206] S. Chen, G. Qi, Z. Hua, H. Yan, Double metal cyanide complex based on Zn_3 [Co(CN)$_6$]$_2$ as highly active catalyst for copolymerization of carbon dioxide and cyclohexene oxide, (2004) 9–12. doi:10.1002/pola.20334.

[207] A. Peeters, P. Valvekens, R. Ameloot, G. Sankar, C.E.A. Kirschhock, D.E. De Vos, Zn–Co double metal cyanides as heterogeneous catalysts for hydroamination: A structure–activity relationship, ACS Catal. 3 (2013) 597–607. doi:10.1021/cs300805z.

[208] C.P. Krap, B. Zamora, L. Reguera, E. Reguera, Stabilization of cubic and rhombohedral phases of zinc hexacyanocobaltate (III), Microporous Mesoporous Mater. 120 (2009) 414–420. doi:10.1016/j.micromeso.2008.12.010.

[209] J. Rodr ́guez-Hern ́andez, E. Reguera, E. Lima, J. Balmaseda, R. Mart ́nez-Garc ́a, H. Yee-Madeira, An atypical coordination in hexacyanometallates: Structure and properties of hexagonal zinc phases, J. Phys. Chem. Solids. 68 (2007) 1630–1642. doi:10.1016/j.jpcs.2007.03.054.

[210] R.K. Motkuri, P.K. Thallapally, B.P. McGrail, S.B. Ghorishi, Dehydrated Prussian blues for CO_2 storage and separation applications, CrystEngComm. 12 (2010) 4003. doi:10.1039/c0ce00199f.

[211] J.C. Wojdeł, S.T. Bromley, F. Illas, J.C. Jansen, Development of realistic models for Double Metal Cyanide catalyst active sites, J. Mol. Model. 13 (2007) 751–756. doi:10.1007/s00894-007-0218-3.

[212] R. Gilson, M.C. Durrant, Estimation of the pKa values of water ligands in transition metal complexes using density functional theory with polarized continuum model solvent corrections, Dalt. Trans. 14 (2009) 10223. doi:10.1039/b911593e.

Acknowledgements

Time always go fast; the three-year doctoral life is going to end. As it's my first-time study abroad, I remembered everything when I first arrived at the University of Tsukuba, maybe my experience was limited, the developed country made me surprised and excited. Gradually, the new lifestyle became one part of my life and make me progress so lot up to now.

Firstly, I would first like to thank my advisor, Professor Zhenya Zhang, for providing me the opportunity to study here, and always support my study. I also wish to express my appreciation to my co-supervisor, associate professor Zhongfang Lei, for her good advice and friendship during my doctoral studies. Besides, I want to give my sincere thanks to the AIST members, Dr. Tohru Kawamoto (Group leader, GL), Dr. Kimitaka Minami (Senior researcher), Dr. Tohru Nakamura-san (Senior researcher), Dr. Akira Takahashi-san (Senior researcher), Mr. Koji Sakurai, Mr. Yutaka Sugiyama and Ms. Miyuki Asai et al., as they gave me many helps and advice during my study. Especially for GL Dr. Tohru Kawamoto, he gave me the opportunity to do research in his lab. and supported me to participate in many academic conferences.

Secondly, I would like to give my thanks to my thesis committee members, Professor Zhenya Zhang, Zhongfang Lei, Kazuya Shimizu and Tohru Kawamoto for their patient check, listening, numerous comments. All instructors provided great insights and a memorable learning experience to me that I would remember in the rest of my life. Fellows like Koji Sakurai-san, Nan Zhang who worked with me together, deserve many contributions to this thesis. And thanks to the others for their selfless help during my three years of doctoral study.

Finally, I would like to thanks for my parents and wife who give me so much love and support during my three-year doctoral study. Meanwhile, thanks for my kid, he took me much happiness and motivation to do research. This dissertation would not have been completed without their love and support.

Appendix

1. ***Yong Jiang***, Akira Takahashi, Tohru Kawamoto, Miyuki Asai, Nan Zhang, Zhongfang Lei, Zhenya Zhang, Keisuke Kojima, Kenta Imoto, Kosuke Nakagawa, Shin-ichi Ohkoshi and Tohru Nakamura. High performance sorption and desorption behaviours at high working temperatures of ammonia gas in cobalt-substituted Prussian blue analogue. *Chem. Commun.*, 54, p 11961–11964, (2018). **(IF=6.392)**

2. ***Yong Jiang***, Kimitaka Minami, Koji Sakurai, Akira Takahashi, Durga Parajuli, Zhongfang Lei, Zhenya Zhang and Tohru Kawamoto. High-capacity and selective ammonium removal from water using sodium cobalt hexacyanoferrate. *RSC Adv*. 8, p 34573–34581, (2018). **(IF=3.111)**

3. Miyuki Asai, Akira Takahashi, ***Yong Jiang***, Manabu Ishizaki, Masato Kurihara, and Tohru Kawamoto. Trace Alcohol Adsorption by Metal Hexacyanocobaltate Nanoparticles and the Adsorption Mechanism, *J. Phys. Chem. C*, 122 (22), p 11918–11925, (2018). **(IF= 4.51)**

4. Yang Yu, Zhongfang Lei, Tian Yuan, ***Yong Jiang***, Nan Chen, Chuanping Feng, Kazuya Shimizu, Zhenya Zhang. Simultaneous phosphorus and nitrogen recovery from anaerobically digested sludge using a hybrid system coupling hydrothermal pretreatment with MAP precipitation, *Bioresource Technology*, 243, p 634-640, 2017. **(IF= 5.458)**